Localization and functional role of Cav2.3 in the medial habenula to interpeduncular nucleus pathway

by

Pradeep Bhandari

December, 2019

A thesis presented to the
Graduate School
of the
Institute of Science and Technology Austria, Klosterneuburg, Austria
in partial fulfillment of the requirements
for the degree of
Doctor of Philosophy

The dissertation of Pradeep Bhandari, titled *Localization and functional role of Cav2.3 in medial habenula to interpeduncular nucleus pathway*, is approved by:

Supervisor: Ryuichi Shigemoto, IST Austria, Klosterneuburg, Austria

Signature: _____

Committee Member: Peter Jonas, IST Austria, Klosterneuburg, Austria

Signature: _____

Committee Member: Francesco Ferraguti, Medical University of Innsbruck, Austria

Signature: _____

Exam Chair: Maxmilian Albert Joesch, IST Austria, Klosterneuburg, Austria

Signature: _____

Signed page is on file

IST Austria Thesis, ISSN: 2663-337X

I hereby declare that this dissertation is my own work and that it does not contain other people's work without this being so stated; this thesis does not contain my previous work without this being stated, and the bibliography contains all the literature that I used in writing the dissertation.

I declare that this is a true copy of my thesis, including any final revisions, as approved by my thesis committee, and that this thesis has not been submitted for a higher degree to any other university or institution.

I certify that any republication of materials presented in this thesis has been approved by the relevant publishers and co-authors.

Signature: _____

Pradeep Bhandari

February 28, 2020

Signed page is on file

Abstract

The medial habenula (MHb) is an evolutionary conserved epithalamic structure important for the modulation of emotional memory. It is involved in regulation of anxiety, compulsive behavior, addiction (nicotinic and opioid), sexual and feeding behavior. MHb receives inputs from septal regions and projects exclusively to the interpeduncular nucleus (IPN). Distinct sub-regions of the septum project to different subnuclei of MHb: the bed nucleus of anterior commissure projects to dorsal MHb and the triangular septum projects to ventral MHb. Furthermore, the dorsal and ventral MHb project to the lateral and rostral/central IPN, respectively. Importantly, these projections have unique features of prominent co-release of different neurotransmitters and requirement of a peculiar type of calcium channel for release. In general, synaptic neurotransmission requires an activity-dependent influx of Ca^{2+} into the presynaptic terminal through voltage-gated calcium channels. The calcium channel family most commonly involved in neurotransmitter release comprises three members, P/Q-, N- and R-type with Cav2.1, Cav2.2 and Cav2.3 subunits, respectively. In contrast to most CNS synapses that mainly express Cav2.1 and/or Cav2.2, MHb terminals in the IPN exclusively express Cav2.3. In other parts of the brain, such as the hippocampus, Cav2.3 is mostly located to postsynaptic elements. This unusual presynaptic location of Cav2.3 in the MHb-IPN pathway implies unique mechanisms of glutamate release in this pathway. One potential example of such uniqueness is the facilitation of release by GABAB receptor (GBR) activation. Presynaptic GBRs usually inhibit the release of neurotransmitters by inhibiting presynaptic calcium channels. MHb shows the highest expression levels of GBR in the brain. GBRs comprise two subunits, GABAB1 (GB1) and GABAB2 (GB2), and are associated with auxiliary subunits, called potassium channel tetramerization domain containing proteins (KCTD) 8, 12, 12b and 16. Among these four subunits, KCTD12b is exclusively expressed in ventral MHb, and KCTD8 shows the strongest expression in the whole MHb among other brain regions, indicating that KCTD8 and KCTD12b may be involved in the unique mechanisms of neurotransmitter release mediated by Cav2.3 and regulated by GBRs in this pathway.

In the present study, we first verified that neurotransmission in both dorsal and ventral MHb-IPN pathways is mainly mediated by Cav2.3 using a selective blocker of R-type channels, SNX-482. We next found that baclofen, a GBR agonist, has facilitatory effects on release from ventral MHb terminal in rostral IPN, whereas it has inhibitory effects on release from dorsal MHb terminals in lateral IPN, indicating that KCTD12b expressed exclusively in ventral MHb may have a role in the facilitatory effects of GBR activation. In a heterologous expression system using HEK cells, we found that KCTD8 and KCTD12b but not KCTD12 directly bind

with Cav2.3. Pre-embedding immunogold electron microscopy data show that Cav2.3 and KCTD12b are distributed most densely in presynaptic active zone in IPN with KCTD12b being present only in rostral/central but not lateral IPN, whereas GABAB, KCTD8 and KCTD12 are distributed most densely in perisynaptic sites with KCTD12 present more frequently in postsynaptic elements and only in rostral/central IPN. In freeze-fracture replica labelling, Cav2.3, KCTD8 and KCTD12b are co-localized with each other in the same active zone indicating that they may form complexes regulating vesicle release in rostral IPN.

On electrophysiological studies of wild type (WT) mice, we found that paired-pulse ratio in rostral IPN of KCTD12b knock-out (KO) mice is lower than those of WT and KCTD8 KO mice. Consistent with this finding, in mean variance analysis, release probability in rostral IPN of KCTD12b KO mice is higher than that of WT and KCTD8 KO mice. Although paired-pulse ratios are not different between WT and KCTD8 KO mice, the mean variance analysis revealed significantly lower release probability in rostral IPN of KCTD8 KO than WT mice. These results demonstrate bidirectional regulation of Cav2.3-mediated release by KCTD8 and KCTD12b without GBR activation in rostral IPN. Finally, we examined the baclofen effects in rostral IPN of KCTD8 and KCTD12b KO mice, and found the facilitation of release remained in both KO mice, indicating that the peculiar effects of the GBR activation in this pathway do not depend on the selective expression of these KCTD subunits in ventral MHb. However, we found that presynaptic potentiation of evoked EPSC amplitude by baclofen falls to baseline after washout faster in KCTD12b KO mice than WT, KCTD8 KO and KCTD8/12b double KO mice. This result indicates that KCTD12b is involved in sustained potentiation of vesicle release by GBR activation, whereas KCTD8 is involved in its termination in the absence of KCTD12b. Consistent with these functional findings, replica labelling revealed an increase in density of KCTD8, but not Cav2.3 or GBR at active zone in rostral IPN of KCTD12b KO mice compared with that of WT mice, suggesting that increased association of KCTD8 with Cav2.3 facilitates the release probability and termination of the GBR effect in the absence of KCTD12b.

In summary, our study provided new insights into the physiological roles of presynaptic Cav2.3, GBRs and their auxiliary subunits KCTDs at an evolutionary conserved neuronal circuit. Future studies will be required to identify the exact molecular mechanism underlying the GBR-mediated presynaptic potentiation on ventral MHb terminals. It remains to be determined whether the prominent presence of presynaptic KCTDs at active zone could exert similar neuromodulatory functions in different pathways of the brain.

Acknowledgments

First of all, I would like to sincerely thank my advisor, Ryuichi Shigemoto, for giving me an opportunity in his lab. His scientific guidance, suggestion and criticism were always very helpful in nurturing scientific temperament in me.

I am grateful to Peter Koppensteiner for performing electrophysiology experiment and providing overall help. His critical comments, thoughtful discussion and encouraging words even during tough times with my experiments helped me move forward smoothly with my project. I offer my gratitude to David Kleindienst for writing a script for analyzing replica sample.

I am thankful to Peter Jonas for insightful discussion of the electrophysiological result. In addition, I thank David Vandael for doing initial electrophysiology experiment. I offer my gratitude to Bernhard Bettler for providing KCTD knock out mice and KCTD antibodies. Besides, I am grateful to Thorsten Fritizius for performing co-immunoprecipitation experiment. Furthermore, I offer my gratitude to Laxmi Kumar Parajuli for teaching me electron microscopy.

Special thanks to Elodie Lemonnier for providing wonderful technical help. I thank all members of Shigemoto Lab for helping me out with my scientific work and providing excellent company due course of my PhD. My gratitude to EM facility team as well for continuous support.

[Optional: Dedication]

About the Author

Pradeep Bhandari completed a BSc in microbiology at Trichandra Multiple Campus, Tribhuvan University and an MSc in human physiology at BP Koirala Institute of Health Sciences. He taught human physiology to medical students from 2009 to 2012 in Nepal. He joined IST Austria in 2013, April. He is interested in studying the role of medial habenula to interpeduncular pathway and calcium channels present in this pathway. During his PhD studies, he presented his research work in Society for Neuroscience (SfN) in 2016 and Federation of European Neuroscience Society (FENS) in 2018.

Besides research, he is interested in long distance trail running and hiking.

List of Publications Appearing in Thesis

Posters

Bhandari P, Parajuli LK, Takao K, Miyakawa T, Kobayashi Y, Tanaka KF, Shigemoto. Role of R-type calcium channel (Cav2.3) in medial habenula to interpeduncular nucleus pathway. Program No. 220.11/J9. 2016 Neuroscience Meeting Planner. San Diego, CA: Society for Neuroscience, 2016. Online.

Vandael P, **Bhandari P**, Shigemoto R, Jonas P. Presynaptic R-type (Cav2.3) channels mediate glutamate release at habenulo-interpeduncular nucleus synapses. Program No. 220.08/J6. 2016 Neuroscience Meeting Planner. San Diego, CA: Society for Neuroscience, 2016. Online.

Bhandari P, Koppensteiner P, Gassmann M, Fritzius T, Bettler B, Kulik A, Shigemoto R. Co-clustering of Cav2.3, GABAB1 and KCTDs in presynaptic active zone of medial habenula to interpeduncular nucleus pathway. Abstract no. F18-2771. 2018. 11th FENS Forum of Neuroscience, 2018. Online.

Bhandari P, Vandael D, Fritzius T, Kleindienst D, Gassmann M, Kulik A, Jonas P, Bettler B, Shigemoto R, Koppensteiner P. Modulation of neurotransmitter release via KCTDs at the medial habenula to interpeduncular nucleus pathway. Program No. 036.05. 2019 Neuroscience Meeting Planner. Chicago, IL: Society for Neuroscience, 2019. Online.

Table of Contents

List of Figures

List of Tables

List of Symbols/Abbreviations

AMPA	α-amino-3-hydroxy-5-methyl-4-isoxazolepropionic acid
Cav	voltage gated calcium channel
CB1	cannabinoid type 1 receptors
CCK	cholecystokinin
dMHb	dorsal medial habenula
EPSC	excitatory post synaptic current
GABA	γ-aminobutyric acid
GB1	GABAB1
GB2	GABAB2
GBR	GABAB receptor
GPCR	G protein coupled receptor
IPN	interpeduncular nucleus
KCTD	potassium channel tetramerization domain containing protein
LHb	lateral habenula
LTP	long term potentiation
MHb	medial habenula
MHbC	central part of MHb
MHbCd	dorsal region of MHbC
MHbL	lateral part of MHb
MHbS	superior part of MHb
nAChRs	nicotinic acetylcholine receptors
NMDA	N-methyl-D-aspartate
NK1	neurokinin 1
PIP_2	phosphoinositol phosphate
POMC	pro-opiomelanocortin
PPR	paired pulse ratio
SK channel	small conductance calcium-activated potassium channel
SNP	single nucleotide polymorphism
SP	supstance P
TBS	Tris-buffered saline
vAchT	vesicular acetylcholine transporter
VGCC	voltage gated calcium channel
Vglut1	vesicular glutamate transporter 1
VgluT2	vesicular glutamate transporter 2

Chapter One

INTRODUCTION

1.1 Input and projection of medial habenula (MHb) to interpeduncular nucleus (IPN) pathway

1.1.1 Medial Habenula

Habenular complex is an epithalamic structure which is a part of dorsal diencephalic system consisting of the stria medularis, habenular complex and the fasciculus retroflexus that is phylogenetically conserved distinctly in all vertebrates. The habenula lies near the dorsal third ventricle and is divided into two different structures: the medial and lateral habenula (Sutherland, 1982). The MHb contains a homogeneous population of darkly staining, small, round or piriform tightly packed neurons with small dendritic fields (Herkenham and Nauta, 1977, 1979, Lecourtier and Kelly, 2007). In contrast, the lateral habenula (LHb) contains a heterogeneous population of mostly medium-sized, loosely packed cells with dendritic fields spanning distances of several hundred microns (Iwahori, 1977, Herkenham and Nauta, 1979). With anterograde and retrograde virus injection, Yamaguchi et al. showed that septal nuclei project to MHb. Dorsal MHb gets projection from bed nucleus of anterior commissure and ventral MHb gets projection from triangular septum (Yamaguchi et al., 2013). MHb receives glutamatergic input along with ATP from triangular septum and GABAergic input from medial septum and nucleus of diagonal band (Qin and Luo, 2009). There is a unidirectional projection from the MHb to the LHb (Kim and Chang, 2005). Electrophysiological and anatomical studies suggest that these two nuclei process and integrate information from the limbic forebrain and the pallidum to the midbrain (Kim and Chang, 2005).

Andres and colleagues divided MHb into different subnuclei based on topographical position: superior part of MHb (MHbS) lies on dorsal superior part by the side of third ventricle; inferior part of MHb (MHbI) lies ventral to MHbS; lateral part of MHb (MHbL) borders with LHb; central part of MHb (MHbC) lies between MHbI and MHbL; and the commissural MHb. Each

subnuclei were reported to have cell types with distinct morphological characteristics in EM (Andres et al., 1999). Aizawa et al. further characterized the neurotransmitter system in each sub-nuclei by mapping the mRNA and protein expression of marker genes for neurotransmitters and their respective receptors (Aizawa et al., 2012). They reported that tachykinin 1 mRNA (*Tac1*), a precursor for substance P, was detected in the dorsal region of MHbC (MHbCd). Complementary to that of *Tac1*, distribution of the cholinergic neurons expressing ChAT was restricted to MHbI, the ventral MHbC (MHbCv), and MHbL. Interestingly, MHbS at the dorsomedial edge of MHb expressed neither *Tac1* nor ChAT (Aizawa et al., 2012). mRNA distribution for the type 1 and 2 vesicular glutamate transporters (*Vglut1* and *Vglut2*), markers of glutamatergic transmission (Fremeau et al., 2001, Varoqui et al., 2002), showed interesting pattern in MHb. *Vglut2* mRNA was present in all MHb neurons, with stronger expression in MHbS and weaker expression in MHbCd. In contrast, *Vglut1* mRNA was restricted to MHbS, MHbI, and MHbCv regions only.

Generally, neurons expressing *Vglut1* and *Vglut2* localize differentially in the adult brain, e.g., *Vglut1* is expressed in the cerebral cortex and hippocampus, whereas *Vglut2* has been localized in subcortical structures such as the thalamus (Fremeau et al., 2001, Varoqui et al., 2002). The habenula is one of the very few exceptional regions expressing both *Vglut1* and *Vglut2* mRNA (Fremeau et al., 2001), and the co-localization of these two markers as observed in MHbS, MHbI, and MHbCv. Similarly, the μ-opioid receptor (*Oprm*) mRNA is present in MHbL (Aizawa et al., 2012). Depending upon the different enzymes and mRNA of various neurotransmitters expressed in MHb subnuclei, it can be categorized as exclusively glutamatergic (MHbS), both substance P-ergic and glutamatergic (MHbCd) in dorsal MHb, or both cholinergic and glutamatergic (MHbI, MHbCv, and MHbL) in ventral MHb (Hamill et al., 1984, Contestabile et al., 1987, Aizawa et al., 2012).

1.1.2 Projection from MHb to IPN

MHb projects almost exclusively to IPN in midbrain via a single compact projection in fasciculus retroflexus (Herkenham and Nauta, 1979). Habenulo-interpeduncular pathway serves as a link between limbic forebrain and midbrain (Sutherland, 1982, Lecourtier and Kelly, 2007). IPN is the prominent structure in the ventral midline of midbrain of vertebrates (Hamill and Lenn, 1984). It is subdivided into different subnuclei. Lenn and Hamill proposed the subdivision of IPN into unpaired median subnuclei as rostral, central and apical; and paired subnuclei as rostral lateral, dorsal

lateral, intermediate and lateral (Lenn and Hamill, 1984). Medial habenular-interpeduncular fibers form the center core of fasciculus retroflexus whereas fibers from lateral habenular nucleus form the outer bundle. Medial habenular compact central portion of fasciculus retroflexus terminate uniquely in IPN; their pattern of termination shows a 90 degree rotation of MHb. The dorsal MHb projects to the lateral IPN region, whereas, ventral MHb projects to all IPN subnuclei such as central, intermediate, and rostral except the lateral IPN. Moreover, fibers of the fasciculus retroflexus entering the IPN have a unique terminal pattern. Each fiber enters and traverses the entire width of the nucleus to the opposite side, then loops back to the first side, probably repeating this zig-zag several times, making synaptic contacts with interpeduncular neurons. On the other hand, lateral habenula project to ventral tegmental area, substantia nigra, median raphe, dorsal raphe, ventral raphe (Herkenham and Nauta, 1979, Sutherland, 1982, Groenewegen et al., 1986).

The majority of synapses of medial habenular neurons in interpeduncular nucleus are en passant synapses (Lenn, 1976). However, intermediate subnucleus of IPN has a unique type of synapse called crest synapse, a special type of synapse in which a dendrite receives afferent inputs from two axons. In 90% of these synapses, the projection consists of one axon from the left and one axon from the right MHb whereas remaining 10% has left MHb or right MHb only (Lenn et al., 1983). Crest synapses are first recognized at 8^{th} day of rat's life. They increase in number and complexity from 8 to 14^{th} days of rat's life (Lenn, 1978).

MHb projects solely to IPN and IPN projects efferents to dopaminergic, serotonergic, and noradrenergic centers through the laterodorsal tegmental area (Groenewegen et al., 1986). IPN sends efferent projections to a variety of midbrain and hindbrain structures implicated in the neurophysiology underlying addiction and a variety of mood related psychiatric conditions such as ventral tegmental area, the raphe nuclei, nucleus incertus, lateral septum, lateral dorsal tegmentum, hippocampus and hypothalamus. In addition, it also projects to dorsal and medial raphe nuclei (McLaughlin et al., 2017). Figure 1.1 shows the possible connection of MHb and IPN with different parts of the brain.

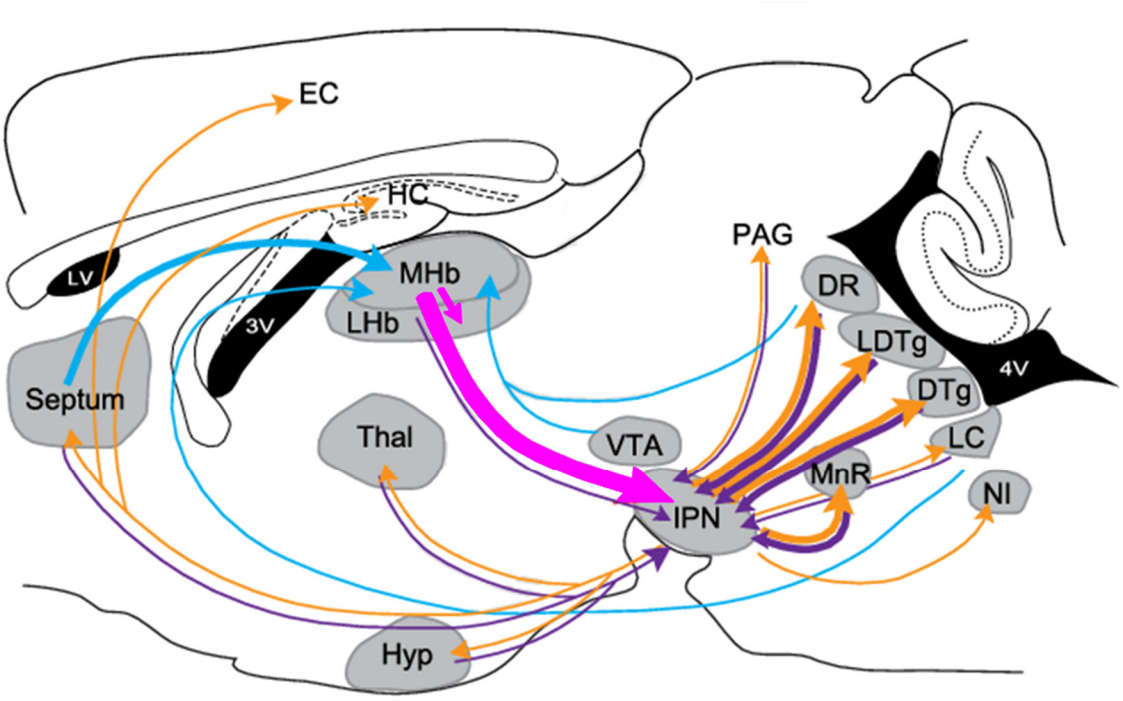

Figure 1.1: Schematic sagittal view of Medial habenula to IPN connectivity. It shows MHb afferents (blue), MHb efferents (pink), IPN afferents (purple) and IPN efferents (orange) with thickness of the arrows reflecting the strength of the connection. 3V, third ventricle; 4V, fourth ventricle; DR, dorsal raphe; DTg, dorsal tegmental nucleus; EC, entorhinal cortex; HC, hippocampus; Hyp, hypothalamus; IPN, interpeduncular nucleus; LC, locus coeruleus; LDTg, laterodorsal tegmental nucleus; LHb, lateral habenula; LV, lateral ventricle; MHb, medial habenula; MnR, median raphe; NI, nucleus incertus; PAG, periaqueductal gray; Thal, thalamus; VTA, ventral tegmental area. Adapted and modified from (Antolin-Fontes et al., 2015).

1.1.3 Release of different neurotransmitters from dorsal and ventral MHb terminals

The dorsal MHb provides substance P-ergic projection to the lateral subnuclei of IPN. Whereas, ventral MHb supplies cholinergic projection to all subnuclei of IPN except the lateral subnuclei. IPN also receives glutamatergic projections from almost all habenular subnuclei (Mroz et al., 1976, Cuello et al., 1978, Groenewegen et al., 1986, Contestabile et al., 1987, Qin and Luo,

2009). IPN has the highest concentration of choline acetyltransferase, an enzyme responsible for synthesis of acetylcholine, in the brain (Palkovits et al., 1974).

Immunohistochemical study shows that the IPN is rich in different neuropeptide positive cell bodies or axon terminals. Fibers in the lateral IPN show positive immunoreactivity to substance P. Rostral half of the IPN also shows relatively sparse substance P-reactive fibers confined to a thin layer marking dorsal border (Groenewegen et al., 1986, Aizawa et al., 2012). Met-enkephalin (ENK) or leu-ENK positive cells are also present in the IPN with the latter one more densely. Enkephalin positive cell bodies are present mostly in the rostral IPN. They are present in the apical and the caudal part of the central IPN as well. Serotonin like immunoreactivity of neuronal cell bodies is present in the apical IPN. Cholesystokinin (CCK) and leu-ENK processes surround the lateral subnuclei. Besides inputs from the MHb, the IPN also receives afferents from the median raphe and dorsal tegmental regions (Groenewegen et al., 1986).

Physiological and immuno-histochemical studies show that MHb is one of the few areas of brain which is rich in GBRs. Other such areas include neocortex, hippocampus, thalamus and cerebellum (Charles et al., 2001). MHb is also rich in nicotinic receptors (Quick et al., 1999). The projections from the MHb to the IPN are exclusively excitatory whereas neurons of the IPN are almost exclusively GABAergic (Qin and Luo, 2009). The immunohistological studies show the presence of GBRs in the IPN as well (Aizawa et al., 2012). Central and rostral subnuclei of the IPN receive inputs from the ventral MHb. These MHb terminals express both vGluT1 and vesicular acetylcholine transporter (vAchT) suggesting possible co-release of glutamate and acetylcholine. vGluT2 mRNA is distributed in almost all nuclei of MHb (Ren et al., 2011, Aizawa et al., 2012). Mu-opioid receptor, the mediator of analgesic and rewarding properties of opioid, is expressed strongly in dorsal medial habenula along with SP-positive axon terminals in the lateral IPN, the projection site of dorsal MHb and a subpopulation of MHb-cholinergic neurons (Herkenham and Nauta, 1979, Sutherland, 1982, Groenewegen et al., 1986, Gardon et al., 2014).

Cav2.3 is present in IPN in axon terminals. This is the sole region in the brain where only Cav2.3 is present predominantly presynaptically (Parajuli et al., 2012). It plays a role in neurotransmitter release in this region (Zhang et al., 2016). Glutamate is released at low stimulation, and acetylcholine at strong stimulation in cholinergic neurons of this pathway. Brief photostimulation of Channelrhodopsin-2 expressing cholinergic neurons in MHb produces fast excitatory postsynaptic current in the IPN mediated by ionotropic glutamate receptors, suggesting wired glutamatergic transmission. On the other hand, tetanic photo-stimulation generates slow inward currents largely mediated by nicotinic acetycholine receptors suggesting volume transmission of acetylcholine in agreement with the co-expression of vesicular transporters of

glutamate and acetycholine in the same axon terminals in the IPN. This also shows dual mode of signal transmission by cholinergic neurons in MHb-IPN pathway (Ren et al., 2011). Similarly, activation of substance P positive dorsal MHb (dMHb) neurons to release substance P and glutamate results in a simultaneous activation of glutamatergic and glycinergic receptors (GlyT1 and GlyT2) in the lateral IPN. Furthermore, glycinergic transmission suppresses activity-dependent synaptic potentiation in lateral IPN neurons, while substance P enhances this plasticity via a (endocannabinoid) CB1 and GABAB receptor (GBR)-dependent manner (Melani et al., 2019a).

MHb express high level of GBR in their cell bodies and their axon terminals in IPN (Margeta-Mitrovic et al., 1999). GBRs are coupled to guanine nucleotide-binding protein ($G\alpha_{i/o}$-$_{\beta\gamma}$). When agonist such as baclofen binds to GBR, Gβγ subunits get released from the GB2 subunit and interact with Cav2.3 modulating it to increase neurotransmitter release (Zhang et al., 2016). Cannabinoid type 1 receptors (CB1) are expressed in MHb and its projection area IPN. Blockade of CB1R specifically enhances cholinergic but not glutamatergic neurotransmission in IPN (Soria-Gomez et al., 2015).

1.1.4 Behavioral relevance of MHb to IPN pathway:

The MHb to IPN pathway plays a role in different behavioral paradigms. Many aversive behaviors are regulated by MHb-IPN pathway. Agetsuma et al. have shown that genetic inactivation of the lateral subnucleus of dorsal habenula in zebra fish, equivalent to the MHb of the mammalian brain, enhances fear responses to electrical shocks proving a role of the dMHb-vIPN in fear-related behavior (Agetsuma et al., 2010). Kobyashi et al. have showed that MHb-IPN pathway in mouse is also involved in anxiety-related behavior (Kobayashi et al., 2013). Zhang et al. have described the MHb-IPN pathway as an extra-amygdalar circuit showing their involvement in fear control (Zhang et al., 2016). Activation of excitatory presynaptic GBRs expressed in cholinergic terminals of IPN enhanced fear extinction whereas, ablation of MHb-IPN pathway or inhibition of $GABA_B$ function impairs fear extinction (Zhang et al., 2016). MHb-IPN synaptic plasticity has a role in aversive behavior as fear conditioning suppresses an activity-dependent potentiation of MHb-IPN synapses, whereas fear extinction reverses this plasticity deficit (Koppensteiner et al., 2017). MHb-diphtheria toxin A transgenic mice, a mouse model equivalent to bilateral lesions of the entire medial habenular complex, showed impulsivity and

compulsivity behavior with increased nose poking to closed door for saccharin. This indicates the inhibitory role of MHb-IPN on impulsive and compulsive behavior. MHb-IPN pathway may also be involved in mental disorders such as schizophrenia, in which impulsive behavior is commonly observed (Kobayashi et al., 2013, Hoptman, 2015). Zhang et al. have also reported that schizophrenic patients have smaller habenula (together lateral and medial) supporting the view of a possible involvement of medial habenula in schizophrenia (Zhang et al., 2017).

Habenulo-interpeduncular pathway plays a role in controlling nicotine intake and/or nicotine addiction. Nicotine activates α5-containing nicotinic acetylcholine receptors (nAChRs), triggering an inhibitory motivational signal that acts to limit nicotine intake (Fowler et al., 2011). This pathway plays a role in physical withdrawal symptoms of nicotinic addiction (Fowler et al., 2011). MHb cholinergic neurons regulate anxiety during nicotine withdrawal by increased signaling through nicotinic acetylcholine receptors (nAchR) containing the α6 subunit in MHb neurons that also express α4 subunits (Pang et al., 2016). Infusion of the non-selective nAchR antagonist, mecamylamine, in MHb or IPN but not in ventral tegmental area or hippocampus precipitates withdrawal syndrome in mice chronically treated with ethanol indicating that nAchR blockade in MHb-IPN pathway causes withdrawal symptom (McLaughlin et al., 2017). Neuropeptide Y knocked out mice show increased alcohol ingestion relative to WT showing the role of neuropeptide Y in alcoholism. This shows that MHb-IPN pathway is involved in both alcohol addiction and withdrawal symptom (McLaughlin et al., 2017).

MHb-IPN pathway is also involved in opioid addiction. Lesions of MHb have been observed to induce hyperalgesia and increase analgesic efficiency of morphine (McLaughlin et al., 2017). Acetylcholinesterase activity is altered and nAchR density increases in MHb following chronic morphine administration; the opioid receptor antagonist, naloxone, shows withdrawal symptom with changed acetylcholinesterase activity (Neugebauer et al., 2013). Administration of 18- methoxycoronaridine, an α3β4 nAChR antagonist, reduces signs of naltrexone-precipitated withdrawal from morphine (McLaughlin et al., 2017).

Hsu et al. showed that dMHb is involved in exercise motivation and the regulation of hedonic state, and is part of an intrinsic reinforcement circuit. Using three mouse models: dMHb lesioned mice by knocking out Brn3a protein, channelrhodopsin-2 expressing mice in dMHb for activation and halorhodopsin expressing mice in dMHb for inhibition, they reported that dMHb ablated mice show little interest in voluntary wheel run without significantly affecting gait and show little interest in sucrose preference test. Similarly, inhibition of dMHb by stimulating halorhodopsin shows acute place aversion. On the other hand, activation of dMHb stimulating channelrhodopsin encourages mouse to perform better in involuntary wheel run (Hsu et al., 2014).

With auto-radiographic deoxyglucose method in male birds, it was shown that the IPN, along with some other brain areas such as rostral preoptic area, nucleus intercollicularis, was activated during appetitive or male consummatory behavior showing the involvement of IPN in male sexual behavior (Dermon et al., 1999).

Function of MHb-IPN pathway	**Reference**
Fear responses in dMHb-IPN pathway to electrical stimulus	(Agetsuma et al., 2010)
Anxiety related behavior	(Kobayashi et al., 2013)
Fear conditioning	(Koppensteiner et al., 2017; Zhang et al., 2016)
Impulsive and compulsive behavior	(Kobayashi et al., 2013, Hoptman, 2015)
Schizophrenia	(Zhang et al., 2017)
Nicotinic addiction and withdrawal symptom	(Fowler et al., 2011)
Alcohol addiction and withdrawal symptom	(McLaughlin et al., 2017)
Morphine addiction	(McLaughlin et al., 2017)
Exercise motivation and the regulation of hedonic state	(Hsu et al., 2014)
Appetitive or male consummatory behavior in birds	(Dermon et al., 1999)
Diabetes associated gene TCF7L2 expressed strongly in MHb regulate the function of nicotinic acetylcholine receptors	(Duncan et al., 2019)
Post mortem analysis of depression patient showed decreased habenular size	(McLaughlin et al., 2017)a
Increased metabolic MHb and LHb activity in helpless rats	(Shumake et al., 2003)

Table 1: Summary of behavioral function of MHb-IPN pathway

1.2 Voltage-gated calcium channels

Voltage gated calcium channel 2.3 (Cav2.3) or R type calcium channel first reported from cerebellar granule cells was “resistant” to most of the subtype specific organic and peptide Cav channel blockers. SNX-482 derived from tarantula *Hysterocrates gigas* blocks R type calcium channels in some cell types (Zhang et al., 1993, Newcomb et al., 1998). Initially, it was classified as a low voltage-activated calcium channel on the basis of functional studies although structurally it looked like a high voltage-activated calcium channel (Soong et al., 1993). Williams et al. showed in their functional studies that Cav2.3 is a high voltage-activated calcium channel opposite to Soong et al.’s conclusion. They showed that R type is similar to high voltage activated N type calcium channels (Williams et al., 1994). The functional expression of Cav2.3 channels have first been reported from marine ray (Soong et al., 1993), then rat (Ellinor et al., 1993) and then human (Williams et al., 1994). $Ca_v2.3$ or R type calcium channel belongs to the family of voltage-gated Ca^{2+} channels comprising ten different genes for ion conducting pore proteins (Figure 1.2) (Schneider et al., 2013). Among the ten different Cavs, P/Q, N and R type calcium channels are commonly found in neurons, whereas L and T types are found in a wide range of cell types (Catterall, 2011).

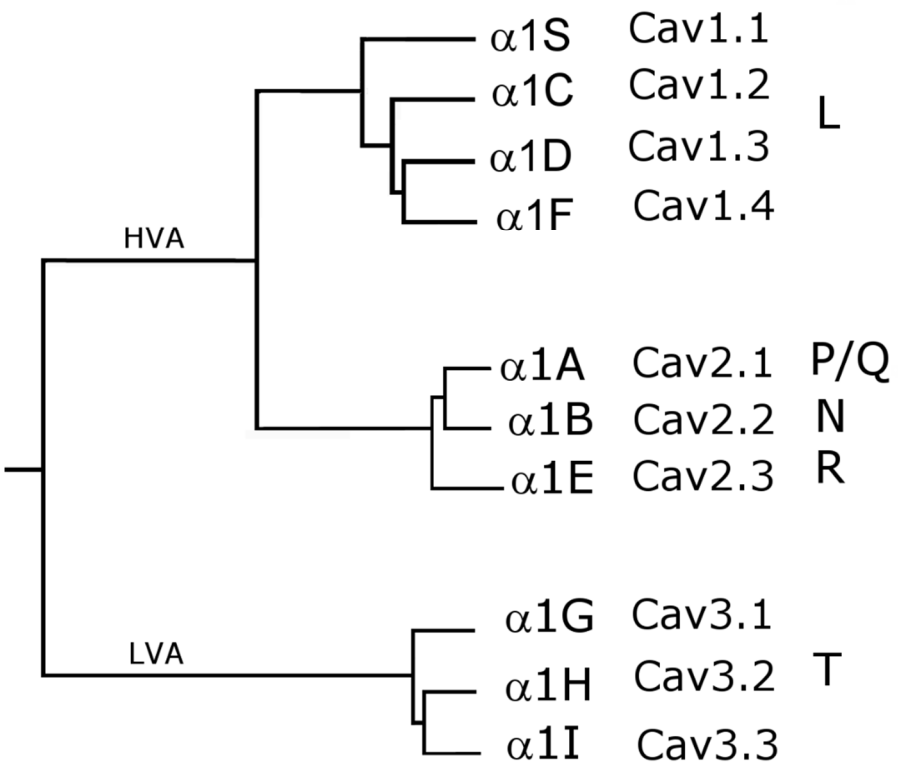

Figure 1.2: Evolutionary tree of voltage gated calcium channel. The cDNA of the pore loops of the human sequence were aligned. HVA- High voltage gated calcium channel, LVA- Low voltage gated calcium channel. Adapted from (Schneider et al., 2013).

1.2.1 Structure

Voltage-gated calcium channel (VGCC) consists of a central pore forming α1 subunit and other auxiliary subunits. The α1 subunit forms the center of the calcium channel which is also the pore forming unit. It consists of four homologous domains each containing 6 transmembrane helices (S1 to S6 as shown in Figure 1.3). These four domains are connected by amino acid loop. Each domain is connected with five protein loops. These four domains are arranged clockwise in Cav molecule (Wu et al., 2015). The pore forming unit is between S5 and S6 whereas S1-S4 act as gating modifiers with each segment acting as voltage sensor. Blockers of calcium channels act within the α1 subunit between the S5 and S6 segments (Catterall, 2011, Zamponi et al., 2015) (Figure 1.3). The size of different components of Cav complexes derived from skeletal muscle cells are α1(approximately 170 kDa), α2(approximately 150 kDa), β(approximately 52 kDa), δ(approximately 17–25 kDa), and γ(approximately 32 kDa), in an approximately stoichiometric ratio (Takahashi et al., 1987, Tanabe et al., 1987, Zamponi et al., 2015).

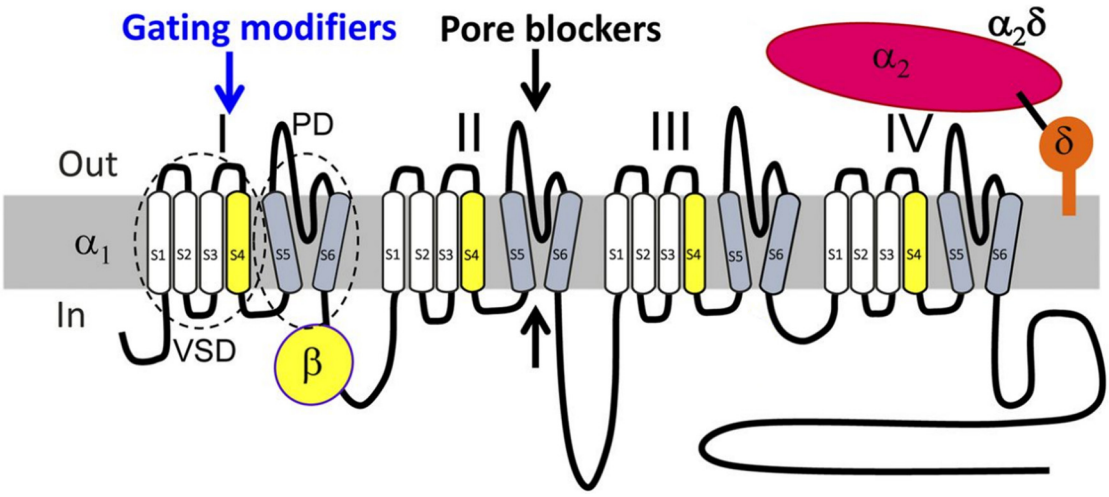

Figure 1.3: Voltage gated calcium channel subunit topology. α1 subunit consist of 4 protein domains (I-IV) each containing six transmembrane helices (S1-S6) which are connected with amino acid loops. I-IV domains are also connected with amino acid loops. Pore forming domain (PD) is between S5-S6 which is acted on by calcium channel blockers. S1-S4 act as voltage sensing domain (VSD). Length of line corresponds to length of polypeptide segment represented. Taken and modified from (Zamponi et al., 2015).

α1 subunits are associated with four auxiliary subunits: $\alpha_2\delta$ and β together with an additional γ subunit in skeletal muscle in all VGCCs except Cav3 channels (T-type) (Dolphin, 2016). β subunit is a cytoplasmic hydrophilic protein. Its structure is composed of an SH3 (Src homology-3) domain and a guanylate kinase domain. The guanylate kinase domain binds to an α-helical segment in the intracellular loop connecting domains I and II leaving the SH3 domain available for interaction with other binding partners (Catterall et al., 2013). $\alpha_2\delta$ is a membrane protein with extracellular N-terminal and hydrophobic C-terminus anchoring with glycosyl-phosphatidylinositol in the membrane. Although encoded by a single gene, $\alpha_2\delta$ molecules are post-translationally cleaved into α_2 and δ and disulfide bonded to yield mature $\alpha_2\delta$. These are present in calcium channels of skeletal muscles, heart and brain. The γ-subunit is present in cardiac and skeletal muscle along with the β subunit (Yang et al., 2011, Dolphin, 2018). Pharmacological and physiological diversity of Cav is provided by the α1 subunit only, whereas auxiliary subunits modulate the Cav. β subunit helps in surface expression of α subunit from endoplasmic membrane to the membrane. It also regulates activation and inactivation of α1 subunit. α2δ also plays a role in surface expression of α1 subunit along with influencing release probability, and linking calcium channel complex to non-calcium proteins. The function of the γ-subunit is not well defined (Dolphin, 2018, Mochida, 2018).

1.2.2 Distribution of R-type or Cav2.3 Ca^{2+} channels:

Cav2.3 channels are expressed ubiquitously in the brain with higher levels in the hippocampus, interpeduncular nucleus, striatum, pallidum, cortex, amygdala, olfactory tubercle, accumbens, and dorsal cochlear (Parajuli et al., 2012). They are predominantly presynaptic in interpeduncular nucleus whereas postsynaptic in other brain regions. Serial section analysis of electron microscopic images from the hippocampal CA1 revealed a higher density of immunogold particles

in the dendritic shaft plasma membrane compared with the pyramidal cell soma (Parajuli et al., 2012).

Six different splice variants of Cav2.3 are present differing in tissue distribution and pharmacological properties. Among 6 different splice variants (Cav2.3a, Cav2.3b, Cav2.3c, Cav2.3d, Cav2.3e and Cav2.3f), Cav2.3c and Cav2.3d are found in human brain; Cav2.3a, Cav2.3c and Cav2.3f are found in rat brain (Schramm et al., 1999, Schneider et al., 2013, Zamponi et al., 2015). Besides the central nervous system, different $Ca_V2.3$ splice variants are also present in endocrine cells, cardiomyocytes and kidneys (Weiergraber et al., 2000). Splice variant α1Ed like isoform is found in insulinoma cell lines INS-1 and β TC-3 in vitro, in cerebellum, and differentiated embryoid bodies of Bl/6 mouse. Splice variant α1Ee is found in kidney and pancreatic islets of Langerhans (Vajna et al., 1998, Pereverzev et al., 2002).

1.2.3 $Ca_V2.3$ pharmacology

In general, calcium channel blockers are divided into two main categories: molecules that physically occlude the channel pore (e.g., conotoxin and charybdotoxin) and those that prevent the channel opening via interactions with the voltage sensing domain (e.g., ω-agatoxin IVA, hanatoxin, ω-grammmotoxin SIA). SNX-482 falls under the latter group (Bourinet et al., 2001). Although its precise site of action on Cav2.3 channels is unknown, it appears to block domains III and IV of the channel as revealed by chimeras between Cav2.3 and Cav1.2 (Bourinet and Zamponi, 2017).

The peptide toxin SNX-482 from the tarantula, Hysterogrates gigas, was found to block the R-type Ca^{2+} currents in rat neurophypophyseal nerve terminals at low nanomolar concentrations, but not in several types of rat central neurons (Newcomb et al., 1998). Later on, it was found that SNX-482 dramatically reduces the A-type K+ current in acutely dissociated dopamine neurons from the mouse substantia nigra pars compacta with an IC50 of less than 3 nM (Kimm and Bean, 2014) Therefore, a highly selective antagonist of Cav2.3/R-type currents is not available yet but needed urgently (Schneider et al., 2018). It is not problematic to study the effect of SNX482 on $Ca_V2.3$ when potassium channels are blocked by toxins. But to study the role of $Ca_V2.3$ in cellular or physiological study in physiological condition could be problematic (Kimm and Bean, 2014).

Hysterogrates gigas secreted SNX482 does not exhibit unequivocal specificity for R-type channels, but highly effectively antagonizes their activation. This peptide also blocks Cav1.2

calcium channels when used higher than 200nM, though incompletely (Bourinet et al., 2001). Besides SNX, other blocker options have also been proposed for Cav2.3. ω-grammotoxin SIA, venom of the tarantula, *Grammostola spatulata*, also acts on $Ca_V2.3$, $Ca_V2.2$ and Cav2.3 channels in micromolar concentration (Turner et al., 1995, Bourinet and Zamponi, 2017). Its action is a reminiscent of ω-agatoxin IVA working as a gating modifier (McDonough et al., 1997). Calcicludine, a 60 amino acid peptide from green mamba *Dendroaspis angusticeps* venom, also blocks Cav2.3 along with other high voltage activated calcium channels in cerebellar granular cells. It shows highest affinity to L-type channels. In heterologous system, the order of blocking is Cav1.2, Cav2.1, Cav2.2 and Cav2.3 channels and the block is irreversible and incomplete at saturating concentrations (Schweitz et al., 1994, Stotz et al., 2000, Bourinet and Zamponi, 2017).

1.2.4 Properties of $Ca_V2.3$

Cav2.3 has been found to be important for neurotransmission in multiple brain areas. Ca_V2 family, of which $Ca_V2.3$ is a member, lies normally in presynaptic terminals as it acts as a driver of evoked synaptic transmission. These channels open to incoming action potentials (Westenbroek et al., 1992, Wheeler et al., 1994, Westenbroek et al., 1995, Zamponi et al., 2015). Mostly, $Ca_V2.1$ channels plays the major role in neurotransmitter release in neuromuscular junction and most synapses in central nervous system. $Ca_V2.2$ channels play a main role in synaptic transmission in autonomic nervous system and some synapses in central nervous system. $Ca_V2.3$ cannels also contribute to central synapses in CNS (Catterall et al., 2013). In CA3-CA1 hippocampal synapses, complete block of Cav2.1 and Cav2.2 by ω-conotoxin-MVIIC (ω-CTx-MVIIC) did not stop presynaptic calcium transient leading Wu and Saggau to suggest possible involvement of Cav2.3 or Cav3 (Wu and Saggau, 1995). Using SNX-482 and low concentration of NiCl2 as a blocker of Cav2.3, Gasparini et al. showed the involvement of Cav2.3 in presynaptic glutamatergic neurotransmission release in hippocampal mossy and associative commissural fiber synapses along with Cav2.1 and Cav2.2. About 15% of calcium influx in these synapses is contributed by Cav2.3 (Gasparini et al., 2001). CaV2.3 channels are present exclusively presynaptically in interpeduncular nucleus showing their unique property and signifying their importance in neurotransmitter release in MHb-IPN pathway (Parajuli et al., 2012). These Cav2.3 channels are conducting neurotransmitter release in MHb-IPN pathway. It is hypothesized that Cav2.3 modulation via Gβγ might be involved in the GBR-mediated increase of neurotransmitter (Zhang et al., 2016) release although there is currently no evidence for this.

Cav2.3 channels also regulate postsynaptic signals in hippocampus (Bloodgood and Sabatini, 2007). They are expressed in dendritic spine heads of CA1 pyramidal neurons suggesting that $Ca_V2.3$ channels get activated via neurotransmission-mediated postsynaptic depolarization when glutamate activate N-methyl-D-aspartate (NMDA) and α-amino-3-hydroxy-5-methyl-4-isoxazolepropionic acid (AMPA) receptors further activating different voltage sensitive channels like voltage gated sodium channels due to local depolarization. The Cav2.3-mediated Ca^{2+} signal, in turn, activates small conductance calcium-activated potassium (SK) channels which regulate synaptic signals by inhibiting NMDA receptors. Absence of synaptically evoked calcium accumulation outside of spines and $Ca_V2.3$ channels' property of activating SK channels suggest that feedback loop is present in active spine. This feedback loop requires substantial local swing in membrane potential and activation of voltage gated sodium channels, Cav2.3, SK channels, and NMDARs. (Bloodgood and Sabatini, 2007).

Presynaptic calcium influx through calcium channel plays various roles in synaptic transmission: involving in vesicle release for neurotransmitter release and short term plasticity (Neher and Sakaba, 2008). Most of the times, if not always, the calcium channels involved for presynaptic synaptic transmission are members of type two voltage gated calcium channels i.e. Cav2.1, Cav2.2 and Cav2.3 (Gasparini et al., 2001). Each Cav2 channels have distinct activity dependence for synaptic transmission. The contribution of Cav2.3 is disproportionately higher at intermediate frequencies (2-5 Hz), Cav2.1 and Ca2.2 are the major source of calcium influx at low frequency stimulation (>1 Hz), and Cav2.2 have a disproportionately reduced contribution to synaptic transmission at higher frequencies (>20 Hz) compared to Cav2.1. Cav2.3 channels' role at intermediate frequency could be due to disproportionate location of Cav2.3 outside active zone making them more important in setting the residual calcium levels (Ricoy and Frerking, 2014).

Cav2.3 is involved in mossy fiber long term potentiation (LTP) induction in which it starts presynaptically (Castillo et al., 1994) although it doesn't have a role in basal synaptic contribution. Cav2.1 and Cav2.2 are responsible for vesicle release during basal synaptic transmission while Ca^{2+} ions passing through Cav2.3 can access the key molecules for mossy fiber LTP, e.g., adenylyl cyclase I. With its absence, LTP still happens in mossy fiber but tetanus of stimuli is required as threshold for LTP increases (Breustedt et al., 2003). Dietrich et al. also showed that Cav2.3 channels accumulate Ca^{2+} in presynaptic terminal leading to presynaptic LTP and post-tetanic potentiation maintaining the low basal release probability that is a prerequisite for mossy fiber synapses plasticity (Dietrich et al., 2003).

R type current mediated by Cav2.3 channels show run up and run down (Almog and Korngreen, 2009). Decline of currents during run-down could be due to changes in voltage

dependence and it can be prevented or slowed down by provision of intracellular ATP through maintained protein phosphorylation and replicated by protein kinase inhibition. Current facilitation during run-up could be due to activation of leupeptin sensitive proteases that may influence the protective action of ATP (Neumaier et al., 2018). Run down in Cav2.1 and Cav2.2 has been linked to constitutive hydrolysis of membrane phosphoinositol phosphate (PIP_2) that can be prevented by ATP through lipid kinase mediated PIP_2 resynthesis (Gamper et al., 2004). Jeong et al. have suggested that depletion of plasma membrane PIP_2 or depletion of its precursor, phosphoinositol phosphate (PIP), affects the expression of Cav2.3 directly or indirectly (Jeong et al., 2016).

1.2.5 Function of $Ca_V2.3$

$Ca_V2.3$ has a functional role in seizure initiation and propagation as $Ca_V2.3$ KO mice do not exhibit spontaneous epileptiform discharges and display reduced pentylenetetrazol-seizure susceptibility (Weiergraber et al., 2006). Zaman et al have also shown the role of Cav2.3 channel in absence epilepsy as Cav2.3 is responsible for oscillatory burst discharge of signals in reticulothalamic nuclei in brain (Zaman et al., 2011). Topiramate, antiepileptic drug, also showed inhibition of cholinergic dependent plateau potentials, intrinsically generated conductance showing ictal-type seizure activity, blocking $Ca_V2.3$. This result also showed the role of $Ca_V2.3$ in epilepsy (Kuzmiski et al., 2005). $Ca_V2.3$ is necessary for spatial memory formation. It doesn't have a role in fear memory (Kubota et al., 2001). As $Ca_V2.3$ is involved in epilepsy and there is unexpected death among patients suffering from epilepsy, $Ca_V2.3$ may play a role in it. $Ca_V2.3$ is also engaged in development of human lungs (Schneider et al., 2015).

Gain of function variants of Cav2.3 gene, CACNA1E, was found to cause neurodevelopmental disorders and developmental and epileptic encephalopathies. Dramatic gain of function may cause increased calcium inward currents that may affect neuronal excitability and synaptic transmission. *CACNA1E*-encephalopathy phenotype included intense impairment with hypotonia and movement disorders (Helbig et al., 2019).

Single nucleotide polymorphism (SNP) of exon 20 in $Ca_V2.3$ gene (The Asp859Glu – rs35737760 SNP of the CACNA1E) was overexpressed in a patient suffering from basilar type migraine with complex neurological auras. This missense variant causes change from aspartate to glutamate at position 859 of Cav2.3 protein modulating its function. This could be the reason for migraine with complex neurological aura (Ambrosini et al., 2017).

$Ca_V2.3$ has a role in visceral inflammatory pain as shown with reduced response by $Ca_V2.3$ KO (Saegusa et al., 2000). It has a role in cancer pain as well. It acts as a target for pro-nociceptive

micro RNA, miR-R34c-5p in cancer pain playing anti-nociceptive role in peripheral sensory neurons (Gandla et al., 2017).

$Ca_V2.3$ channels have a role in sleep as $Ca_V2.3$ deficient mice showed reduced wake duration and increased slow wave sleep. 51% of the high-voltage gated calcium channel in reticulothalamic nuclei is Cav2.3. Cav2.3 channels are essential for rhythmic burst discharge of reticulothalamic neurons. In Cav2.3 deficient mice, oscillatory burst charge was suppressed and slow after hyperpolarization reduced. They regulate sleep architecture in thalamocortical loop and extra thalamocortical circuitries in brain (Siwek et al., 2014).

$Ca_V2.3$ is necessary for long-term leptin depolarization and excitation of hypothalamic pro-opiomelanocortin (POMC) neurons. Mouse with Cacna1e knockdown of POMC neuron had increased glucose production than normal. This shows that Cav2.3 plays an active role in normal glucose homeostasis (Smith et al., 2018).

1.3 GABAB receptor

Neuronal activity in central nervous system is maintained by interplay between synaptic excitation and inhibition (Gassmann and Bettler, 2012). Excitation is chiefly maintained by glutamate and inhibition is by γ-aminobutyric acid (GABA) and glycine. Glutamate acts on postsynaptic cation permeable AMPA receptors, kainite type receptors, and NMDA receptors. GABA, one of the main inhibitory neurotransmitters, acts chiefly on anion permeable post synaptic GABAA receptors. All these ionotropic receptors maintain fast conductance (<10ms). Glutamate and GABA also act on slow conducting (sub seconds to minute) metabotropic glutamate receptors and GBRs respectively. These are G-protein coupled receptors (GPCRs) which mediate a slow response via guanine nucleotide-binding protein (G protein) signaling. (Gassmann and Bettler, 2012, Pin and Bettler, 2016).

G protein coupled receptors (GPCRs) are the largest family of human membrane proteins acting as signaling proteins which are considered control panel of the cells (Lefkowitz, 2013). These molecules detect array of different chemical molecules present outside the cell and start intracellular signaling cascades. Transducing the extracellular signal to biochemical and genetic machineries intracellularly affect different responses like taste, vision, olfaction, vascular tone, muscular contraction, pain and behavior. GPCRs regulate virtually all physiological functions in human (Lefkowitz, 2013, Latorraca et al., 2017, Rajagopal and Shenoy, 2018). There are five different families of GPCRs in human genomes: rhodopsin (A), secretin (B), glutamate (C),

adhesion and frizzled families. GBR is in glutamate (C) family (Fredriksson et al., 2003). Structurally, core of GPCRS consist of extracellular N terminal, 7 membrane spanning αhelices and intracellular C terminal (Gurevich and Gurevich, 2019).

1.3.1 Structure of GBR

Metabotropic GBR was first discovered by Norman Bowery in 1979; it is a vital inhibitory neurotransmitter receptor found in both ends of synapses i.e. presynaptic and postsynaptic area throughout central nervous system (Bowery et al., 1980, Bowery et al., 1987). GBR is the first GPCR to be reported in which agonist and G protein coupling domain are located in two distinct subunits- GABAB1 (GB1) and GABAB2 (GB2). GB1 binds with agonist whereas GB2 activates G protein separately. Both subunits are necessary for GBR to be functional both in neurons and in heterologous expression systems (Duthey et al., 2002). GB1 and GB2 are heptahelical structures formed by 7 transmembrane helices with 3 intracellular and 3 extracellular loops connecting the helices. Inside end of the receptor activates G protein upon agonist activation of the receptor in the outside end in GPCR (Duthey et al., 2002). The extracellular domains of GB1 are further sub-divided into two types- GB1a and GB1b. Both GB1a and GB1b subunits are generated from GABBR1 gene. These proteins differ in GB1a having, two N-terminal protein interaction motifs of around 160 amino acids each, the sushi domains, though it doesn't provide unique kinetic or physiological difference to GB1a subunit while expressing in heterologous system (Figure 1.4) (Bettler et al., 2004, Blein et al., 2004). However, studies with KOs of GB1a and GB1b KO mice showed that absence of GB1a and GB1b differentially influence synaptic plasticity processes, network oscillations and behavior (Fritzius and Bettler, 2019).

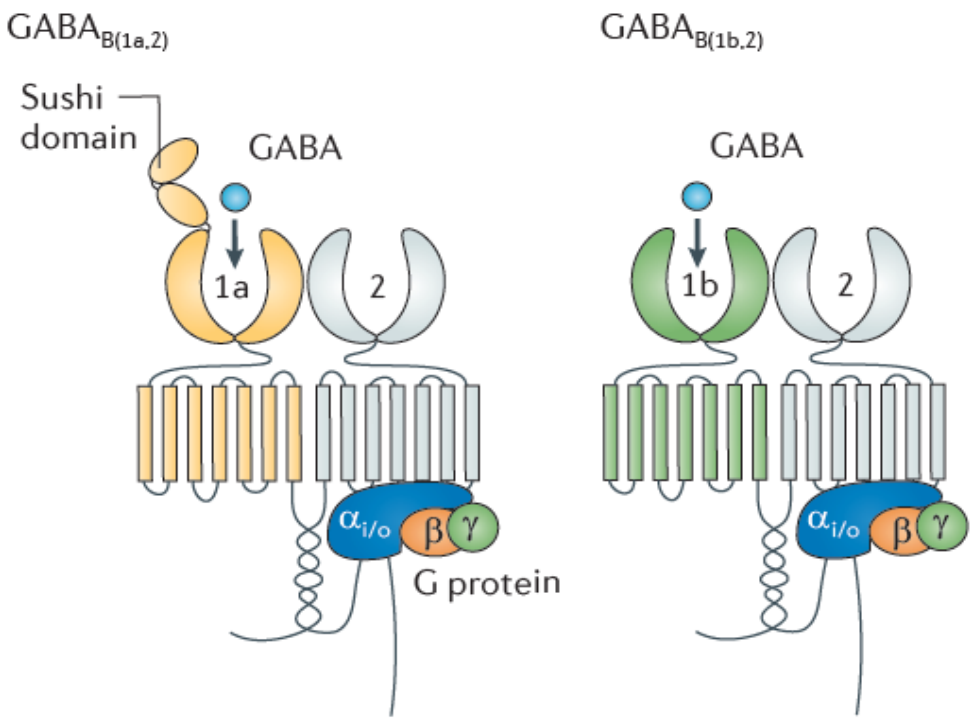

Figure 1.4: Principal subunits of GABAB receptor (GBR). GB1a, GB1b and GB2 have seven transmembrane domains of G protein-coupled receptors and form two distinct core units: GB1a,2 and GB1b,2. GB1a and GB1b are subunit isoforms that differ by presence of two amino-terminal sushi domains in GB1a. GB1a and GB1b contain GABA binding site while GB2 couple to G protein. Adapted from (Gassmann and Bettler, 2012).

GB1b is present in spine just opposite to excitatory release sites (Vigot et al., 2006).GB1a is present in somato-dendritc compartment and in axon terminals. Its transfer to axon terminal is assisted by the presence of sushi domain. They function as an important axonal targeting signal. When fused to CD8α, uniformly distributed transmembrane protein, sushi domain polarizes it to the axons. Similarly, sushi domain also directs the somatodendritic protein, mGluR1, to axons when fused proving its function in bringing GB1a to axon (Biermann et al., 2010). With proteomic study, Schwenk et al reported presence of interactor proteins of the sushi domains of GB1a such as α-amyloid precursor protein (APP), the adherence junction associated protein 1 (AJAP-1) and the PILRα associated neural protein (PIANP) (Schwenk et al., 2016). With the discovery of auxiliary subunits of GBR by Bettler group in 2010, GBR is found to have both principal and auxiliary subunits. GB1a, GB1b and GB2 act as principal subunit whereas potassium channel tetramerization domain containing proteins (KCTDs): KCTD8, KCTD12, KCTD12b and KCTD16

act as auxiliary subunits. KCTDs are cytoplasmic proteins (Schwenk et al., 2010, Metz et al., 2011).

1.3.2 Function of GABAB receptor (GBR)

GABA binds to the GB1 subunit which leads to a conformational change in the GB2 subunit and a subsequent exchange of GDP by GTP in the associated inhibitory G proteins $G\alpha_i\beta\gamma$. GBRs regulate VGCC or G-protein activated inwardly rectifying potassium (GIRK) channels. When agonist stimulates GBR, it activates heterotrimeric Gi/o-type G proteins, then Gαi from the activated G protein inhibits adenylyl cyclase enzyme inhibiting cAMP production. In presynaptic terminals, Gβγ subunit from the activated G protein can directly bind with VGCC reducing Ca^{2+} current (Couve et al., 2000) and also inhibits docking of vesicles. Moreover, the activated G proteins disrupt synaptic vesicle fusion by blocking SNARE (soluble *N*-ethylmaleimide-sensitive factor attachment protein (SNAP) receptor) proteins (Wells et al., 2012). Both inhibiting adenylyl cyclase activity and decreasing vesicle docking to active zone decrease neuro-transmitter release (Gassmann and Bettler, 2012). Thus, GBR generally shows inhibitory action in presynaptic terminals (Gassmann and Bettler, 2012). Usually GBRs are present at inhibitory and excitatory synapses as autoreceptor and heteroreceptor respectively. In autoreceptors, GABA acts directly to the GBR and inhibits further release of GABA. In heteroreceptor, spilled over GABA acts and inhibits glutamate release in neighboring excitatory synapse (Gassmann and Bettler, 2012). In postsynaptic compartments, GBRs cause inhibition mainly through activation of GIRKs via Gβγ. GIRK activation reduces neuronal excitability by shunting excitatory currents, and generating slow inhibitory postsynaptic potentials (IPSPs). It also inhibits back-propagating action potentials, which restrict synaptic plasticity processes and the generation of dendritic Ca^{2+} spikes (Xie et al., 2010). Dendritic Ca^{2+} spikes are also affected by Gβγ inhibiting VGCC (Simpson, 1988). GBR-mediated inhibition of adenylyl cyclase reduces protein kinase A (PKA) activity. Reduction of PKA activity by GBRs inhibits the Ca^{2+} permeability of NMDA-type glutamate receptors (NMDARs) (Chalifoux and Carter, 2010). Gene expression is also influenced by GBR-mediated PKA downregulation (Fukui et al., 2008).

Both pre- and postsynaptic GBRs downstream effectors are known to regulate the expression of long term potentiation (LTP), a form of synaptic plasticity that is implicated in learning and memory processes (Vigot et al., 2006). GBRs reduce the excitability of the postsynaptic neuron indirectly influencing LTP processes. LTP process is influenced by direct

inhibition of the Ca^{2+} permeability of NMDARs by postsynaptic GBRs via the cAMP-dependent PKA signaling pathway (Chalifoux and Carter, 2010, Gassmann and Bettler, 2012). Interestingly, GBRs have an important role in the control of spontaneous network activity that is fundamental for cognitive processes (Mann et al., 2009).

Contrary to the long held dogma that GBRs block Ca^{2+} channels and neurotransmitter release, recent report reported that activation of GBRs facilitates R-type mediated Ca^{2+} release in MHb projection in IPN (Zhang et al., 2016, Fritzius and Bettler, 2019). In heterologous system, GBRs conventionally inhibit R-type Ca^{2+} channel; it remains to be elucidated the mechanism behind the facilitation of R-type mediated Ca^{2+} release in MHb neurons (Fritzius and Bettler, 2019).

It is well-accepted fact that imbalance in excitation/inhibition in neuronal networks in brain causes many neurological and psychiatric illnesses. Too little inhibition can cause diseases like anxiety, depression, epilepsy, spasticity, sleep disorder and chronic pain. On the other hand, too much inhibition can also cause diseases like schizophrenia, and cognitive disorders (Kato and Witkin, 2018). Having modulatory role of GBRs in synaptic transmission and neuronal activity in most neurons, drugs have been designed targeting GBRs. Chiefly, two drugs are currently in use targeting GBRs. Baclofen is used to treat muscle rigidity and spasm associated with multiple sclerosis (Fritzius and Bettler, 2019). It is also used to treat alcoholism in France (Rolland et al., 2018). Moreover, it is used to treat muscle spasticity (Fritzius and Bettler, 2019). γ-hydroxybutyrate (GHB), GABA metabolite, is used to treat daytime sleepiness and reduce sudden attacks of weak/paralyzed muscles in narcoleptic patients (Bay et al., 2014).

1.3.3 KCTDs as auxiliary subunits of GBR

GBR responses in heterologous systems show different kinetics compared to native GBRs. This observation led Schwenk et al. to propose that there must be some regulator of G-protein signaling or phosphorylation or distinct subunit combination downstream. Proteomics, electron microscopy, immunohistochemistry, in situ hybridization and functional studies identified four KCTDs: KCTD8, KCTD12, KCTD12b and KCTD16 act as auxiliary subunit of GBR (Schwenk et al., 2010). This protein family comprises 26 members in humans which are divided into seven (A-G) subgroups. KCTD 8, 12, 12b and 16 are the sole members of group D. Homologous KCTD members in the same subgroups may share similar functional roles in proliferation, transcription, protein degradation, regulation of G-protein coupled receptors and other molecular or biological

processes (Liu et al., 2013). Interestingly, there is no human homologue of KCTD12b, even though the protein is present in many other species, including fish (Gamse et al., 2005). KCTDs have common structural motif, N-terminal tetramerization (T1) domain. The T1 domains contain a BTB motif (Zollman et al., 1994). Originally identified in *Drosophila melanogaster* zinc finger proteins, BTB (also called Poxviurs zinc finger, POZ) motifs are protein-protein interaction modules that mediate both self-association and interaction with non-BTB partners. KCTD proteins are soluble with N-terminal BTB domains (Stogios et al., 2005) and highly variable C-termini (Liu et al., 2013, Skoblov et al., 2013). Except within subgroups of closely related family members, KCTD proteins lack obvious sequence similarity in their highly variable C-terminal regions (Teng et al., 2019). T1 domain's function in voltage-gated K^+ channels is to assemble four subunits around a central channel pore. Crystal structure analysis of T1 domain of Shaker potassium channel revealed that four identical subunit structures are arranged in four fold symmetry (tetramerization) around centrally located pore of 20 A° in length (Kreusch et al., 1998). In contrast, a recent study showed that the T1 domains in KCTDs assemble into a homo-pentameric ring that tightly binds to the C terminal domain of GB2 while the H1 domains of KCTD bind a total of 5 Gβγ subunits (Figure 1.5) (Zheng et al., 2019). Thus, T1 domains of KCTD proteins are structurally and functionally distinct from T1 domains of voltage gated K+ channel proteins (Kv proteins), making KCTD sound more like a misnomer (Ji et al., 2016). Tyr 902 in the C terminal domain of GB2 is required for binding to the T1 domains of KCTD. Besides T1 domains, KCTDs have sequence related H1 homology domains, with KCTD8 and KCTD16 also having sequence related H2 homology domains. H1 and H2 domains are not sequence related to each other (Schwenk et al., 2010, Gassmann and Bettler, 2012). C terminal GB2 binding domain is absent in invertebrates and hence KCTDs are not accessory subunits of GBRs in them even though they do have KCTDs (Seddik et al., 2012). Depending on the type of KCTD protein with specific homology domain expressed, they are either involved in desensitization (KCTD12 or 12b) or inhibition of desensitization of the GB2 receptor (KCTD8 and KCTD16). A particular sequence motif, T/NFLEQ, in H1 domains in KCTD12 and -12b mediate desensitization. This sequence motif is absent in H1 domains of KCTD8 and -16. Moreover, the H2 domains in KCTD8 and -16 inhibit desensitization when expressed in C-terminal to the H1 domains but not when expressed as a separate protein in *trans* (Seddik et al., 2012).

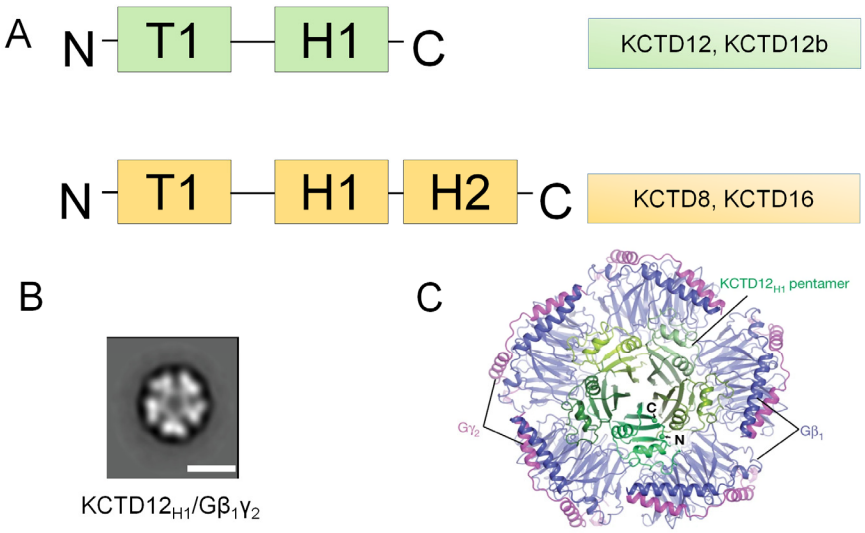

Figure 1.5: Potassium channel tertramerization domain containing protein (KCTD) topology. A Schematic diagram of KCTD with a conserved tetramerization T1 domain and carboxy-terminal homology domains (H1 and H2). B view of negative-stain electron-microscopy two-dimensional class averages for $KCTD12_{H1}$-$G_{\beta\gamma}$ complex pentameric structure. Scale bar, 10 nm. C Crystal structure of KCTD12H1 pentamer in complex with five copies of $G_{\beta1\gamma2}$ heterodimer. Adapted and modified from (Gassmann and Bettler, 2012, Zheng et al., 2019).

1.3.4 Expression of KCTDs in medial habenula

KCTD8, 12, 12b and 16 transcripts are expressed in various parts of mouse brain. GB1a, GB1b and GB2 are expressed in various parts of brain with highest expression in cortex, thalamus including habenula, cerebellum and hippocampus (Metz et al., 2011). So is true for transcripts of KCTDs (accessory subunit ones) as well. In some parts of brain, they are expressed alone whereas in others, they are together. KCTD12 and KCTD16 are the most abundant types in different neuronal populations of brain (Metz et al., 2011). They are expressed together strongly in dentate gyrus granule cells layer, pyramidal layer of hippocampus. Their expression is strong in entorhinal complex as well. Thalamus has strong expression of both of these molecules but KCTD16 is absent in medial habenula. In brain areas like cerebellum, their expression is rich. Besides these two molecules, KCTD8 molecule shows by far the strongest expression in medial habenula and weak expression in olfactory bulb, cerebellar granule cells, brainstem. On the other

hand, KCTD12b is present exclusively in the medial-habenula, only concentrated in ventral part. KCTD12 is weakly present in medial habenula and KCTD16 is absolutely absent there. In general, areas where GBR expression is strong e.g. medial habenula have strong expression of different KCTD molecules like 8, 12 and 12b. And, in others, single type of KCTD molecules are present incorporating with GBR (Metz et al., 2011).

Generally assumed to function as homo-oligomers, KCTDs also assemble as hetero-oligomers in all possible combinations. And these hetero oligomers form pentamers and directly interact with GABAB receptor and the G protein modulating physiologically induced K^+ and Ca^{2+} current responses in the brain. Two thirds of the KCTD16 in adult mice hippocampus form hetero-oligomer with KCTD12 and the hetero-oligomer prolongs duration of slow IPSCs in pyramidal cells (Fritzius et al., 2017). Activity-dependent binding of KCTD to Gβγ is unique to KCTD12 and 12b which results in desensitization: constitutive binding provides stabilization of the G protein at the receptor whereas dynamic binding with Gβγ gives desensitization by uncoupling Gβγ from effector K^+ or Ca^{2+} channel. While receptor-free KCTD12 desensitizes K^+ currents activated by other GPCRs in vitro, native KCTD12 is exclusively associated with GBRs. Accordingly, genetic ablation of KCTD12 specifically alters GBR responses in the brain showing that GBRs are provided with fast and reversible desensitization by harnessing KCTD12 that intercepts Gβγ signaling (Turecek et al., 2014).

Several KCTD family members are expressed in neuronal development during the embryonic stage (Gharbi et al., 2012). For example, reduced expression of KCTD11 is associated with pediatric mellanoblastoma (Di Marcotullio et al., 2004, Zawlik et al., 2006), KCTD7 mutation is associated with neurodegeneration and progressive myoclonic epilepsy (Van Bogaert et al., 2006). These are also involved in diseases like chronic tinnitus (KCTD12), HDL cholesterol concentration (KCTD10), abnormal head size (KCTD13), progressive myoclonic epilepsy (KCTD7), and medulloblastoma (KCTD11, KCTD21, KCTD6) (Liu et al., 2013). Interestingly, variations in the KCTD8 gene correlate with brain size and detrimental effects of prenatal nicotine exposure on neuronal development may partly be mediated via KCTD8 (Paus et al., 2012).

GBR is reported to be involved in synaptic inhibition in most of the brain regions like cerebellum, hippocampus, cortex, and thalamus. Interestingly, it has excitatory role in medial habenula to IPN pathway (Zhang et al., 2016). And medial habenula has strong expression of KCTD12, KCTD12b and KCTD8, with the latter two being basically absent in the rest of the brain. In fact, KCTD12b is expressed exclusively in ventral medial habenula in brain, whereas KCTD8 is expressed strongly throughout medial habenula (Metz et al., 2011). As only Cav2.3 is present at presynaptic terminal in this pathway, KCTD8 and KCTD12b, the auxiliary subunits of GBR, may

be involved in modulation of Cav2.3 for neurotransmitter release in this pathway. Thus to study the functional role of these molecules in the MHb-IPN pathway, morphological, biochemical and functional/electrophysiological study was designed.

1.4 Aim of this project

1. To study the localization and function of Cav2.3, GABAB receptor and its auxiliary subunits KCTDs in MHb to IPN pathway.

2. To study the involvement of KCTD subunits in facilitation of Cav2.3-mediated release by GABAB receptor activation in MHb to IPN pathway.

2 Chapter Two

METHODS

2.1 Animals:

Experiments on genetically modified mice were performed in strict accordance with institutional, national, and European guidelines for animal experimentation and were approved by the Bundesministerium für Wissenschaft, Forschung und Wirtschaft of Austria (Animal license number: BMWFW-66.018/0012-WF/V/3b/2016). We used the following mouse strains: wild type (WT, C57Bl/6J, Jax #000664 and, where noted, BALB/c, Jax #000651), Cav2.3 KO (background: C57Bl/6, 129/Sv), KCTD8 KO (background: mixed C57Bl/6J, 129), KCTD12 KO (background: mixed C57Bl/6J, 129) and KCTD12b KO (background: BALB/c), offspring of Tac1- Cre (Jax # 021877; background: mixed C57Bl/6J, 129) x Ai32 (Jax #024109; background: C57Bl/6J) crossings, termed Tac1-ChR2. All animal experiments were done strictly in accordance with institutional, Austrian and European regulations. All KCTD KO strains were generated in the lab of Bernhardt Bettler (University of Basel, Switzerland). Only male mice were used at the age of 8 – 16 weeks. The mice were housed and bred at the animal facility at IST Austria on 12h light/dark cycle with access to food and water ad libitum.

2.2 Transcardial perfusion for brain fixation:

Mice were anaesthesized with ketamine (90 mg/kg) xylazine (4.5 mg/kg) solution intraperitoneally. After 5-10 minutes, mouse was fully anesthetized which was confirmed by toe-pinch reflex test. Once there were no responses to pinching the toe, the diaphragm was opened and the heart was exposed. The right atrium was cut open with scissors and 25 mM ice cold phosphate buffer saline (PBS) was transcardially perfused to left ventricle via 27 G needle with a perfusion pump to flush blood from the circulatory system at flow rate of 7 ml/min. Once the liver turned pale, the mouse was transcardially perfused with paraformaldehyde solution (PFA) solution for 12 minutes. PFA solutions of different concentrations were used for confocal imaging [4% PFA (TAAB) and 15% picric acid in 0.1 M phosphate buffer, PB], pre-embedding [4% PFA and 15% picric acid in 0.1

M PB+0.05% glutaraldehyde(TAAB)] and SDS-digested freeze-fracture replica labeling (SDS-FRL, 2% PFA and 15% picric acid in 0.1M PB). The pH of all PFA solutions was adjusted to 7.4±0.05 with HCl. After perfusion, the mouse brain was removed from the skull and placed in 0.1 M phosphate buffer (PB) and slices were prepared within 3 days. Slices of different thickness (50 µm for confocal microscopy and pre-embedding, 130 µm or 70 µm slices for SDS-FRL replica) were cut with a vibrotome (Linear-Pro7, Dosaka) in ice-cold 0.1M PB.

2.3 Immunohistochemistry for light microscopy

Slices were washed once in 0.1 M PB for 10 minutes and three times in 50 mM PBS for 10 minutes followed by blocking in immersion buffer (10% normal goat serum (NGS), 2% bovine serum albumin (BSA), 0.5% Triton-X in 50 mM PBS) for 1 hour followed by incubation with primary antibody in immersion buffer for overnight (O/N) at 4°C. Concentration of primary antibodies was 1 µg/ml:anti-Cav2.3 (Genovac), anti-GABAB1 (Kulik et al., 2002), anti-KCTD8 (Bettler Lab, Univ. of Basel), anti-KCTD12 (Bettler Lab, Univ. of Basel) and anti-KCTD12b (Bettler Lab, Univ. of Basel) (Schwenk et al., 2010, Metz et al., 2011). Slices were washed in PBS 3 times (10 minutes each) and incubated in secondary antibody solution [1:500, Alexa-488 anti-guinea pig (Molecular Probe), Alexa-488 anti-rabbit (Molecular Probe)] in the dark for one hour at RT. Slices were washed in PBS for 10 minutes (3 times) and mounted onto glass slides with Mowiol (Sigma Aldrich) as a mounting media and left to dry O/N at RT in the dark. Once dry, slides were stored at 4 °C. The mounted slices were observed in LSM 800 (Zeiss) inverted confocal microscope.

2.4 Co-immunoprecipitation

Plasmids encoding N-terminally Flag-tagged KCTDs were described earlier (Seddik et al., 2012). Plasmids expressing Cav2.3 Flag-tagged in C-terminal were obtained from GenScript. Cultured human embryonic kidney 293 (HEK293) cells were transfected using 2 µg/µl polyethylenimine (Sigma-Aldrich) with above mentioned plasmids for the expression of either Flag-KCTDs alone or in combination with Flag-Cav2.3. HEK293 cells were washed 48 h after transfection in ice cold PBS and lysed in NETN buffer (100 mM NaCl, 1 mM EDTA, 0.5% Nonidet P-40, 20 mM Tris-HCl, pH 7.4, supplemented with complete EDTA-free protease inhibitor mixture (Roche)), followed by rotation for 10 min at 4 °C. Cell lysates were then cleared by centrifugation at 10,000 × g (4 °C, 10 min) and directly used for immunoblot analysis (Input) or for co-immunoprecipitation assay, in

which they were precleared for 1 h using 30 µL (dry volume) of a 1:1 mixture of protein-A and protein-G-agarose beads (GE Healthcare). Thereafter, lysates were incubated by rotating for 16 h at 4 °C in the presence of 2.5 µl of 0.3 µg/µl anti-Cav2.3 (CACNA1E) antibody (ACC-006, Alomone Labs). The next day, 10 µL (dry volume) of a 1:1 mixture of protein-A and protein-G-agarose beads were added and incubated by rotating for 40 min at 4 °C. Afterward, they were washed with 5 × 1 mL of NETN buffer and pulled down proteins were eluted with 25 µL of 4 × sample loading buffer containing 200 mM DTT. Proteins were resolved using standard one-dimensional SDS-PAGE on 10% polyacrylamide gels (for 45 min at 70 mV, followed by an additional 1.5 h at 120 mV). For immunoblotting analysis, proteins were transferred to 0.45 µM polivinylidene fluoride membranes (Milipore) for 2 h at 200 mA and probed with the primary antibodies rabbit anti-Flag (F7425, Sigma) and anti-Cav2.3 (ACC-006, Alomone Labs) in combination with peroxidase-coupled secondary donkey anti-rabbit antibodies (NA934, GE Healthcare, 1:10000).

2.5 Pre-embedding immunolabeling:

Mice were perfused with 4% PFA and 15% picric acid solution in 0.1 M PB along with 0.05% glutaraldehyde (TAAB). 50 µ slices were cut with vibrotome (Linear-Pro7, Dosaka) in ice cold PB (0.1 M). Brain slices were washed in 0.1 M PB for 10 minutes (2 times). Cryo-protection was done with 5 % sucrose solution in 0.1M PB for 20 minutes followed by 10% sucrose solution in 0.1 M PB for half an hour at RT. Finally, slices were kept in 20% sucrose solution for ON at 4 °C. It was followed by freeze thawing. Cryo-protected slices were spread in 6 well plate removing sucrose solution. Thereafter, the plate was kept on liquid nitrogen for a minute. Thawing was done by adding 20% sucrose solution in the sections and putting the plate on hot plate (50°C) for 2 minutes. Freeze thawing step was continued for two more times. Slices were washed in 0.1 M PB (10 min) followed by washing in TBS for 20 minutes (3 times). Free aldehyde quenching was done by washing slices in 50 mM glycine (Sigma Aldrich) in TBS for 10 minutes. After washing in TBS for 20 minutes (3 times), slices were blocked with BB (10% NGS, 2% BSA in TBS) for an hour. Primary antibody incubation was done with respective antibodies in 2% BSA solution for 2 overnights (ONs) at 4 °C. Concentration of antibodies used was 8 µg/ml for Cav2.3, 4 µg/ml for KCTD8, KCTD12 and KCTD12b and 2µg/ml for GABAB1. Afterward, slices were rinsed in TBS for 20 minutes (3 times). They were further incubated in respective secondary antibodies (1:100) for overnight at 4 °C in 2% BSA in TBS. For Cav2.3, 1.4 nm gold-conjugated anti guinea pig

antibody (Nanoprobes) and for all other antibodies, i.e. GABAB1, KCTD8, KCTD12 and KCTD12b, 1.4 nm gold-conjugated anti-rabbit antibody (Nanoprobes) was used. Washing was done with TBS for 20 minutes followed by PBS for 20 minutes (2 times). Post-fixation was done in 1 % glutaraldehyde in PBS for 10 minutes at RT. Slices were washed in PBS for 10 minutes (3 times) followed by quenching of free glutaraldehyde in 50 mM glycine in PBS for 10 minutes. After washing slices for 10 minutes (3 times) in PBS, they were washed in milli-Q (MQ) water for 5 minutes (3 times).

Silver intensification of immunogold particles followed next. Nanoprobes silver intensification (Nanoprobes) component A (initiator) and B (moderator) were mixed first by vortexing followed by component C (activator). After mixing well by vortexing, slices were incubated in the mixture solution for 9 minutes 15 second in the dark. Tubes were tapped every 2 minutes for uniform intensification. Slices were washed with MQ water for 10 minutes (3 times). Slices were washed in 0.1 M PB for 10 minutes and post fixation was done with 1% OsO_4 in 0.1 M PB to fix lipids and provide contrast to the sample. Before post fixing with OsO_4, slices were separated and straightened to avoid being oxidized/burnt in overlapped or folded condition. After osmification for 20 minutes in dark, slices were washed in 0.1M PB for 10 minutes followed by washing in MQ for 5 minutes (3 times). Counter-staining was done with 1% uranyl acetate (Al-labortechnik) in water in dark. After incubating for 35 minutes in 1% uranyl acetate in dark, slices were serial dehydrated in ethanol solution of different concentration in ascending order i.e 50%, 70%, 80%, 90%, 95%, to 100%. Slices were incubated for 5 minutes in each ethanol solution except for 100% ethanol which was for 10 minutes (twice). Slices were washed with propylene oxide (Sigma Aldrich) for 10 minutes (2 times) to let Durcupan resin (Sigma Aldrich) to enter easily inside the tissue. Slices were then put in Durcupan resin (mixture of components A, B, C and D in proportion of 10:10:0.3:0.3 respectively) for 1 O/N at RT.

Flat embedding of resin-infiltrated slices was done by putting each slice separately on a silicon-coated glass slide with a small amount of Durcupan resin. Thereafter, slices were covered with a ACLAR® fluoropolymer film as coverslip (Science Services); the slide was kept on oven at 37 °C for an hour. The slides were then transferred to oven at 60 °C for 2 ON for polymerization of resin and a lead weight block was placed on top of it. Re-embedding was done by trimming rostral or lateral IPN with a surgical blade, placing the IPN tissue into the lid of a plastic tube (TAAB) and filling the tube with Durcupan resin. The sample was incubated at 60 °C for 2 O/Ns to allow for resin polymerization.

Each resin block was trimmed using a Leica EM TRIM2 removing the resin surrounding the sample. The resin above the sample in the trimmed block was further cut at 200 nm

increments using a glass knife in the Ultramicrotome Leica EM UC7 until the sample was exposed. Once it was confirmed using a mirror of ultramicrotome that sample was exposed, 70 nm sections were cut with a diamond knife (Diatome Ultra 45 °). A small ribbon of floating sections was collected in the water-filled boat of the diamond knife and was mounted in copper-grid coated with formvar. Once the grid was dry, it was stored in a grid box for further observation in Tecnai10 (FEI; AV 80 KV) or Tecnai 12 (FEI; AV 120 KV) transmission electron microscopes.

For the analysis of pre-embedding immunolabeled ultrathin sections, the presynaptic active zone was manually demarcated based on rigid alignment of pre- and postsynaptic membranes and the presence of a postsynaptic density with the same length as the presynaptic active zone, as previously described (Rubio et al., 2017). Active zone length and silver-intensified gold particle densities and distances were measured using Reconstruct software. Synapses with more than two silver-intensified gold particles clumped together were excluded.

2.6 SDS-digested freeze-fracture replica labelling (SDS-FRL):

Brain slices were cryo-protected in graded glycerol concentration in PB. Slices were washed in 10% glycerol solution (Sigma Aldrich) in 0.1 M PB for 20 min at RT, 20% glycerol solution for 1 hour (RT) followed by 30% glycerol in 0.1 M for overnight at 4 °C. Whole interpeduncular nucleus (IPN) was manually excised with a surgical blade under a stereomicroscope and transferred to a clean gold/copper carrier (Wohlwend) which is double-sided taped (80 or 140 µm thickness) gently around the stage with a wet brush. The carrier was covered by the other clean carrier with its stage covering the sample lying inside the taped area. Pressure was applied to tape/glue two carriers together with sample inside. Gentle force was applied to carrier to stick the two carriers with sample in between. It was rapidly frozen by high-pressure freezing machine (HPM010, BAL-TEC, Balzers). The frozen sample was stored in liquid nitrogen until fractured. The frozen sample was fractured at -117°C by double replica method in a freeze-etching device (BAF060, BAL-TEC). The fractured sample was coated with a carbon layer (thickness: 5 nm evaporated at a 90 ° angle), followed by a platinum layer (thickness: 2 nm at a 60 ° angle) and another carbon layer (thickness: 15 nm from a 90 ° angle). The separated gold carriers containing the two halves of the fractured tissue were transferred into ceramic wells containing 50 mM Tris-buffered saline (TBS, pH 7.4). The undigested replica was subsequently mounted onto the center of a calibrated nickel grid (Science Services) with the replicated surface facing the grid. After removal of excess solution from the sample, the grid was placed atop a drop (<0.5 µl) of UV sensitive glue (Norland optical

adhesive 61) on a glass plate. The glue was cured with UV light (Nitecore, MTIU) for 20 s and the grid was then carefully scraped off the glass using a razor blade. The remaining tissue of the glued replica sample was digested in SDS solution (15 mM Tris·HCl, 20% sucrose, and 2.5% SDS in TBS, pH 8.3) for 48 hours at 60 °C and 12 – 15 h at 37 °C under constant agitation at 50 rpm.

SDS digested sample was washed in SDS solution in porcelain spot plate for 10 minutes. It was further washed in washing buffer, WB (50 mM TBS, 0.1%Tween-20, BSA 0.05%, NaN_3 0.05%, pH 7.4), and non-specific binding sites blocked with blocking buffer (BB) (5% BSA in WB) for 1 hour at RT. For double labelling experiment, first primary antibody (Cav2.3) was added in 30 µl droplet of 1% BSA in WB in plastic plate which was sealed with parafilm and humidity was maintained with wet tissue paper. The sample was incubated for 2 overnights (ONs) shaking (16 rpm) at 15°C. After washing in WB, it was again blocked with BB for 20 minutes. 5 nm gold-conjugated anti-guinea pig secondary antibody (1 µl in 30 µl blocking solution, British Biocell International, BBI) was added to the solution and was incubated at 15°C for 1 overnight. After washing the sample in porcelain spot plate for 10 min (3 times) with WB, it was blocked with BB for 1 hour. Next, the primary rabbit antibodies against either KCTD8, KCTD12b or GABAB1 (4 µg/ml for KCTDS, 2 ug/ml for GABAB1) or against the active zone (AZ) markers [mixture of anti-RIM ½ (140203, Synaptic system): 5 µg/ml, anti-Neurexin: 5µg/ml (Prof. Watanabe, Hokkaido Uni.), and anti-CAST (Prof. Ohtsuka, Uni. of Yamanashi): 3 µg/ml)] were added to each sample in 1% BSA in WB droplet (30µl) and were incubated for 2 O/Ns like above. After washing with WB and blocking non-specific sites with 5% BSA in WB (for 20 min), second secondary antibody (i.e. 2 or 10 nm gold-conjugated anti-rabbit antibody) was added (1 µl/30 µl blocking buffer) and incubated O/N at 15°C. On 7th day, sample was washed with WB for 10 minute once, with TBS for 10 minutes twice and with MilliQ water for 10 min. Thereafter, sample was picked up, dried and stored in grid box. Carbon coating was done with High Vacuum Coater Leica EM ACE600 depositing 20 nm thick carbon on sample. This protective carbon coat was applied to the replica-containing side of the grid to protect gold particles from the subsequently applied solvent and to prevent the replica from dissociating off the grid. Glue of grid glued replica was dissolved in a tube with 1 ml Dynasolve 711 solution at 60 °C (60 rpm). The replica was washed for 1.5 h followed by replacement with fresh Dynasolve solution and incubation for another 45 minutes. Thereafter, the grid was washed with 100% methanol for 10 minutes. It was followed by serial dilution of 100%, 95%, 90%, 70% and 50% ethanol for 5 minutes each. The grid (with replica) with dissolved glue was picked up, dried in air, and stored for observation in Tecnai10 (FEI; AV 80 KV) or Tecnai 12 (FEI; AV 120 KV) transmission electron microscopes. Images were acquired in Tecnai 12 at

110kx, 150kx magnification and in Tecnai 10 at 93kx magnification. Images were analyzed with GPDQ software (Lujan et al., 2018). Demarcation of presynaptic active zones was performed manually based on two morphological criteria: there had to be a visible alteration in surface curvature in the P-face and/or a concentration in intramembrane particles (IMPs) of variable sizes that appeared clearly different from those of the surrounding P-face. For density measurements, incomplete active zones were analyzed whenever there was a visible transition to the postsynaptic E-face that displayed the characteristic IMP clusters of a glutamatergic postsynapse (Tanaka et al., 2005). For confirmation, the complete active zone area demarcated based on protoplasmic surface depression and concentrated IMP cluster were compared with the area of complete postsynaptic E-face IMP clusters. In addition, the area of manually demarcated complete active zones were also compared with those demarcated using a mixture of active zone-marker antibodies (Neurexin C2, CAST II, and RIM1/2). To analyze clustering of molecules (Cav2.3, GABAB1, KCTD8, and KCTD12b), we performed 100 Monte Carlo simulations using GPDQ software (Lujan et al., 2018). For each simulation, the same number of particles was redistributed randomly, with each pixel having the same probability of becoming the center of a particle, on the demarcated area of interest under the condition that two particles could not be closer to each other than 10 nm. We then compared nearest neighbor distances (NNDs) between real particles with the NNDs of simulated particles using Kolmogorov-Smirnov test.

2.7 Brain slice preparation and electrophysiological measurements

Mice were anesthetized with a mixture of ketamine (90 mg/kg) and xylazine (4.5 mg/kg) and transcardially perfused with ice-cold, oxygenated (95% O_2, 5% CO_2) artificial cerebrospinal fluid (ACSF) containing (in mM): 118 NaCl, 2.5 KCl, 1.5 $MgSO_4$, 1 $CaCl_2$, 1.25 NaH_2PO_4, 10 Glucose, 30 NaH_2CO_3, (pH = 7.4). The brain was rapidly excised and coronal brain slices of 250 µm thickness were prepared with a Dosaka Linear-Pro7. Slices were recovered at 35 °C for 20 min and thereafter slowly cooled down to RT over the course of one hour. After recovery, one slice was transferred to the recording chamber (RC-26GLP, Warner Instruments) and superfused with the ACSF containing 2.5 mM $CaCl_2$, 20 µM bicuculline methiodide, 50 µM hexamethonium-bromide and 5 µM mecamylamine hydrocholride at a rate of 3-4 ml/min. Rostral or lateral IPN nuclei were visually identified using an infrared differential interference contrast video system in an Oympus BX51 microscope. Electrical signals were acquired at 10 – 50 kHz and filtered at 2 kHz using a HEKA EPC 10. Glass pipettes (BF150-86-10, Sutter Instrument) with resistances of

3-4 MΩ were crafted using a P97 horizontal pipette puller (Sutter Instrument) and filled with internal solution containing (in mM): 130 K-Gluconate, 10 KCl, 5 $MgCl_2$, 5 MgATP, 0.2 NaGTP, 0.5 EGTA, 5 HEPES; pH 7.4 adjusted with KOH. Whole-cell patch clamp recordings were performed at 29.5±2 °C in voltage-clamp mode at a holding potential of -60 mV and access resistance was constantly monitored via a -10 mV voltage step at the end of each sweep. Recordings with access resistances exceeding 20 MΩ or with changes in access resistance or holding current by more than 20% were discarded. To evoke glutamatergic excitatory postsynaptic currents (EPSCs) in rostral IPN neurons, voltage (0.5 – 3.5 V, 0.2 ms duration) was applied with an ISO-Flex stimulus isolator (AMPI) to a concentric bipolar stimulating electrode (CBBPC75, FHC) located inside the IPN, 150 – 200 µm distal to the recorded neuron. For optogenetic stimulation in Tac1-ChR2 mice, blue light (λ = 465 nm) was emitted directly onto the lateral IPN through a 5 mm long mono fiber-optic cannula (fiber diameter 200 µm, total diameter 230 µm, Doric lenses) connected to a PlexBright LED (Plexon) with an optical patch cable (fiber diameter 200 µm, total diameter 230 µm, 0.48 NA). The LED was triggered via 200 –ddd 290 mA current pulse (2 ms duration) from a LED Driver (LD-1, Plexon) which was controlled directly via the HEKA EPC10 amplifier. The sweep interval of all stimulation protocols (electrical and optogenetic) was 10s. For the application of SNX-482 (1 µM), 0.1% BSA was added to the ACSF. For variance mean analysis, ACSF with four different Ca^{2+} concentrations (1.5 – 8 mM) were applied to measure variance and mean EPSC amplitude at different release probabilities. To study the effect of $GABA_B$ receptors on EPSC amplitude, R(+)-Baclofen hydrochloride (1 µM) was used. Electrophysiology data were analyzed in python using a custom made script, Excel (Microsoft) and Prism (GraphPad).

2.8 Data analysis and statistics

All statistical tests and graph preparations were done using Prism (GraphPad) and figure assembly was done in Photoshop (Adobe) and Powerpoint (Microscoft). To determine whether to use parametric or non-parametric statistical tests, Shapiro-Wilk test for normality of residuals was applied. Unless otherwise noted, averaged data is presented as mean ± SEM, and P values < 0.05 were considered to indicate statistical significance.

3 Chapter Three

RESULTS

3.1 R-type mediated neurotransmission and differential effects of GABAB receptor activation at two distinct MHb – IPN pathways

The MHb to IPN pathway comprises two major projections (Figure 3.1A). The dorsal MHb projects to the lateral subnuclei of the IPN and releases glutamate and substance P whereas the ventral MHb projects to the rostral and central IPN subnuclei and co-releases glutamate and acetylcholine (Ren et al., 2011, Aizawa et al., 2012, Molas et al., 2017, Melani et al., 2019a). In confocal light microscopy, both the rostral/central regions as well as the lateral subnuclei show prominent Cav2.3 immunofluorescent signal (Figure 3.1B, C), in accordance with a previous study showing strong, exclusively presynaptic Cav2.3 signal in the IPN (Parajuli et al., 2012). To confirm R-type-dependent neurotransmission in both pathways, we performed whole-cell recordings from IPN neurons in acute brain slices and applied the selective Cav2.3 blocker SNX-482 (Newcomb et al., 1998; Zhang et al., 1993). In rostral and lateral IPN neurons, 1 µM SNX-482 strongly reduced the amplitude of excitatory postsynaptic currents (EPSCs) by 83% and 52%, respectively (Figure 3.2A, B). Similarly to Cav2.3, GBR also are present in all IPN subnuclei (Figure 3.1D, E). Rostral IPN neurons experience a strong increases in EPSC amplitudes following GABAB receptor activation with 1 µM baclofen (Figure 3.2C), whereas EPSC amplitudes were reduced by baclofen in lateral IPN neurons (Figure 3.2D). Therefore, the modulation of R-type mediated release via GABAB receptors appears fundamentally different between the two MHb-IPN pathways. This result suggests a comparison of presynaptic molecules between dorsal MHb terminals and ventral MHb terminals as a possible approach to better understand the modulation of neurotransmitter release by GBRs.

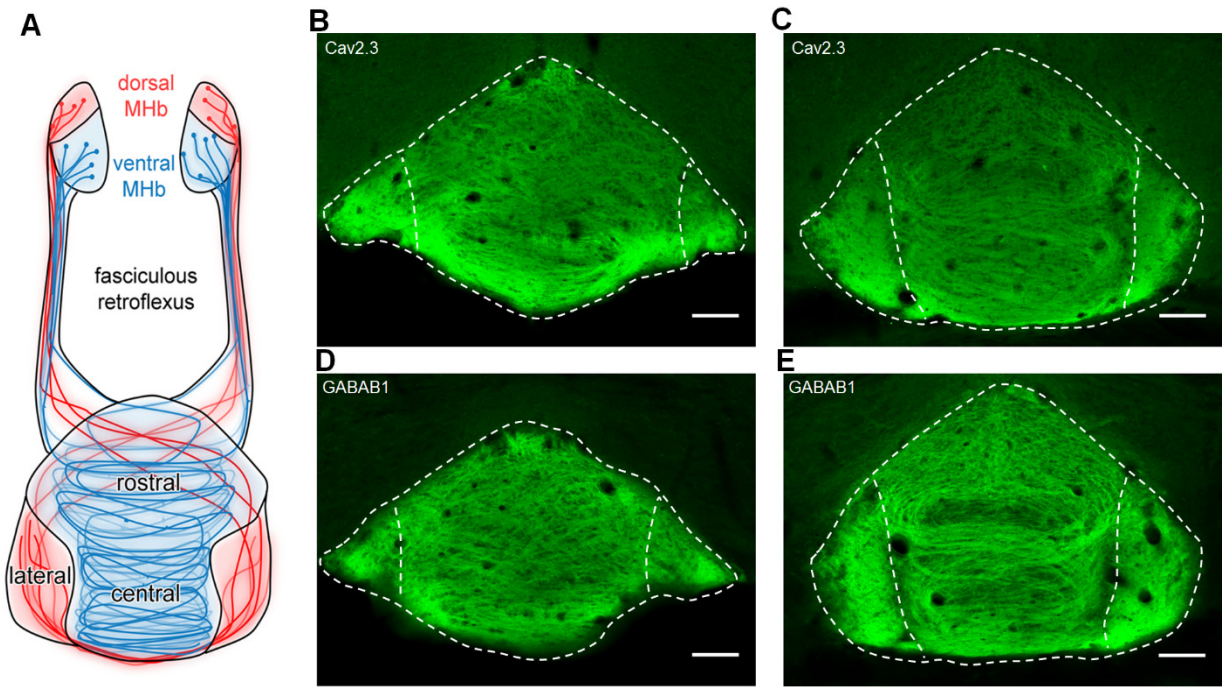

Figure 3.1: Expression of Cav2.3 and GABAB receptors at two parallel MHb-IPN pathways

A Schematic drawing of the two MHb-IPN pathways. In red: the dorsal part of the MHb projects to the lateral subnuclei of the IPN. In blue: the ventral part of the MHb projects to the rostral/central subnuclei of the IPN **B**, **C** Confocal image of Cav2.3 immunofluorescence signal indicates Cav2.3 presence in MHb axonal projections of both MHb-IPN pathways **D**, **E** Confocal image of GABAB1 immunofluorescence signal indicates the presence of GABAB receptors (GBRs) in all IPN subnuclei. Scale bars 100 µm.

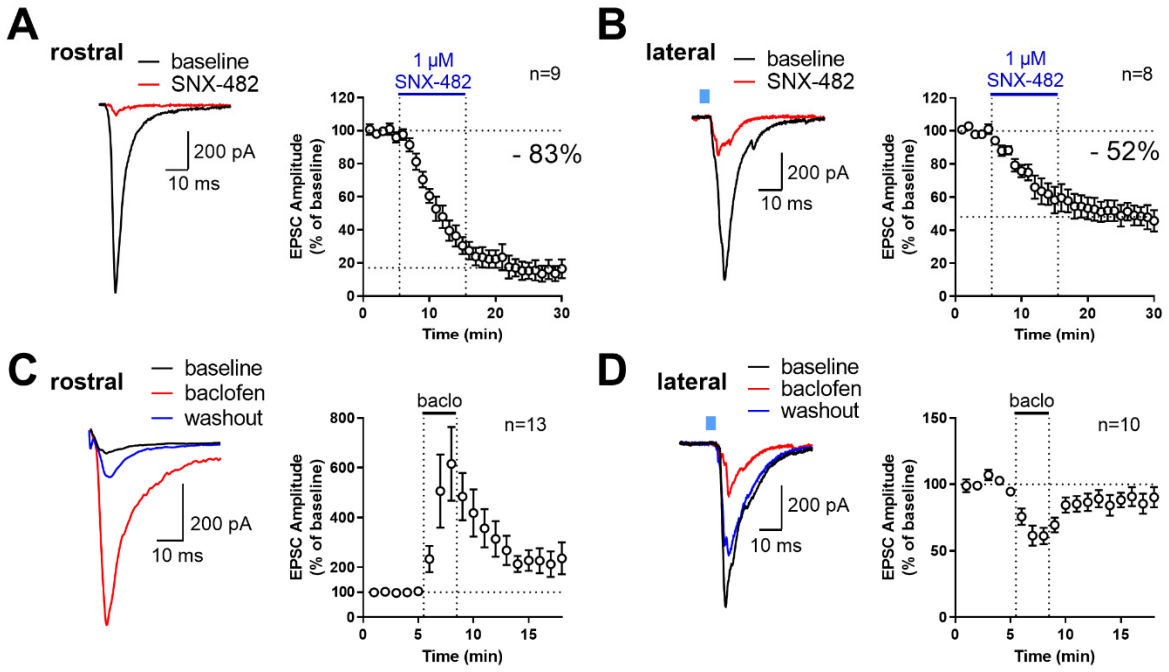

Figure 3.2: Function of Cav2.3 and GABAB receptors at two parallel MHb-IPN pathways

A Pharmacological inhibition of presynaptic Cav2.3 with SNX-482 in whole-cell recordings of rostral IPN neurons. Left: example traces before and after the application of SNX-482; middle: example time course of EPSC amplitude reduction by SNX-482; right: averaged time course of relative EPSC amplitude reduction by SNX-482. EPSC amplitudes were reduced by 83% on average. **B** In Tac1-ChR2-EYFP mice, SNX-482 reduced light-evoked glutamatergic EPSC amplitudes on average by 52%. **C** In whole-cell recordings of rostral IPN neurons, activation of GBRs by 1 µM baclofen produced a potentiation of electrically evoked EPSC amplitudes. Left: example EPSC traces before (black) and after the application of baclofen (red) and after washout of baclofen (blue); middle: example time course of EPSC amplitudes in one cell; right: averaged time course of relative EPSC amplitude change after baclofen **D** In contrast, GBR activation reduced the amplitude of light-evoked glutamatergic EPSCs in lateral IPN neurons. Averaged data I presented as mean ± SEM. (Fig. A from David Vandael, Jonas Lab; Fig. C-D from Peter Koppensteiner, Shigemoto Lab).

3.2 Differential presence of KCTDs in IPN subnuclei

In order to better understand the differential modulation of neurotransmitter release by GABAB receptors at the two MHb-IPN pathways, we investigated the expression of the auxiliary subunits of GABAB receptors, called K-channel tetramerization domain-containing (KCTD) proteins. We found widespread expression of KCTD8 in all IPN subnuclei, with habenular fiber path-like signal patterns in the rostral/central subnuclei (Figure 3.3A). Of note, KCTD8 is also expressed postsynaptically in the rostral and intermediate IPN subnuclei, according to the Allen Brain Atlas. In contrast, KCTD12 and KCTD12b were only present in the rostral and central but not the lateral IPN subnuclei (Figure 3.3B, C), suggesting their absence in the dorsal MHb-IPN pathway. While KCTD12 immunofluorescence patterns in the rostral region suggested mostly postsynaptic expression, KCTD12b signal showed the characteristic crisscross pattern of MHb fiber paths inside the rostral/central IPN, suggesting presynaptic expression. Antibody specificity for all KCTD antibodies was confirmed using the corresponding KO animals (Figure 3.3 A-C)

In a brain-wide proteomics study, presynaptic Ca^{2+} channels were found to be at the center of macromolecular complexes that also contained GABAB receptors and KCTDs (Muller et al., 2010). Furthermore, KCTDs were found to directly bind to N-type Ca^{2+} channels, even in the absence of GABAB receptors (Schwenk et al., 2016). To test whether the KCTDs expressed in the MHb-IPN pathway may interact with Cav2.3, we performed a co-immunoprecipitation experiment in HEK293 cells. Interestingly, we found selective binding of Cav2.3 to KCTD8 and KCTD12b, but not KCTD12 (Figure 3.4). These results suggest that KCTD8 and 12b in MHb-derived axons may directly interact with presynaptic Cav2.3, even in the absence of GABAB receptors.

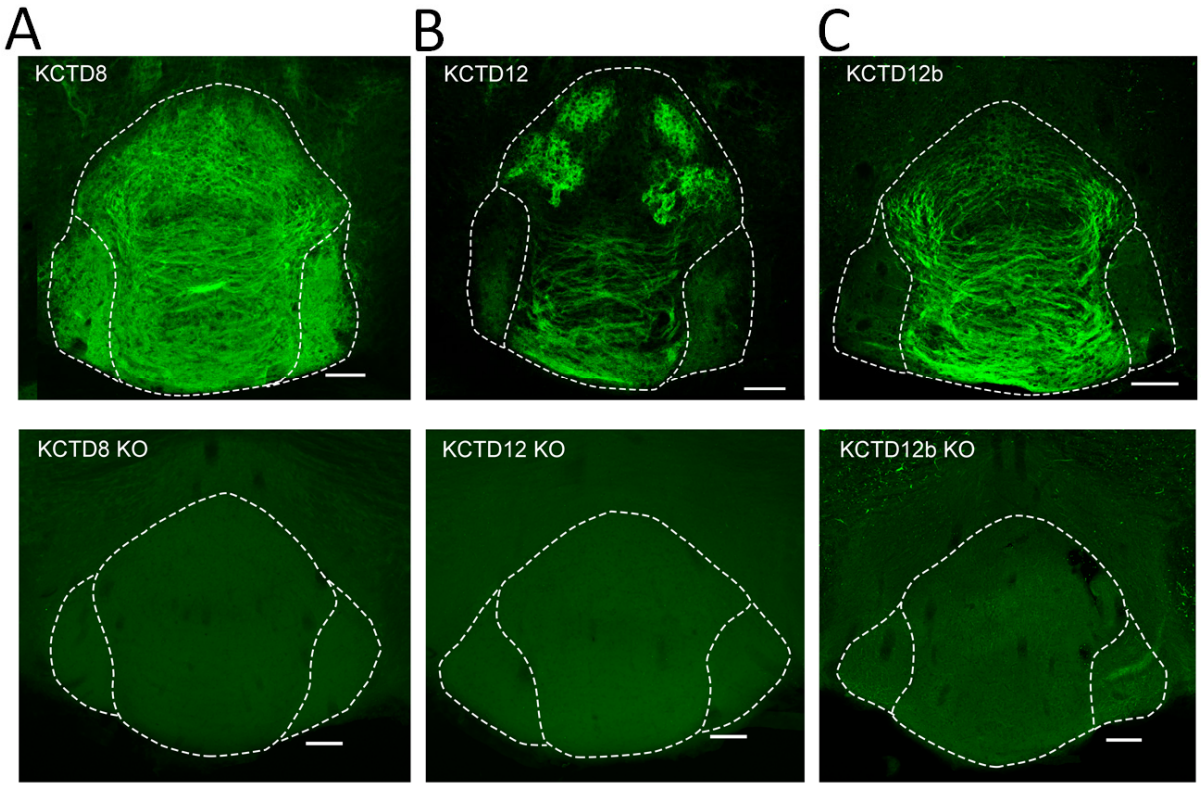

Figure 3.3: Presynaptic KCTDs in distinct IPN subnuclei

A – C: Confocal images of immunofluorescence signals of KCTD8, KCTD12 and KCTD12b in the IPN in WT (upper panels) and the respective KO mice (lower panels). KCTD8 immunofluorescence was present in all IPN subnuclei whereas KCTD12 and KCTD12b signal was observed only in the rostral/central but not the lateral IPN subnuclei. Scale bars: 100 µm

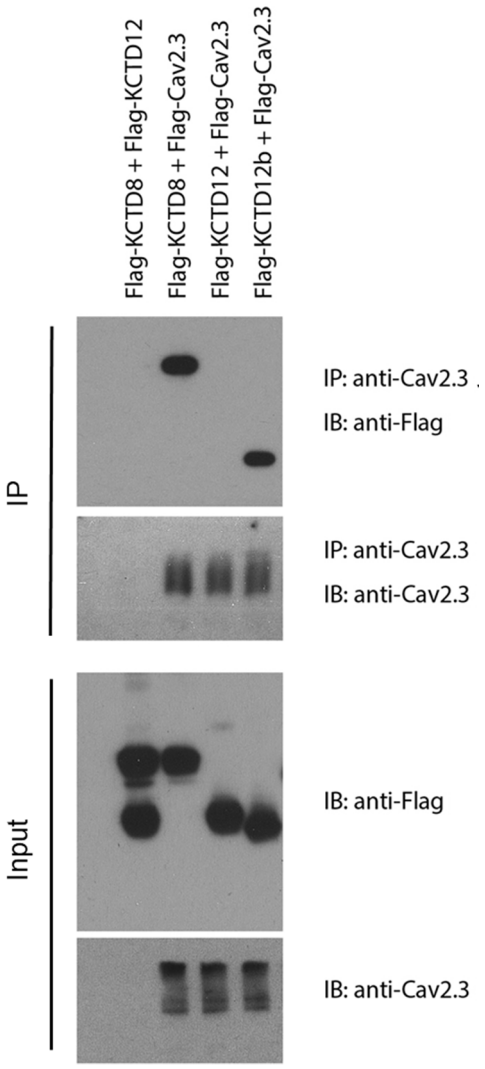

Fig 3.4: Interaction of KCTDs with Cav2.3 in vitro

Co-immunoprecipitation in HEK293 cells transfected with flag-tagged KCTDs and Cav2.3. Immunoprecipitation of Cav2.3 co-precipitated KCTD8 and KCTD12b, but not KCTD12. (From Bettler Lab).

3.3 Pre-embedding and SDS-FRL immunolabeling of presynaptic Cav2.3, GABAB1 and KCTDs in rostral and lateral IPN subnuclei

Next, we studied the sub-synaptic localization of Cav2.3, GABAB1 and KCTDs in ventral and dorsal MHb terminals. We performed pre-embedding immunolabeling and quantified the number

of silver-intensified gold particles in the AZ, the peri-synaptic region (0-50 nm distance from the AZ) and extra-synaptic regions (50-100, 100-150 and 150-200 nm distance from the AZ; Figure 3.5 to 3.10). In accordance with our immunohistochemical data (Figure 3.3B, C), KCTD12 and KCTD12b labeling was detected only in MHb terminals in the rostral but not the lateral IPN subnuclei (Figure 3.8D, 3.9B, 3.10D, E). In addition, KCTD12 labeling was mostly observed in postsynaptic elements (Figure 3.8C). In MHb terminals in the rostral IPN, Cav2.3 and KCTD12b showed similar localization patterns, with peak particle densities in the AZ and a gradual decrease in density with increased distance from the AZ (Figure 3.5, 3.10A, 3.9A, and 3.10E). Labelling for Cav2.1 and Cav2.2 was not detected in MHb terminals with pre-embedding immunolabelling tecnhinque (result not shown). In contrast, GABAB1, KCTD8 and KCTD12 showed peak localization in the perisynaptic region with lower particle densities inside the AZ in rostral and lateral IPN (Figure 3.6-3.8, 3.10B – D). These results suggest that KCTD12b dominates the AZ of ventral MHb terminals in the rostral IPN whereas KCTD8 dominates the AZ of dorsal MHb terminals in the lateral IPN (Figure 3.10F).

To circumvent potential antigen-masking due the protein-dense AZ region in conventional pre-embedding immunolabeling, we performed SDS-digested freeze-fracture replica labeling (SDS-FRL) (Fujimoto, 1995). This method enables unhindered access of antibodies to proteins inside/close to the pre- or postsynaptic membrane and allows for multiple gold-conjugated immunolabelings simultaneously (Tanaka et al., 2005, Indriati et al., 2013, Nakamura et al., 2015, Miki et al., 2017). In order to distinguish IPN subnuclei, we used an improved version of the grid-glued SDS-FRL method (Harada and Shigemoto, 2016) which facilitates the preservation of complete replicas during the handling procedures which is required for the identification of IPN subnuclei in the electron microscope (Figure 3.11A). We detected Cav2.3 on the P-face of the presynaptic AZ and confirmed antibody specificity using Cav2.3 KO mice (Figure 3.11B, C, F; average density WT: 147.8 ± 23.9, mean ± SEM, particles/μm², n=4 replicas; KO 3.4 ± 0.99 particles/μm², n=4 replicas; WT vs. KO: P = 0.0099, paired t-test). In addition, we confirmed that Cav2.3 was localized in the AZ using co-immunolabelings with a mixture of antibodies against the AZ proteins RIM1/2, Neurexin and CAST (Figure 3.11D). In the absence of AZ protein labeling, demarcation of the presynaptic AZ was based on multiple criteria, including P-face curvature and intramembrane particle (IMP) size and density. The area of AZs demarcated without AZ protein labeling ($AZ_{unmarked}$) was not significantly different from that of AZ-marker labeling ($AZ_{unmarked}$ n=46, AZ_{marked} n = 80; P = 0.8692, Kolmogorov-Smirnov test) or from the area of unlabeled postsynaptic IMP clusters on the E-face, the replica equivalent of the postsynaptic density (PSD) seen in

conventional ultrathin sections (PSD n = 68; P > 0.9999, Kolmogorov-Smirnov test), verify our morphological criteria of AZ.

The result of our pre-embedding immunolabeling suggested that Cav2.3 and other tested presynaptic molecules are localized in and around the AZ of MHb terminals (Figure 3.5-3.10). In order to confirm that these molecules are actually co-localized inside the same AZ, we performed double immunolabelings for Cav2.3 and either GABAB1, KCTD8 and KCTD12b in SDS-FRL (Figure 3.12). We omitted double labeling for Cav2.3 and KCTD12 because a) KCTD12 is unable to directly bind Cav2.3 (Figure 3.4), b) the signal for KCTD12 was found in small population of presynaptic terminals inside the rostral IPN (Figure 3.8, 3.10D) and c) KCTD12 appeared to be located rather post-synaptically in the rostral IPN (Figure 3.8C). We found that in ventral MHb terminals in the rostral IPN, Cav2.3 is co-localized with GABAB1, KCTD8 and KCTD12b in over 97% of all Cav2.3 positive synapses (Figure 3.12A and B upper panel, 3.13A; GABAB1: 98.81 ± 1.19%, n=2 animals; KCTD8: 98.06 ± 1.10%, n=3 animals; KCTD12b: 97.48 ± 1.8%, mean ± SEM, n=4 animals). The same labeling patterns were seen in dorsal MHb terminals located inside the lateral IPN, with the exception of an absence of KCTD12b (Figure 3.12A and B lower panel, 3.13A; GABAB1: 99.31 ± 0.69%, n=2; KCTD8: 97.16 ± 0.57%, n=3). Particle numbers and densities of all tested molecules except KCTD12b, which is absent in the lateral IPN, were comparable between ventral and dorsal MHb terminals in the rostral and the lateral IPN, respectively (Figure 3.13A). In addition, the nearest-neighbor distances (NND) of all tested molecules were significantly smaller than those obtained from simulations of randomly distributed particles (Figure 3.13B), suggesting that Cav2.3, GABAB1 and KCTDs are clustered inside the AZ.

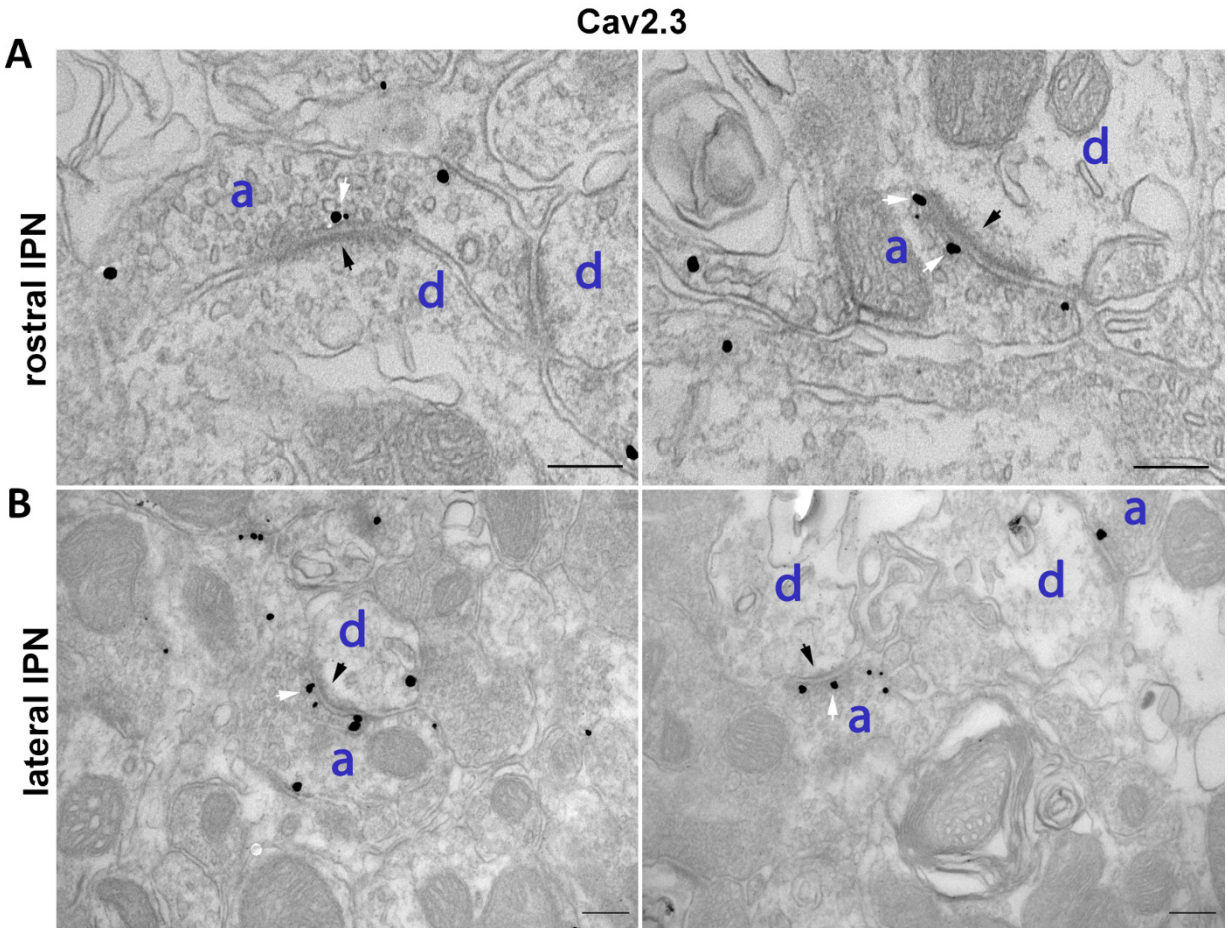

Figure 3.5: Sub-synaptic localization of Cav2.3 in presynaptic terminals in both MHb-IPN pathways

Transmission electron microscope images of 70 nm thick sections following pre-embedding immunolabeled slices for Cav2.3 from synapses in the rostral (**A**) and lateral (**B**) IPN subnuclei. Black arrows show post synaptic density (PSD); white arrows show silver enhanced gold particles for Cav2.3 in presynaptic terminal. a: axon terminal, d: dendrite. Scale bars: 200 nm.

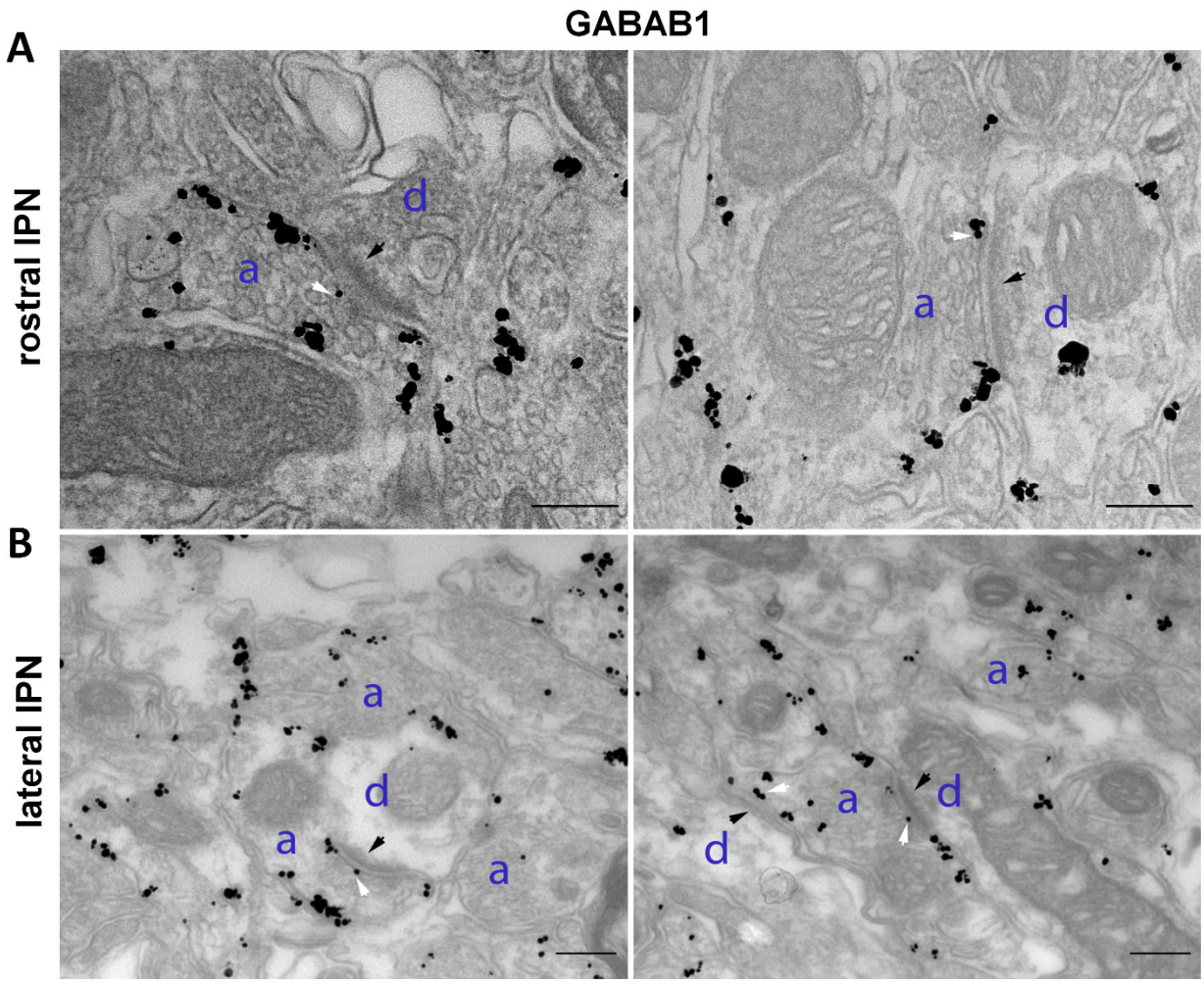

Figure 3.6: Sub-synaptic localization of GABAB1 in presynaptic terminals in both MHb-lPN pathways

Transmission electron microscope images of 70 nm thick sections following pre-embedding immunolabeled slices for GABAB1 from synapses in the rostral (**A**) and lateral (**B**) IPN subnuclei. Black arrows show post synaptic density (PSD); white arrows show silver enhanced gold particles for GABAB1 in presynaptic terminal. a: axon terminal, d: dendrite. Scale bars: 200 nm.

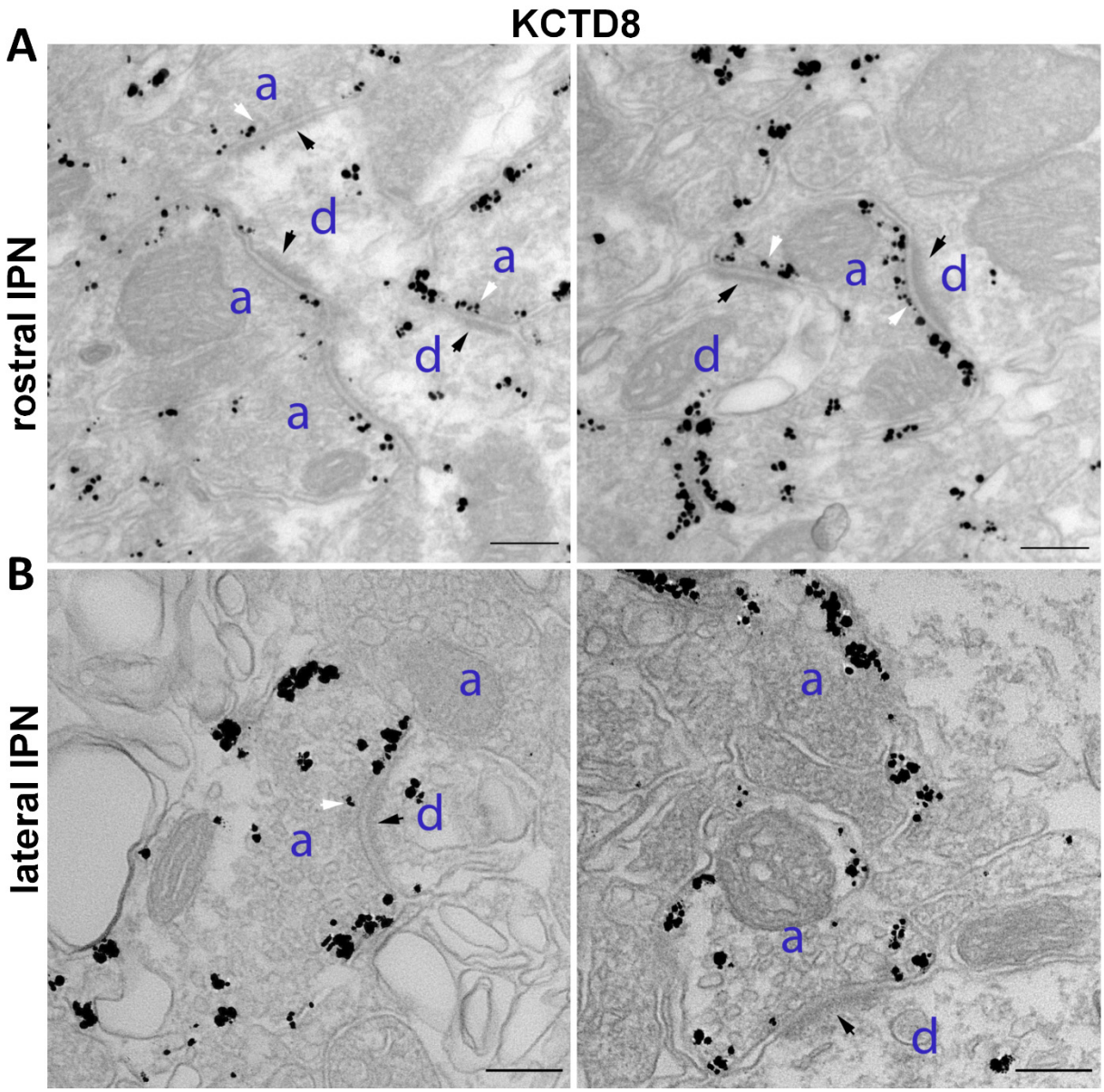

Figure 3.7: Sub-synaptic localization of KCTD8 in presynaptic terminals in both MHb-IPN pathways

Transmission electron microscope images of 70 nm thick sections following pre-embedding immunolabeled slices for KCTD8 from synapses in the rostral (**A**) and lateral (**B**) IPN subnuclei. Black arrows show post synaptic density (PSD); white arrows show silver enhanced gold particles for KCTD8 in presynaptic terminal. a: axon terminal, d: dendrite. Scale bars: 200 nm.

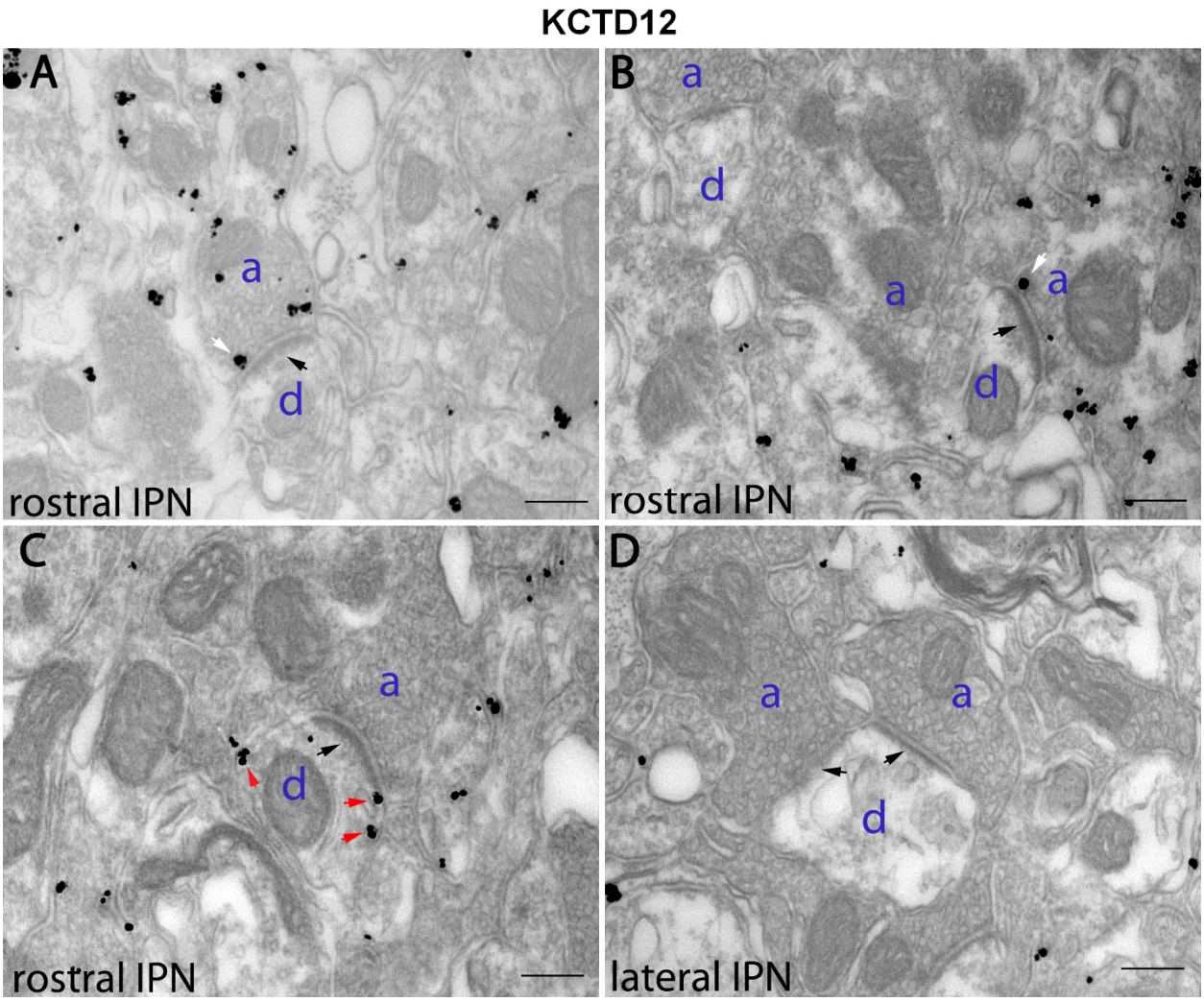

Figure 3.8: Sub-synaptic localization of KCTD12 in terminals in both MHb-IPN pathways

Transmission electron microscope images of 70 nm thick sections following pre-embedding immuneolabeled slices for KCTD12 from synapses in the rostral (**A, B and C**) and lateral (**D**) IPN subnuclei. Black arrows show PSD; white arrows show silver-enhanced gold particles for KCTD12 in presynaptic terminals; red arrows show KCTD12 localized along postsynaptic membrane. a: axon terminal, d: dendrite. Scale bars: 200 nm.

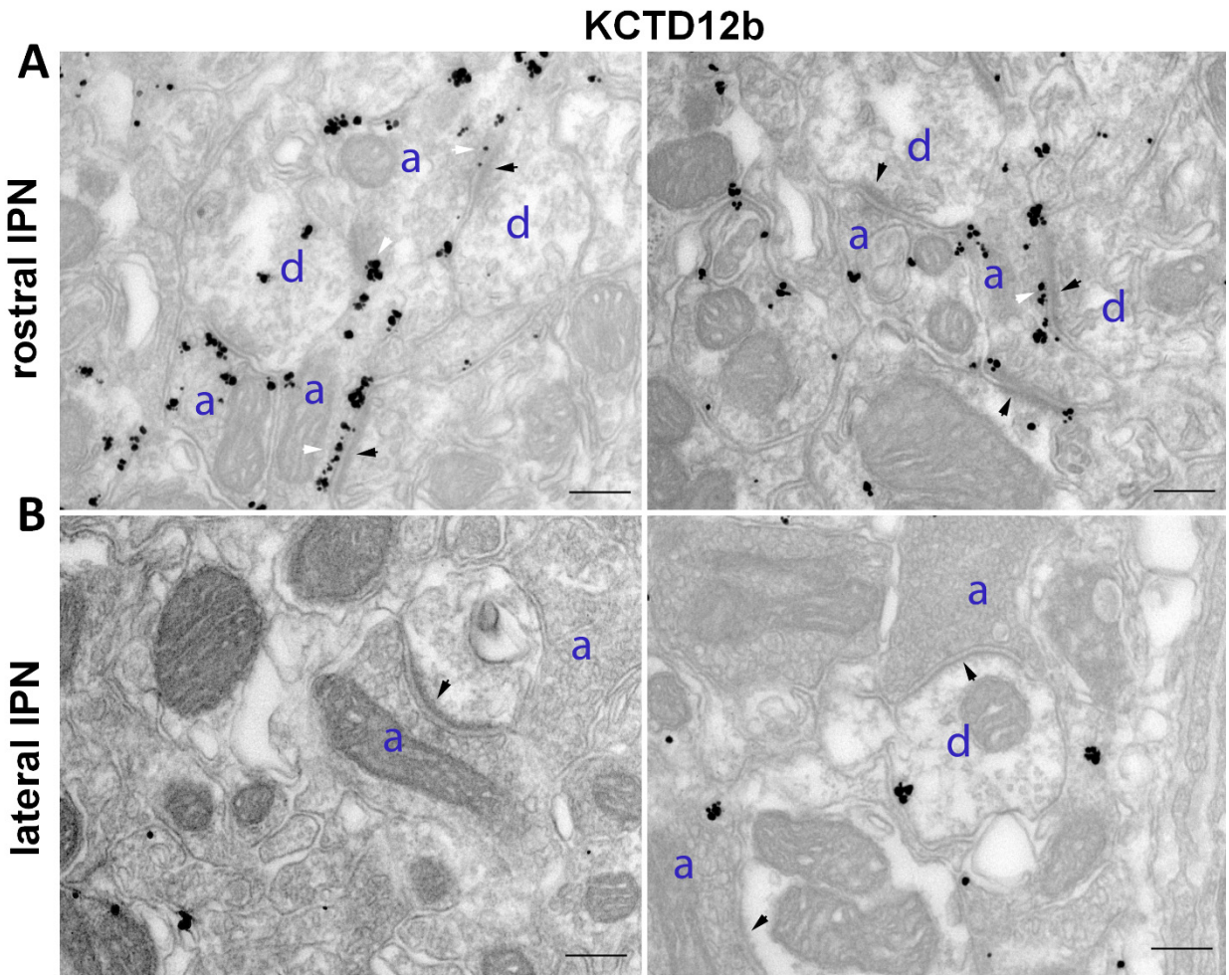

Figure 3.9: Sub-synaptic localization of KCTD12b in terminals in both MHb-IPN pathways

Transmission electron microscope images of 70 nm thick sections following pre-embedding immunolabeled slices for KCTD12b from synapses in the rostral (**A**) and lateral (**B**) IPN subnuclei. Black arrows show post synaptic density (PSD); white arrows show silver enhanced gold particles for KCTD12b in presynaptic terminal. a: axon terminal, d: dendrite. Scale bars: 200 nm.

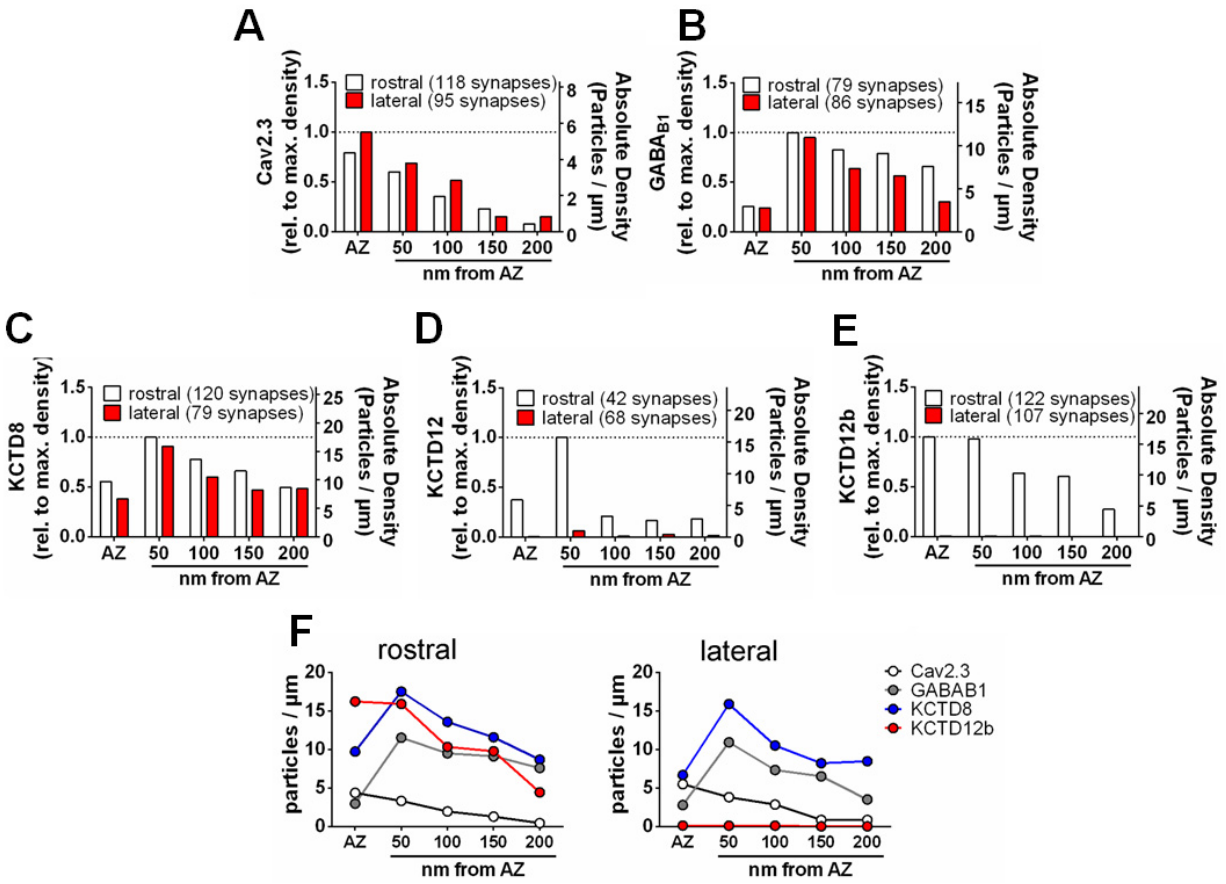

Figure 3.10: Quantitative analysis of sub-synaptic localization of presynaptic molecules along both MHb-IPN pathways

Bar graphs indicate relative and absolute silver-enhanced gold particle densities in the AZ and at distances of 50 – 200 nm from the AZ (50 nm bins) for Cav2.3 (**A**), GABAB1 (**B**), KCTD8 (**C**), KCTD12 (**D**) and KCTD12b (**E**). **F** Absolute labeling densities are summarized for synapses in the rostral (left panel) and lateral IPN (right panel). Note the absence of KCTD12 and KCTD12b particles in presynaptic terminals inside the lateral IPN subnuclei. KCTD12 was not included in panel F because of mostly postsynaptic localization inside the rostral IPN. Data was pooled from two animals following confirmation of same distribution patterns using Kolmogorov-Smirnov test (see also Figure 3.5 to 3.9).

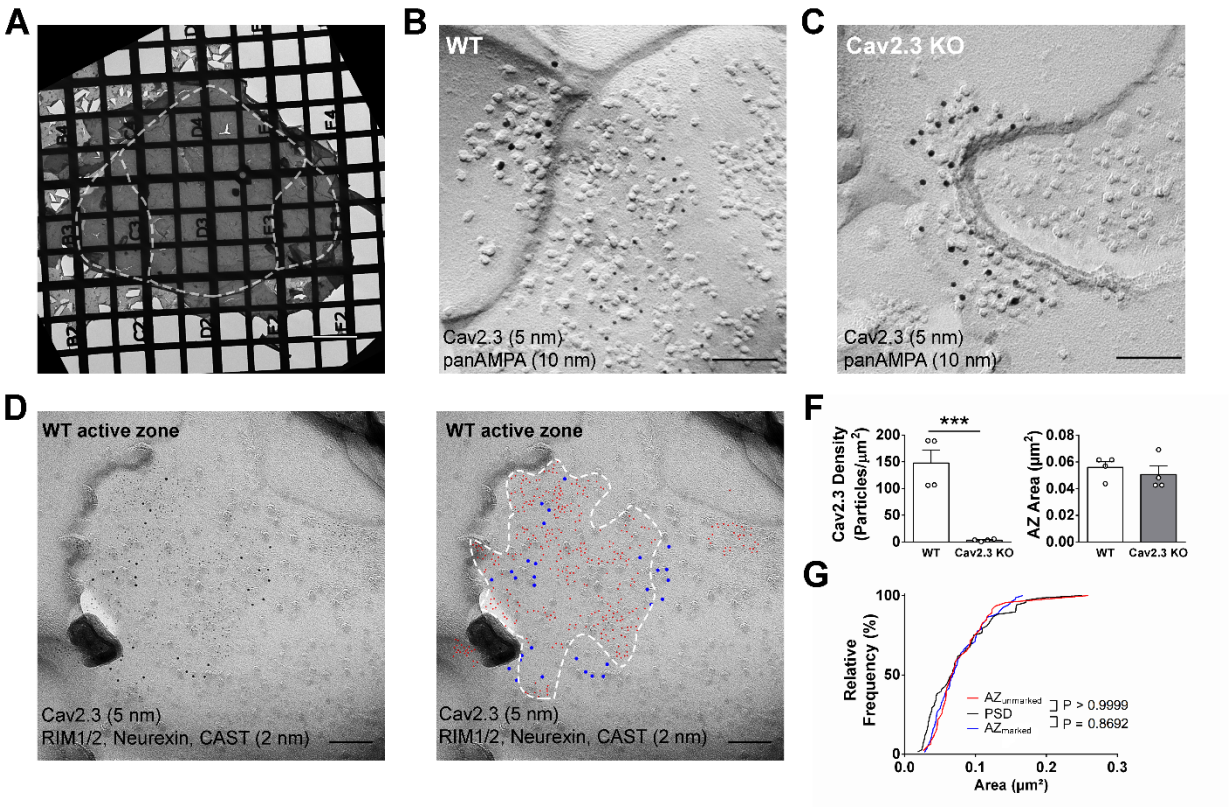

Figure 3.11: SDS-digested freeze-fracture replica labeling confirms Cav2.3 in the active zone of medial habenula terminals in the IPN

A Example image of a grid-glued replica containing the whole IPN. White line indicates demarcation of rostral/central and lateral subnuclei. Scale bar: 20 µm **B** Example image of a presynaptic P-face and a postsynaptic E-face of a habenular synapse in the rostral IPN that was double labeled with antibodies against AMPA receptors (10 nm) and Cav2.3 (5 nm). Scale bar: 100 nm **C** Example image of a similar synaptic profile double-labeled with antibodies against AMPA receptors (10 nm) and Cav2.3 (5 nm) in the rostral IPN of a Cav2.3 KO mouse. Scale bar: 100 nm **D** Left panel: double labeling of a WT carbon-only replica with antibodies against Cav2.3 (5 nm) and a mixture of active zone proteins (2 nm), including RIM1/2, CAST and Neurexin1. Right panel: the same image with additional coloring of 2 nm and 5 nm particles and demarcation of the active zone area based on active zone marker labeling. Scale bar: 100 nm **F** Left panel: quantification of Cav2.3 labeling densities in the presynaptic P face in WT and Cav2.3 KO mice. *** indicates $P < 0.0001$, unpaired t-test. Right panel: area of demarcated active zones was not significantly different between replicas from WT and Cav2.3 KO mice. Data were obtained from 4 replicas from 4 mice of each genotype. **G** Comparison of active zone area demarcated with or

without active zone markers and the size of the glutamatergic postsynaptic IMP clusters. P value indicates result of Kolmogorov-Smirnov test.

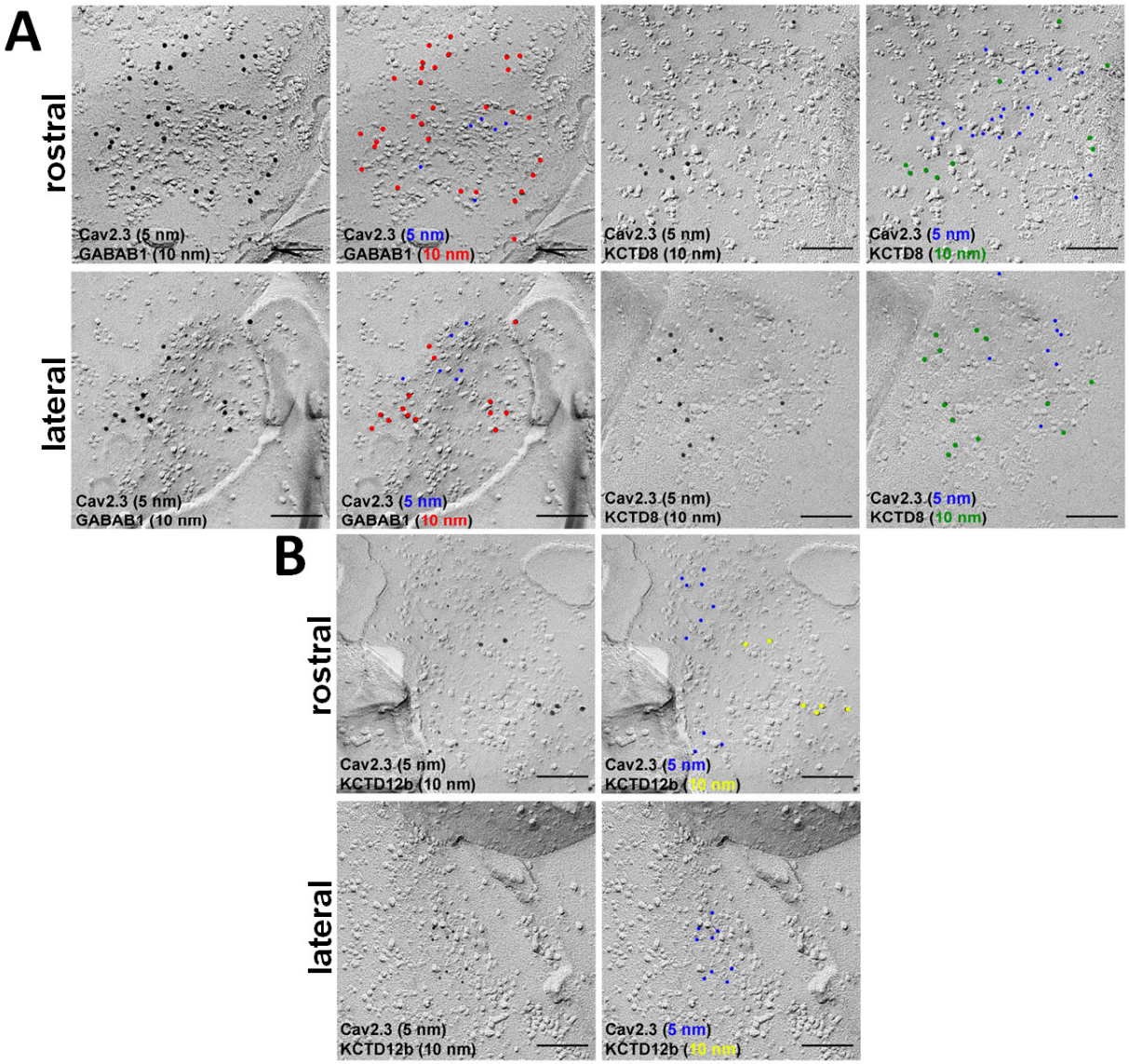

Figure 3.12: Co-localization of Cav2.3 with GABAB receptors and KCTDs in the active zone of medial habenula terminals

Double Labeling of WT replicas for Cav2.3 and either GABAB1 (**A**, left), KCTD8 (**A**, right) or KCTD12b (**B**) along with respective color marking for each particles in the right side of each image. Upper panel Images in **A** and **B** are from presynaptic terminals in the rostral IPN. Lower panel Images in **A** and **B** are from presynaptic terminals in the lateral IPN. Gold particles of replica pictures in both panels are highlighted by separate colors for each type of molecules (blue for Cav2.3, red for GABAB1, green for KCTD8 and yellow for KCTD12b) in the right side of each picture. Scale bar: 100 nm**.**

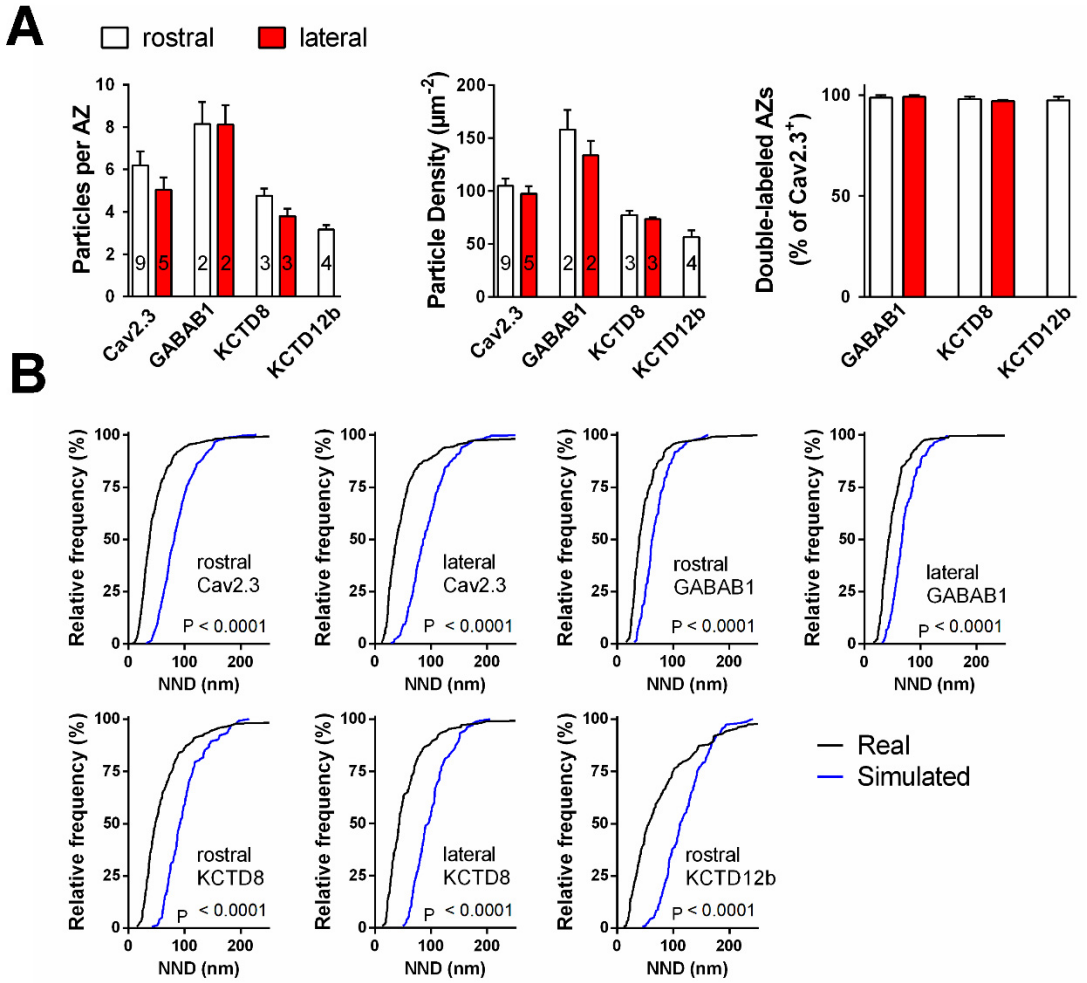

Figure 3.13: Quantitative analysis of co-localization of Cav2.3 with GABAB receptors and KCTDs in the active zone of medial habenula terminals

A Quantification of active zone immunolabeling in the rostral and lateral IPN. With the exception of the absence of KCTD12b in lateral IPN terminals, absolute particle numbers (left graph) and particle densities (middle graph) were comparable between MHb terminals in the rostral and lateral IPN. Right graph: Over 97% of active zones showing Cav2.3 labeling also showed labeling for either of the other molecules (GABAB1, KCTD8 or KCTD12b), suggesting co-localization of all presynaptic molecules inside the same active zone. Numbers inside the bars indicate the number of replicas used for each quantification **B** Nearest neighbor distance (NND) for all the presynaptic molecules in MHb terminals inside the rostral and lateral IPN based on the real (black line) and simulated random distribution (blue line). Smaller NND values in real distributions compared to the simulated ones suggest clustering of all presynaptic molecules. P value obtained via Kolmogorov-Smirnov test. (see also Figure 3.12)

3.4 KCTDs bi-directionally modulate neurotransmitter release probability from ventral MHb terminals

Next, we wanted to investigate the functional significance of the presence of KCTDs in the AZ and their ability to bind to Cav2.3. Because KCTD12b is absent in the lateral IPN, we focused on ventral MHb terminals inside the rostral IPN and performed whole cell recordings from rostral IPN neurons in acute brain slices of WT and KCTD8 and 12b KO mice. Using electrical stimulation, we measured the paired-pulse ratio (PPR) of two consecutively evoked EPSCs at 20 Hz (Figure 3.14A) and found a significant reduction in PPR in KCTD12b KO mice (1.19 ± 0.12, n=20) compared with both WT (2.17 ± 0.32, n=23; P = 0.0435, Kruskal-Wallis test with Dunn's multiple comparison test) and KCTD8 KO mice (2.25 ± 0.28, n=17; P = 0.0074). PPR values inversely correlate with release probability (Dobrunz and Stevens, 1997), therefore, our result suggests that release probability might be higher in KCTD12b KO mice compared to WT or KCTD8 KO mice. To confirm this possibility, we performed variance-mean analysis (Figure 3.14B – D) to estimate the values of release probability (at 2.5 mM Ca^{2+}) and quantal size (Figure 3.14E). Compared with WT mice (WT release probability: 0.26 ± 0.04, n = 16), the release probability from ventral MHb terminals of KCTD12b KO mice (0.49 ± 0.05, n = 9) was significantly increased (Figure 3.14E; $F_{2, 34}$ = 21.23, P < 0.0001; WT vs. KCTD12b KO: P = 0.0005, one-way ANOVA with Tukey post hoc test). Surprisingly, release probability in KCTD8 KO mice (0.12 ± 0.02, n = 12) was significantly lower than that of WT or KCTD12b KO mice (WT vs. KCTD8 KO: P = 0.0176; KCTD8 KO vs. KCTD12b KO: P < 0.0001; Tukey post hoc test). The quantal size remained unaffected by genotype ($F_{2, 34}$ = 1.613, P = 0.2142). This result suggests that KCTD8 and KCTD12b have opposite effects on the probability of neurotransmitter release from ventral MHb terminals, with KCTD8 enhancing and KCTD12b reducing release.

Next, we investigated nano-anatomical changes associated with the increased release probability in KCTD12b KO mice. To this aim, we performed SDS-FRL and co-labeled Cav2.3/GABAB1 or Cav2.3/KCTD8 in replicas of WT and KCTD12b KO IPN samples. Since KCTD12b is not expressed in MHb terminals in the lateral IPN, we normalized the densities of presynaptic molecules in MHb terminals in the rostral IPN to the average density of the same molecule in MHb terminals of the corresponding lateral IPN of the same replica. Thereby, we avoided interference by variabilities in labeling efficiencies between individual replicas. Contrary to our expectation, there was no significant difference in the relative densities of Cav2.3 in the

presynaptic AZ (Figure 3.15A-C; WT rostral: 1.01 ± 0.04 fold of lateral IPN, n = 8 replicas from 8 mice; KCTD12b KO: 1.06 ± 0.13 fold of lateral IPN, n = 8 replicas from 8 mice; P = 0.5054, Mann-Whitney test). Similarly, GABAB1 expression in the presynaptic AZ of MHb terminals was not significantly different between WT and KCTD12b KO (Figure 3.15C; WT rostral: 1.30 ± 0.18 fold of lateral IPN, n = 3 replicas from 3 mice; KCTD12b KO: 0.89 ± 0.07 fold of lateral IPN, n = 3 replicas from 3 mice; P = 0.4000, Mann-Whitney test). Next, we tested the possibility that absence of one KCTD subtype may result in a compensatory invasion of the other into the AZ. Interestingly, the relative density of KCTD8 in the AZ of MHb terminals was increased by 149% in KCTD12b KO mice compared with those of WT mice (WT rostral: 0.84 ± 0.12 fold of lateral IPN, n = 5 replicas from 5 mice; KCTD12b KO: 2.09 ± 0.45 fold of lateral IPN, n = 5 replicas from 5 mice; P = 0.0079, Mann-Whitney test). These results suggest that the presence of KCTDs in the AZ may be dynamically regulated and that this regulation may be important in scaling of synaptic strength.

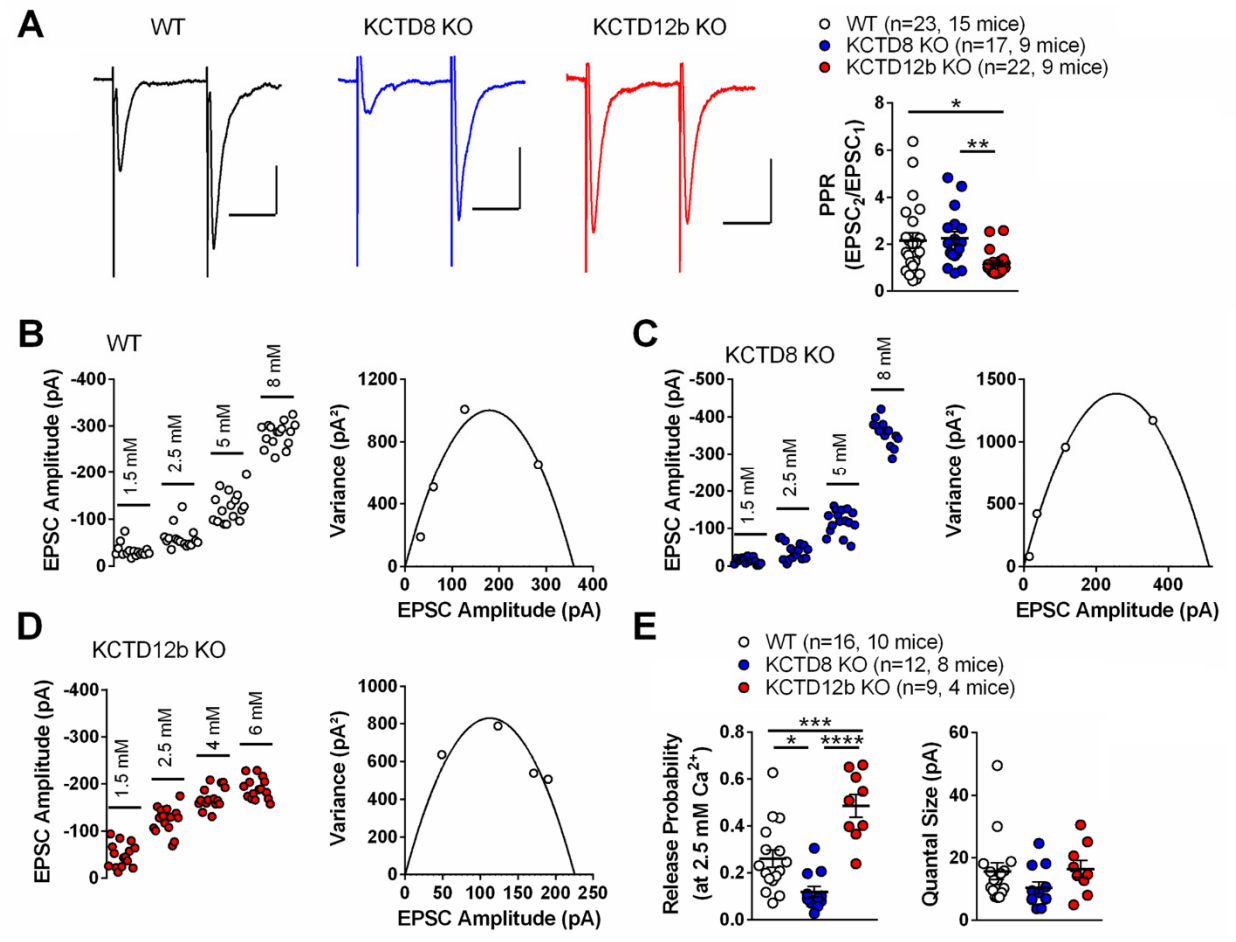

Figure 3.14: KCTDs modulate release probability

Whole-cell recordings of paired-pulse ratios (PPR) of electrically evoked glutamatergic excitatory postsynaptic currents (EPSCs) in rostral IPN neurons of WT, KCTD8 KO and KCTD12b KO mice. PPR, calculated as EPSC2 amplitude/EPSC1 amplitude, was significantly lower in KCTD12b KO mice compared to WT and KCTD8 KO, * indicate $P < 0.05$, ** indicate $P < 0.01$, Kruskal-Wallis with Dunn's post hoc test. scale bars: WT, KCTD12b KO: 25 ms/20 pA; KCTD8 KO: 25 ms/50 pA **B-D** Example variance-mean measurements of electrically evoked EPSC amplitudes at varying external Ca^{2+} concentrations recorded in rostral IPN neurons of WT (**B**), KCTD8 KO (**C**) and KCTD12b KO mice (**D**). **E** Release probability and quantal size deduced from the variance-mean analysis in **B-D** Data represents mean ± SEM; * indicates $P < 0.05$, *** indicates $P < 0.001$, **** indicates $P < 0.0001$ in one-way ANOVA with Tukey post hoc test. (From Peter Koppensteiner, Shigemoto Lab).

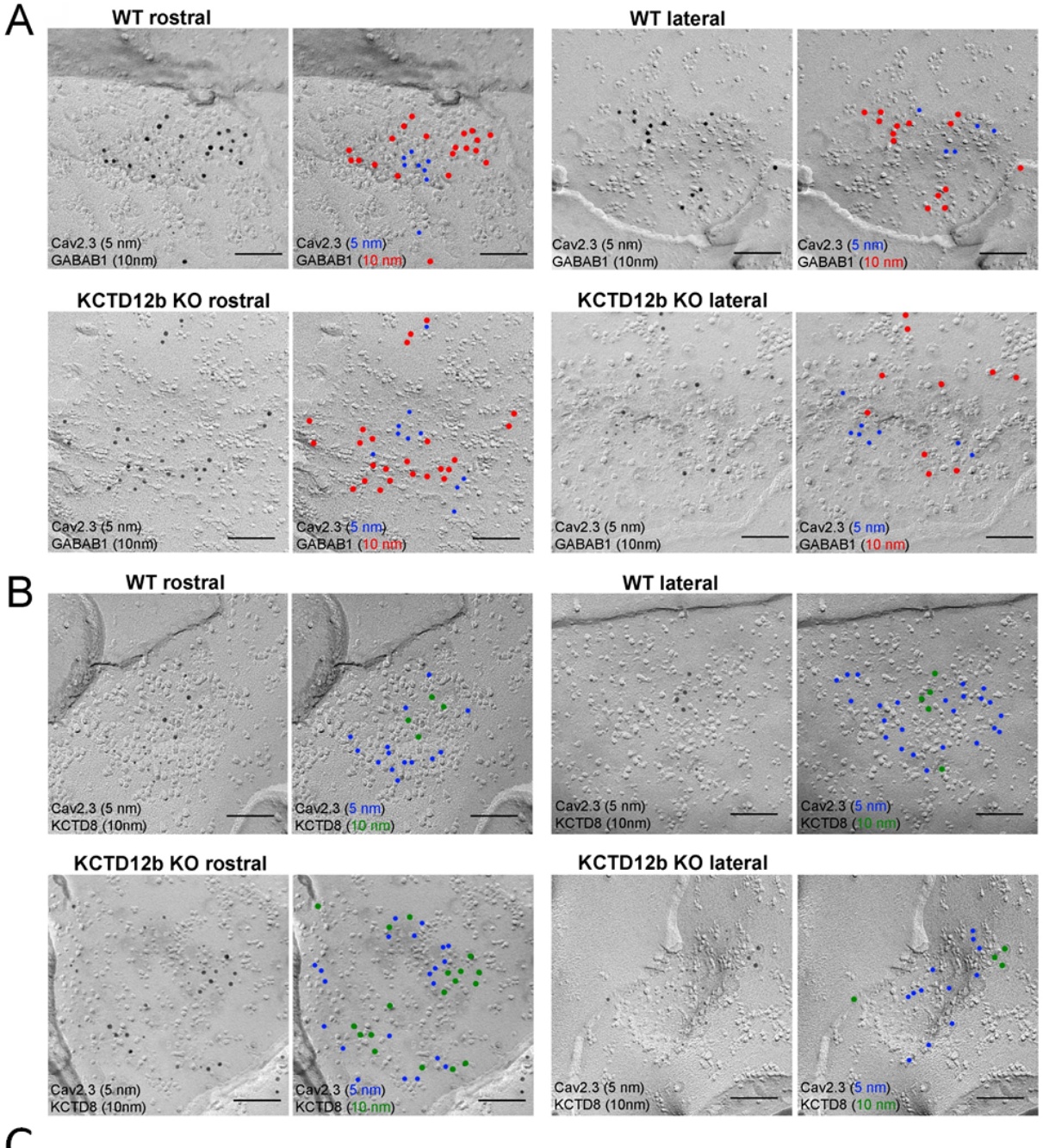
A
WT rostral
WT lateral
KCTD12b KO rostral
KCTD12b KO lateral
Cav2.3 (5 nm)
GABAB1 (10nm)
GABAB1 (10 nm)
B
KCTD8 (10nm)
KCTD8 (10 nm)
C
Cav2.3 Density (Relative to lateral IPN)
P = 0.5054
8
WT
KCTD12b KO
KCTD8 Density (Relative to lateral IPN)
**
5
GABA1 Density (Relative to lateral IPN)
P = 0.4000
3

Figure 3.15: KCTDs are localized to the active zone

Example images of active zones containing Cav2.3 and either GABAB1 (**A**) or KCTD8 (**B**) in replicas of WT (upper row in both panels) and KCTD12b KO IPN tissue (lower row in both panels). Gold particles of replica pictures in both panels are highlighted by separate colors for each type of molecules (blue for Cav2.3, red for GABAB1, and green for KCTD8) in the right side of each picture. Scale bar: 100 nm **C** Quantification of relative densities for Cav2.3, GABAB1 and KCTD8 in active zones located in the rostral IPN of WT and KCTD12b KO mice. Densities were normalized to the average density in medial habenula terminals inside the lateral IPN of the same replica. The number inside the bars indicate the number of replicas used for quantification. Data represents mean ± SEM; ** indicates $P < 0.01$ in a t-test.

3.5 KCTD8 may facilitate termination of GBR-mediated presynaptic potentiation of neurotransmitter release in rostral IPN

Finally, we tested the impact of KCTDs on the GBR-mediated potentiation of neurotransmitter release from ventral MHb terimals in the rostral IPN (Figure 3.16). Please note that data of the WT group is identical to that presented in Figure 3.2C. The application of 1 µM baclofen still potentiated EPSC amplitudes in all KCTD KO lines with similar relative increases of around 500% of baseline, suggesting that KCTDs are not required for the induction of the GBR-mediated enhancement in EPSC amplitude. However, termination of the GBR-mediated enhancement in KCTD12b KO mice was significantly faster compared with WT, KCTD8 KO and KCTD8/12b KO mice (Figure 3.16A, B; $F_{3, 634} = 10.79$; WT vs. KCTD12b KO: $P < 0.0001$; KCTD8 KO vs. KCTD12b KO: $P < 0.0001$; KCTD8/12b vs. KCTD12b KO: $P = 0.0007$; two-way ANOVA with Tukey post hoc test). Interestingly, the faster termination of the GBR-mediated potentiation was abolished in KCTD8/12b double KO mice (Figure 3.16B), suggesting that it is mediated via the previously observed compensatory invasion of KCTD8 into the AZ in KCTD12b KO mice (Figure 3.15C). In addition, there was no difference in the kinetics or relative increase in GBR-mediated enhancement between WT and KCTD8 KO mice, suggesting that KCTD8 does not interfere with the termination of the baclofen effect when KCTD12b is present. Since the GBR-mediated presynaptic potentiation has been implicated in the induction of synaptic plasticity in this pathway (Koppensteiner et al., 2017), the subtype composition of the presynaptic KCTD-heteromers may modulate both basal release as well as synaptic plasticity.

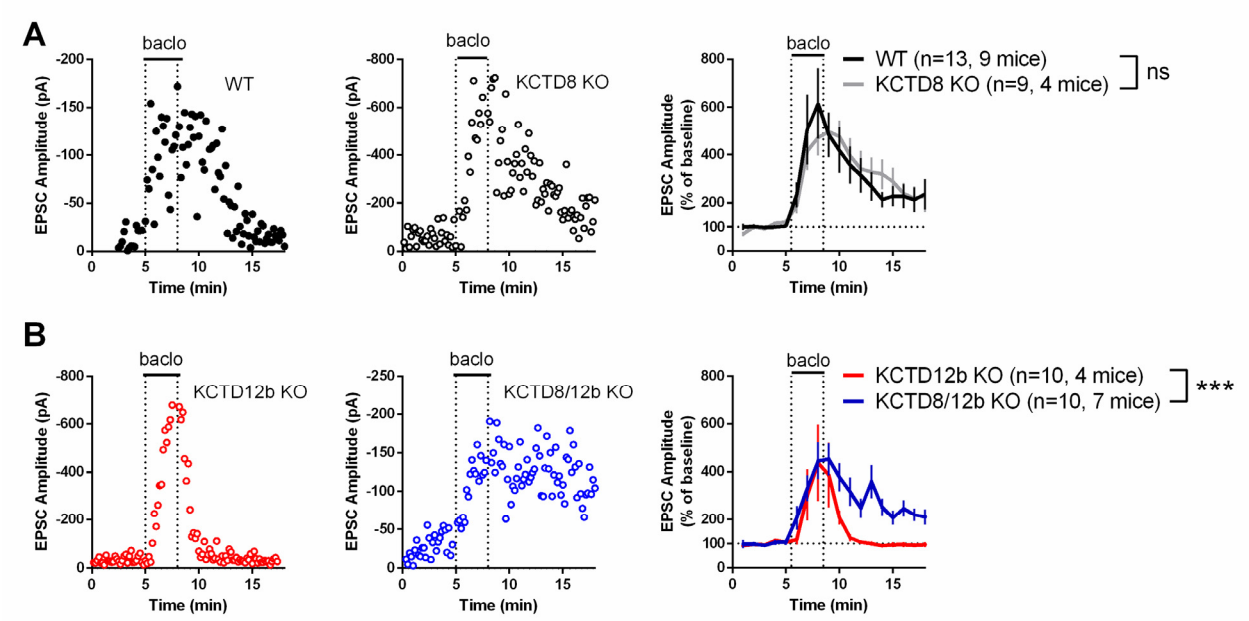

Figure 3.16: KCTD8 enhances termination of presynaptic potentiation by GABAB receptors

A In whole-cell recordings from rostral IPN neurons, a three minute application of 1 μM baclofen produced a strong increase in electrically evoked glutamatergic EPSC amplitude in both WT (example time course in the left graph) and KCTD8 KO mice (example time course in the middle graph). Right graph: neither the increase in EPSC amplitude relative to baseline nor the time course of the potentiation was significantly different between WT and KCTD8 KO mice (ns, two-way ANOVA with Tukey post hoc test). **B** Baclofen application produced a similarly strong increase in KCTD12b KO mice (example time course in the left graph) and in KCTD8/12b double KO mice (example time course in the middle graph) but the potentiation returned to baseline values significantly faster in KCTD12b KO mice compared to all other groups. *** indicates $P < 0.0001$ in a two-way ANOVA with Tukey post hoc test. (From Peter Koppensteiner, Shigemoto Lab).

4 Chapter Four

DISCUSSION

Cav2.3 in MHb-IPN pathway was studied with morphological, biochemical and functional approaches to decipher mechanism of its role in neurotransmission. We demonstrate that Cav2.3, an exclusive presynaptic calcium channel in this pathway is required for neurotransmitter release from both dorsal and ventral MHb terminals in the lateral and rostral IPN, respectively. However, activation of GBRs modulate neurotransmitter release from dorsal and ventral MHb terminals in opposite ways: neurotransmission is facilitated by GBRs in ventral MHb terminals but inhibited in dorsal MHb terminals. To understand the modulatory actions of Cav2.3-mediated release by GBRs, we investigated the role of GBR auxiliary subunits along both MHb-IPN pathways. We show that KCTD8 is expressed in both dorsal and ventral MHb terminals whereas, KCTD12b is exclusively located in ventral MHb terminals. Furthermore, we identified a bi-directional regulation of the release probability by KCTD8 and KCTD12b from ventral MHb terminals as well as a modulation of decay kinetics of the GBR mediated potentiation. Thereby, we identified a novel role of KCTDs in the modulation of R-type Ca^{2+} channel-dependent neurotransmission.

4.1 Unique features of MHb-IPN pathway

Our result of Cav2.3 being the only VDCC in the MHb terminal concentrated mostly in active zone in presynaptic area in IPN is one of the unique features of the MHb-IPN pathway. Previously, it was reported to be present in hippocampal presynaptic terminals in mossy and commissural fiber synapse in small percentage, about 15% (Gasparini et al., 2001) of the total Ca^{2+} channels as ~50-60% of EPSCs amplitude was contributed by Cav2.3. In CA3-CA1 synapses also, it contributes one quarter of total EPSP showing its presence and supportive role in neurotransmission with P/Q and N-type calcium channel (Wu and Saggau, 1995). Unlike presynaptic Cav2.3 in the stratum oriens in hippocampus which has less than 1% of the total Cav2.3 (Parajuli et al., 2012), presynaptic Cav2.3 is mostly concentrated in the active zone in rostral and lateral IPN nuclei. Both pre-embedding and the replica labelling showed Cav2.3 concentrated in presynaptic AZ of MHb terminals indicating an important role of Cav2.3 in neurotransmitter release in this pathway. However, in their pre-embedding immunogold studies, Parajuli and colleagues have reported that Cav2.3 is diffusely distributed along presynaptic

terminal membrane with occasional presence in active zone of MHb terminal in IPN (Parajuli et al., 2012). The discrepancy with our pre-embedding immunogold result could be due to the difference in IPN nuclei we observed as IPN nucleus is not specified in their study. Moreover, further quantitative analysis of their data may also show concentration of Cav2.3 in active zone as only qualitative data is shown.

In the present study, we confirmed the functional significance of presynaptic Cav2.3 electrophysiologically using the specific Cav2.3 blocker SNX-482 (Newcomb et al., 1998). Neurotransmission from dorsal MHb terminals appeared to be less sensitive to SNX-482 than that from ventral MHb terminals, a finding not reflected in our electron microscopy data showing similar expression patterns in both MHb-IPN pathways. There are multiple possibilities to explain this apparent discrepancy. For example, it could be that the morphological structure of IPN neurons in rostral and lateral IPN are different. If the dendritic trees of lateral IPN neurons extend to deeper layers of the acute slice, SNX-482 may not efficiently diffuse to such depths at pharmacologically relevant concentration, given the adhesive properties of peptide toxins. In addition, the mode of stimulation in acute brain slices for selective targeting of either ventral or dorsal MHb-derived fibers was different: We used electrical stimulation of the fasciculus retroflexus to evoke EPSCs in rostral IPN neurons but light stimulation of Tac1-ChR2 mice to measure EPSCs in lateral IPN neurons. The 12-15 mW photo-stimulation was sufficiently strong to activate all ChR2-positive terminals, independent of tissue-depth. In contrast, electrical stimulation of fibers close to the slice surface may have targeted only a fraction of ventral MHb-fibers and this fraction may have been more accessible to the peptide toxin due to proximity to the slice surface. Hence percentage of EPSC amplitude block in lateral IPN is not as effective as in rostral IPN. Therefore, we suspect that both pathways may exclusively rely on Cav2.3 for release. There is currently no data available comparing the morphology of neuronal cells in each nuclei of IPN. Our data is compatible with in situ hybridization data of the Allen brain atlas which has shown strong expression of Cav2.3 in MHb cell bodies and an absence of Cav2.2 and Cav2.1 mRNA, key VGCCs for neurotransmitter release in almost all other brain areas (Gasparini et al., 2001, Catterall et al., 2013). It is also consistent with the result of Zhang et al. (Zhang et al., 2016) who showed the role of Cav2.3 in neurotransmission from cholinergic MHb terminals in the IPN, using nickel as a blocker although nickel is not a specific Cav2.3 antagonist.

Along with Cav2.3, GBRs show their strongest expression brain-wide in MHb neurons and we confirmed GBR expression in MHb-derived axons and axon terminals inside the IPN with immunolabeling for both light and electron microscopy. Although the GABAB1a/b antibody targets GB1 subunit only, both heptahelical GBR subunits, i.e. GB1 and GB2, are always expressed

together (Bettler et al., 2004). This is due to the fact that only fully-assembled GBRs are capable of translocation from the ER to the plasma membrane. Hence, GB1 labeling on the plasma membrane reflects completely assembled GBRs. Pre-embedding results show that the majority of GBR is localized peri- and extra-synaptically whereas some are expressed in active zone as well. GBR could modulate Cav2.3 mediated neurotransmission in MHb-IPN pathway (Zhang et al., 2016). But interestingly, GBR showed opposite effects in two different MHb terminals in IPN when acted upon by its agonist, baclofen (Bowery et al., 1980). GBR showed an excitatory role in ventral MHb terminal as it potentiated the glutamate release (Figure 3.2C) in rostral IPN when acted upon by its agonist. This property of GBR is opposite to the general inhibitory effect of GBRs on neurotransmitter release in other presynaptic terminals (Frangaj and Fan, 2018; Zhang et al., 2016). The mechanism of the excitatory function of GBR on ventral MHb terminals is not clear yet (Zhang et al., 2016). Zhang et al. have shown that selective knock-out of GBRs in cholinergic neurons prevented the baclofen-induced potentiation, suggesting that presynaptic GBRs on cholinergic MHb terminals are mediating the effect. Furthermore, they found that both infusions of pertussis toxin into the IPN, which selectively inhibits $G\alpha_{i/o}\beta\gamma$ signaling, as well as genetic ablation of Cav2.3 prevented the potentiation (Zhang et al., 2016). Surprisingly, GBR had an inhibitory role on neurotransmission from MHb terminals in the lateral IPN like its usual role in other brain areas even when majority of VGCC is Cav2.3. Since both pathways rely on Cav2.3 for release, a direct, excitatory effect of Cav2.3 by GBRs appears unlikely.

To understand the differential modulation of Cav2.3-mediated neurotransmission by GBRs, we studied the localization and function of accessory subunits of GBRs in MHb terminals inside the IPN. Among four accessory subunits, KCTDs 8, 12 and 12b mRNA transcripts are expressed in MHb neurons (Metz et al., 2011). Using immunofluorescence, we confirmed that these mRNAs are translated and the resulting proteins are detectable in MHb axons inside the IPN. The MHb-IPN pathway is the only area in the brain where KCTD12b is present (Metz et al., 2011). KCTD12b and KCTD12 are not splice variants but encoded in different chromosomes, X-chromosome and chromosome 14, respectively. Although they are highly similar in function, their amino acid sequences differ much in their C terminal domains, as other KCTD proteins do (Teng et al., 2019). As reported by Metz et al, KCTD12b mRNA is absent in dorsal MHb and its projection target area i.e. lateral IPN is devoid of KCTD12b proteins. It is the uniqueness of GBR in ventral MHb that it has KCTD12b as an accessory subunit along with KCTD8 and KCTD12. Since KCTDs form homo- and hetero-pentamers, with KCTD12 and 12b commonly associating with KCTD8 (Zheng et al., 2019), we hypothesized that a pentameric ring containing MHb-specific KCTD subtypes may be involved in the unusual excitatory action of GBRs in ventral MHb terminals. One

hypothesis was that the desensitization of the GBR-mediated effector ion channel response such as activation of G-protein gated inwardly rectifying K (GIRK) channels or inhibition of VGCCs may be altered by the presence of KCTD12b. Specifically, previous studies have shown that the association of either KCTD12 or 12b with GBRs produces a desensitization that is followed by a slight overshoot after removal of the GBR agonist. In the case of Ca^{2+} channel currents, this means that Ca^{2+} currents were inhibited by GBR activation but subsequently transiently increased following the termination of the GBR response (Schwenk et al., 2010, Schwenk et al., 2016). Since the ventral MHb is the only place in the CNS where KCTD12 and 12b are present together, we further hypothesized that the combined desensitizing properties of KCTD12 and 12b may favor this overshoot of Ca^{2+} channel currents upon the activation of GBR. However, the potentiation of release from ventral MHb terminals remained intact in the absence of either KCTD8 or KCTD12b rejecting our hypothesis. Nevertheless, recovery from potentiation was significantly faster in KCTD12b KO mice but returned to wild type levels when KCTD8 was additionally removed. This suggests a possible interplay between KCTD8 and KCTD12b with GBR affecting Cav2.3 has a role of this unique feature of GBR in IPN. The faster deactivation kinetics in KCTD12b KO mice is unlikely due to technical differences, such as fast wash out of baclofen from the preparation. As mice of all genotypes were recorded in similar condition showing similar speed of baclofen application and they were recorded randomly, this rules out the possibility of different washout speed affecting deactivation kinetics. Moreover, when KCTD12b is genetically removed, KCTD8 increased in AZ compensating the lack of KCTD12b in AZ, which could support the faster recovery from potentiation by KCTD8 and explain the slow recovery in KCTD8 /12b double KO mice. One possible technical caveat could be that the increase in KCTD8 density seen in replica labelling may be due to better accessibility of KCTD8 epitope in KCTD hetero-pentamers. Steric hindrance created by KCTD12b in WT mice may have gone in KCTD12b KO even though the KCTD8 molecule number is the same. Instead of KCTD8 homo-pentamer formation, KCTD8 and KCTD12 hetero-pentamer may have formed without changing KCTD8 number but with decreasing steric hindrance for anti-KCTD8 antibody. If KCTD8 is upregulated at the mRNA level in KCTD12b KO mice, it could be detected by *in situ* hybridization in ventral medial habenula.

Although we did not identify the molecular mechanism underlying the GBR-mediated potentiation of Cav2.3-mediated neurotransmission, there are a number of candidate molecules uniquely expressed in ventral but not dorsal MHb neurons, which might be involved. For example, ventral MHb neurons selectively express synaptoporin (Marqueze-Pouey et al., 1991), whereas dorsal MHb neurons only express its homolog, synaptophysin (Hashikawa et al., 2019). This suggests that the release machinery might differ between terminals from dorsal and ventral

subnuclei. Moreover, ventral but not dorsal MHb neurons selectively express a unique isoform of protein kinase C (PKCθ) which is absent in most neurons of the brain (Allen Brain Atlas). Importantly, GBR signals via the $G\alpha_i$ pathway and the GBR-mediated potentiation is abolished by pre-treatment with pertussis toxin (Zhang et al., 2016). Although PKC is not activated in the classical $G\alpha_i$ pathway, it was reported that $G\alpha_i$ signaling can activate PKC in heterologous expression system, resulting in activation of the phospholipase C pathway and cytosolic Ca^{2+} increase (Schmidt et al., 1998). Interestingly, PKCθ exerts regulatory control over guanine nucleotide exchange factors involved in the modulation of $G\alpha_i$ signaling (Lopez-Sanchez et al., 2013). Thus, differential GBR-mediated effects in dorsal and ventral MHb terminals may result from distinct release mechanisms or the involvement of peculiar PKC-mediated signaling.

Facilitation of release by GBR activation in rostral IPN and inhibition in lateral IPN may have distinct physiological significance. Zhang and colleagues have reported that cholinergic projections, which are also positive for GBRs, in rostral IPN facilitates fear extinction when stimulated with baclofen whereas lateral IPN doesn't show such effect (Zhang et al., 2016). Melani and colleagues have reported that substance P pathway is also involved in fear extinction in rostral MHb to lateral IPN. When the NK1 (neurokinin 1) receptor, primary receptor for substance P, was blocked injecting the antagonist, L732138, in lateral IPN, fear extinction was significantly lesser (Melani et al., 2019b). Considering that GBR activation causes inhibition in lateral IPN, it would negatively affect fear extinction. This means that GBR activations in rostral and lateral IPN may have opposite effects on fear extinction.

4.2 Co-immunoprecipitation and co-localization of KCTDs with Cav2.3

The presynaptic localization of GBRs and their auxiliary subunits in synapses throughout the brain has been confirmed by multiple studies. For example, Schwenk and colleagues found that Cav2.2 directly binds to KCTD8 and KCTD16 in native tissue (Schwenk et al., 2016). The principal and auxiliary subunits of GBR are commonly co-purified with VGCC complexes (Muller et al., 2010) and, in turn, VGCCs are co-purified with native GBR complexes (Schwenk et al., 2010). Laviv et al. have shown using fluorescence resonance energy transfer spectroscopy that GBR, G protein and VGCC form a complex in hippocampal boutons (Laviv et al., 2011). Our biochemical approach in a heterologous system revealed that both KCTD8 and 12b, but not KCTD12 may

directly bind Cav2.3. However, such interactions have been overlooked in these previous reports, most likely due to the brain wide proteomics approach that may not be suitable to identify interactions specific for single brain areas.

In SDS-FRL, we found that Cav2.3, GBRs and KCTDs are together in the same active zone. Although all tested molecules showed clustering, clusters rarely overlap, contrary to expectations for proteins in the same complex. This could be due to steric hindrance between antibodies targeting proteins in close proximity to each other. Another explanation could be that the synapses were at rest during fixation and direct interactions between these presynaptic molecules may be more apparent when the synapse undergoes activity. An important question for future studies would be to investigate which interactions are present at rest and how do these interactions change during neurotransmission. An indication for the resting state interactions may be found in our pre-embedding immunolabeling result. There, we found that the sub-synaptic localization patterns of KCTD8 and GBRs were similar, with peak expressions in the peri-synaptic zone. Furthermore, patterns of Cav2.3 and KCTD12b were similar, with peak densities in the active zone. Therefore, we suspect that KCTD8 may be associated mostly with GBRs whereas KCTD12b may be associated mostly with Cav2.3 at rest. A recent study described the interaction of the GBR with KCTDs, using crystallography (Zheng et al., 2019). Zheng and colleagues revealed that KCTDs bind on the C-terminal intracellular tail of the GB2 subunit and this tail may be up to 40 – 50 nm in length. Therefore, a theoretical radius of 40 – 50 nm around the GBR plus 30 nm for primary and secondary antibodies could result in a distance of up to 80 nm between gold particles for GBRs and KCTDs in SDS-FRL, even if they are directly bound to each other. Another important consideration is the fact that KCTDs are cytosolic proteins – meaning that they will not be detectable in SDS-FRL unless they are in a stable complex with membrane-associated proteins. Therefore, KCTD signals observed in SDS-FRL should mostly be in tight protein complexes with either GBRs, Cav2.3 or additional, unknown membrane-associated molecules.

4.3 Technical Consideration for immunolabelling with modified SDS-FRL

To confirm whether the theoretical binding of Cav2.3 to KCTD8 and KCTD12b was actually taking place in vivo, we performed SDS-FRL for Cav2.3 and KCTDs. We performed a modified glue grid method for SDS-FRL technique. Our modified glue grid method for SDS-FRL provided extra advantage over regular labelling method for replica (Harada and Shigemoto, 2016; Nakamura et al., 2015). Gluing the replica with remnant tissue after fracturing to the nickel grid provided stability

to the replica so that whole IPN was intact till the end. Hence, it was easier to compare labelling in lateral and rostral nuclei without difficulty. Besides, it was easier to handle the replica during labelling process and identifying the anatomical area in IPN during EM observation was also easier which could have been confusing otherwise. We were concerned whether the glue could hinder labelling of immuno-particles to the epitope in the edges of the replica and in possible cracks. This risk should have been avoided using the lowest possible amount of glue (~0.4 µl). However, no remaining glue was observed during EM observation in almost all of the cases. Thus the chance of glue hindering labelling is minimal.

All molecules tested i.e. Cav2.3, GBR, KCTD8 and KCTD12b are present strongly in AZ (Figure 3.12). Compared to Cav2.3 distribution observed in immune-gold pre-embedding immunohistochemistry, the number of Cav2.3 in SDS-FRL was very high (Figure 3.13A). This could be because of easy accessibility of anti-Cav2.3 antibody to Cav2.3 in the replica whereas antibody has to penetrate through the thicker section for immunoreaction to occur in pre-embedding. In addition, the labelling is even in replica compared to pre-embedding materials because of different thickness to be penetrated for antibody to access antigen in sections. Moreover, the SDS treatment also denatures Cav2.3 epitope making it easy for Cav2.3 antibody to react with Cav2.3 molecule trapped in two dimensional surface of carbon replica (Masugi-Tokita and Shigemoto, 2007, Masugi-Tokita et al., 2007).

Similar to pre-embedding data, SDS-FRL also showed strong expression of GBR in active zone along with extrasynaptic area. It also showed KCTD8 and KCTD12b in active zone as well. It is interesting though that these molecules do not seem to be expressed strongly in replica labelling compared to GBR. In pre-embedding, their expression densities were comparable in AZ (Figure 3.10, 3.13A). This could be due to the reason that these two molecules are cytoplasmic in nature which cannot be retained on membrane on their own (Liu et al., 2013). They bind their BTB complex with GB2 to the membrane forming a long tail (Zheng et al., 2019). SDS digestion somehow may disrupt the bond of these molecules with GB2 decreasing the labelling intensity in replica. Besides, denaturing of these proteins during SDS digestion could have made them less suitable for antibody binding even if they are there in the membrane binding with GBR.

Besides these advantages of SDR-FRL technique, there was high variability of labelling in each replica, especially for Cav2.3. Hence it would be difficult to compare labelling strength in different samples. This could be overcome by normalizing density of molecules in rostral IPN to corresponding lateral IPN as whole IPN is intact with glued grid method. This worked for Cav2.3, GABAB1, and KCTD8, while it did not work for KCTD12b as it is expressed only in the rostral IPN.

4.4 Bidirectional effects of KCTDs

To investigate the functional significance of KCTD8 and KCTD12b being in AZ of MHb-IPN pathway and their ability to couple with Cav2.3, we performed electrophysiological studies. The observation of increased and reduced release probability in the absence of KCTD12b or KCTD8, respectively, suggests that the theoretical interaction between KCTDs and Cav2.3 without GBR activation may have a potential role in fine tuning synaptic strength. In zebrafish, KCTD8 and 12b equivalents are differentially expressed in the right and left habenulae, respectively. This asymmetry may be associated with different sizes of the two dorsal fish habenulae as well as with different functional roles in aversive behaviors (deCarvalho et al., 2014, Duboue et al., 2017). Although there is no apparent size asymmetry in the rodent MHb, it is an intriguing idea that perhaps there is an evolutionary conserved molecular asymmetry on the level of KCTDs expression. Future studies may be required to test this hypothesis.

Synaptic facilitation in KCTD12b KO could be due to facilitation of VGCC currents by direct interaction between Cav2.3 and KCTD8. Importantly, the density of Cav2.3 and GBRs remained unaffected in KCTD12b KO (Figure 3.15C). Possibly, KCTD12b was recruiting Gβγ to Cav2.3 and when it was absent in KO, KCTD8 compensated the KCTD12b location and Gβγ did no longer interact with Cav2.3 resulting in facilitation. This argument fits with the result that KCTD8 KO has decreased release probability as only KCTD12b is present there. One may envision the possibility that the G-proteins may exhibit constitutively higher GTP binding at rest, due to a uniquely strong expression of the GTP exchange factor Rapgef4, also called Epac2 (Sugawara et al., 2016), in the ventral MHb (Allen Brain Atlas). This may lead to constitutive binding of active Gβγ to both KCTD12 and KCTD12b – the only KCTD capable of directly binding this G-protein. Future pharmacological interventions may be able to test this hypothesis by blocking Rapgef4. Through direct binding of Cav2.3 and KCTD12b, Gβγ may be recruited to the VGCC and selectively suppress Ca^{2+} conductance at rest. Other reason of facilitation besides upregulated conductance of VGCC could be due to altered availability of free Ca^{2+}, calcium binding protein and Ca^{2+} sensor (Fioravante and Regehr, 2011). According to the Allen Brain Atlas and Marqueze-Pouey and colleagues, the ventral MHb selectively shows strong expression of synaptoporin as well as synaptotagmins1 and 9, suggesting potential unique mechanisms of calcium sensing and vesicle fusion (Marqueze-Pouey et al., 1991). Similarly, synaptic depression in KCTD8 KO could be due to different reasons besides calcium channel inactivation such as decrement of readily releasable pool of vesicles, longer time taken for endocytosis of vesicles, and long-time taken for vesicle replenishment (Fioravante and Regehr, 2011). Future studies will be required to investigate the

role of these presynaptic molecules and their function in neurotransmitter release from the MHb to the IPN.

Contrary to their name, KCTDs are neither potassium channels nor do they form tetramers. Instead, they merely contain a multimeriziation domain similar to voltage-gated potassium channels and exclusively form pentameric rings (Zheng et al. 2019, Fritzius and Bettler, 2019). While the C-termini of KCTD subtypes are highly variable, the N-termini of all KCTD subtypes contains a so-called Bric-a-brack, Tram-track, Broad complex (BTB) domain (Liu et al., 2013). This protein-protein interaction domain is not only responsible for the formation of protein complexes but is also involved in the regulation of gene transcription, interaction with the cytoskeleton as well as the protein degradation machinery (Melnick et al., 2000, Furukawa et al., 2003, Kang et al., 2004). Although KCTDs are known to modulate signaling pathways, including sonic hedgehog and Wnt/beta-catenin (De Smaele et al., 2004, Dutta and Dawid, 2010), there is currently only sparse information available on the exact function of distinct KCTD subtypes. For example in zebrafish, KCTD8 and KCTD12 are differentially expressed in left and right habenulae and serve as markers of asymmetry (Husken et al., 2014). However, their exact involvement in asymmetry remains completely unknown.

We identified a direct interaction between Cav2.3 and KCTD8 and KCTD12b. It is unclear whether KCTDs exert a modulatory role on Cav2.3 or rather serve as adaptor proteins linking Cav2.3 to other modulatory proteins. Our result might be explained by a direct effect of KCTDs on currents through Cav2.3. For example, the increase in release probability in KCTD12b KO mice may be caused by a KCTD8-mediated increase of Cav2.3 conductance. However, there is no previous example of direct modulatory action of KCTDs on any ion channel. Hence, there is limited insight into the possible mechanisms underlying such a modulation. Other functions of KCTDs that might be responsible for changes in release probability may be due to their BTB domains, such as alterations of the presynaptic cytoskeleton or changes in presynaptic protein repertoire through modulations protease-related processes. Furthermore, there is the possibility of KCTD-mediated changes in gene transcription.

5 Chapter Five

SUMMARY

Our results show Cav2.3 as the exclusive VGCC in MHb terminal which is modulated by KCTDs in its neurotransmitter release function. The major findings are as follows:

1. Cav2.3 is the only VDCC expressed in MHb terminals in IPN, which is mostly concentrated in the presynaptic active zone.
2. GABAB1 and KCTD8 are expressed in MHb terminals throughout IPN, whereas KCTD12 and KCTD12b are expressed in ventral MHb to rostral/central IPN but not in lateral IPN. Immunoreactivity for KCTD12b was exclusively observed in ventral MHb and their IPN terminals in the whole brain.
3. Cav2.3 shows strongest expression in active zone of MHb terminals along with KCTD12b, while GABAB1, KCTD8, and KCTD12 show the highest expression perisynaptically.
4. Cav2.3 co-immunoprecipitates with KCTD8 and KCTD12b but not KCTD12 in HEK cell preparation.
5. Replica labelling shows that Cav2.3, GABAB1, KCTD8 and KCTD12b are co-localized with each other in active zone of MHb terminal.
6. Release probability in rostral IPN of KCTD12b KO is significantly higher than that of WT and KCTD8 KO, while KCTD8 KO mice show significantly lower release probability than WT mice.
7. GABAB1 agonist, baclofen, shows facilitatory effects on glutamatergic transmission in rostral IPN, while inhibitory effects in lateral IPN in WT mice. The facilitatory effects remained in KCTD8 and KCTD12b KO mice.
8. Presynaptic potentiation of evoked EPSC amplitude by baclofen application in rostral IPN of KCTD12b KO mice falls sharply to baseline faster than those in WT, KCTD8 KO mice and KCTD8/12b KO mice indicating that KCTD12b is involved in the sustained potentiation of vesicle release by GABAB receptor activation, whereas KCTD8 facilitates its termination in the absence of KCTD12b.

6 Chapter Six

REFERENCES

Agetsuma M, Aizawa H, Aoki T, Nakayama R, Takahoko M, Goto M, Sassa T, Amo R, Shiraki T, Kawakami K, Hosoya T, Higashijima S, Okamoto H (2010) The habenula is crucial for experience-dependent modification of fear responses in zebrafish. Nature neuroscience 13:1354-1356.

Aizawa H, Kobayashi M, Tanaka S, Fukai T, Okamoto H (2012) Molecular characterization of the subnuclei in rat habenula. The Journal of comparative neurology 520:4051-4066.

Almog M, Korngreen A (2009) Characterization of voltage-gated Ca(2+) conductances in layer 5 neocortical pyramidal neurons from rats. PloS one 4:e4841.

Ambrosini A, D'Onofrio M, Buzzi MG, Arisi I, Grieco GS, Pierelli F, Santorelli FM, Schoenen J (2017) Possible Involvement of the CACNA1E Gene in Migraine: A Search for Single Nucleotide Polymorphism in Different Clinical Phenotypes. Headache 57:1136-1144.

Andres KH, von During M, Veh RW (1999) Subnuclear organization of the rat habenular complexes. The Journal of comparative neurology 407:130-150.

Antolin-Fontes B, Ables JL, Gorlich A, Ibanez-Tallon I (2015) The habenulo-interpeduncular pathway in nicotine aversion and withdrawal. Neuropharmacology 96:213-222.

Bay T, Eghorn LF, Klein AB, Wellendorph P (2014) GHB receptor targets in the CNS: focus on high-affinity binding sites. Biochemical pharmacology 87:220-228.

Bettler B, Kaupmann K, Mosbacher J, Gassmann M (2004) Molecular structure and physiological functions of GABA(B) receptors. Physiological reviews 84:835-867.

Biermann B, Ivankova-Susankova K, Bradaia A, Abdel Aziz S, Besseyrias V, Kapfhammer JP, Missler M, Gassmann M, Bettler B (2010) The Sushi domains of GABAB receptors function as axonal targeting signals. The Journal of neuroscience : the official journal of the Society for Neuroscience 30:1385-1394.

Blein S, Ginham R, Uhrin D, Smith BO, Soares DC, Veltel S, McIlhinney RA, White JH, Barlow PN (2004) Structural analysis of the complement control protein (CCP) modules of GABA(B) receptor 1a: only one of the two CCP modules is compactly folded. The Journal of biological chemistry 279:48292-48306.

Bloodgood BL, Sabatini BL (2007) Nonlinear regulation of unitary synaptic signals by CaV(2.3) voltage-sensitive calcium channels located in dendritic spines. Neuron 53:249-260.

Bourinet E, Stotz SC, Spaetgens RL, Dayanithi G, Lemos J, Nargeot J, Zamponi GW (2001) Interaction of SNX482 with domains III and IV inhibits activation gating of alpha(1E) (Ca(V)2.3) calcium channels. Biophysical journal 81:79-88.

Bourinet E, Zamponi GW (2017) Block of voltage-gated calcium channels by peptide toxins. Neuropharmacology 127:109-115.

Bowery NG, Hill DR, Hudson AL, Doble A, Middlemiss DN, Shaw J, Turnbull M (1980) (-)Baclofen decreases neurotransmitter release in the mammalian CNS by an action at a novel GABA receptor. Nature 283:92-94.

Bowery NG, Hudson AL, Price GW (1987) GABAA and GABAB receptor site distribution in the rat central nervous system. Neuroscience 20:365-383.

Breustedt J, Vogt KE, Miller RJ, Nicoll RA, Schmitz D (2003) Alpha1E-containing Ca2+ channels are involved in synaptic plasticity. Proceedings of the National Academy of Sciences of the United States of America 100:12450-12455.

Castillo PE, Weisskopf MG, Nicoll RA (1994) The role of Ca2+ channels in hippocampal mossy fiber synaptic transmission and long-term potentiation. Neuron 12:261-269.
Catterall WA (2011) Voltage-gated calcium channels. Cold Spring Harbor perspectives in biology 3:a003947.
Catterall WA, Leal K, Nanou E (2013) Calcium channels and short-term synaptic plasticity. The Journal of biological chemistry 288:10742-10749.
Chalifoux JR, Carter AG (2010) GABAB receptors modulate NMDA receptor calcium signals in dendritic spines. Neuron 66:101-113.
Charles KJ, Evans ML, Robbins MJ, Calver AR, Leslie RA, Pangalos MN (2001) Comparative immunohistochemical localisation of GABA(B1a), GABA(B1b) and GABA(B2) subunits in rat brain, spinal cord and dorsal root ganglion. Neuroscience 106:447-467.
Contestabile A, Villani L, Fasolo A, Franzoni MF, Gribaudo L, Oktedalen O, Fonnum F (1987) Topography of cholinergic and substance P pathways in the habenulo-interpeduncular system of the rat. An immunocytochemical and microchemical approach. Neuroscience 21:253-270.
Couve A, Moss SJ, Pangalos MN (2000) GABAB receptors: a new paradigm in G protein signaling. Molecular and cellular neurosciences 16:296-312.
Cuello AC, Del Fiacco M, Paxinos G (1978) The central and peripheral ends of the substance P-containing sensory neurones in the rat trigeminal system. Brain research 152:499-500.
De Smaele E, Di Marcotullio L, Ferretti E, Screpanti I, Alesse E, Gulino A (2004) Chromosome 17p deletion in human medulloblastoma: a missing checkpoint in the Hedgehog pathway. Cell cycle (Georgetown, Tex) 3:1263-1266.
deCarvalho TN, Subedi A, Rock J, Harfe BD, Thisse C, Thisse B, Halpern ME, Hong E (2014) Neurotransmitter map of the asymmetric dorsal habenular nuclei of zebrafish. Genesis (New York, NY : 2000) 52:636-655.
Dermon CR, Stamatakis A, Tlemcani O, Balthazart J (1999) Performance of appetitive or consummatory components of male sexual behavior is mediated by different brain areas: a 2-deoxyglucose autoradiographic study. Neuroscience 94:1261-1277.
Di Marcotullio L, Ferretti E, De Smaele E, Argenti B, Mincione C, Zazzeroni F, Gallo R, Masuelli L, Napolitano M, Maroder M, Modesti A, Giangaspero F, Screpanti I, Alesse E, Gulino A (2004) REN(KCTD11) is a suppressor of Hedgehog signaling and is deleted in human medulloblastoma. Proceedings of the National Academy of Sciences of the United States of America 101:10833-10838.
Dietrich D, Kirschstein T, Kukley M, Pereverzev A, von der Brelie C, Schneider T, Beck H (2003) Functional specialization of presynaptic Cav2.3 Ca2+ channels. Neuron 39:483-496.
Dobrunz LE, Stevens CF (1997) Heterogeneity of release probability, facilitation, and depletion at central synapses. Neuron 18:995-1008.
Dolphin AC (2016) Voltage-gated calcium channels and their auxiliary subunits: physiology and pathophysiology and pharmacology. The Journal of physiology 594:5369-5390.
Dolphin AC (2018) Voltage-gated calcium channel alpha 2delta subunits: an assessment of proposed novel roles. F1000Research 7.
Duboue ER, Hong E, Eldred KC, Halpern ME (2017) Left Habenular Activity Attenuates Fear Responses in Larval Zebrafish. Current biology : CB 27:2154-2162 e2153.
Duncan A, Heyer MP, Ishikawa M, Caligiuri SPB, Liu XA, Chen Z, Vittoria Micioni Di Bonaventura M, Elayouby KS, Ables JL, Howe WM, Bali P, Fillinger C, Williams M, O'Connor RM, Wang Z, Lu Q, Kamenecka TM, Ma'ayan A, O'Neill HC, Ibanez-Tallon I, Geurts AM, Kenny PJ (2019) Habenular TCF7L2 links nicotine addiction to diabetes. Nature 574:372-377.
Duthey B, Caudron S, Perroy J, Bettler B, Fagni L, Pin JP, Prezeau L (2002) A single subunit (GB2) is required for G-protein activation by the heterodimeric GABA(B) receptor. The Journal of biological chemistry 277:3236-3241.

Dutta S, Dawid IB (2010) Kctd15 inhibits neural crest formation by attenuating Wnt/beta-catenin signaling output. Development (Cambridge, England) 137:3013-3018.

Ellinor PT, Zhang JF, Randall AD, Zhou M, Schwarz TL, Tsien RW, Horne WA (1993) Functional expression of a rapidly inactivating neuronal calcium channel. Nature 363:455-458.

Fioravante D, Regehr WG (2011) Short-term forms of presynaptic plasticity. Current opinion in neurobiology 21:269-274.

Fowler CD, Lu Q, Johnson PM, Marks MJ, Kenny PJ (2011) Habenular alpha5 nicotinic receptor subunit signalling controls nicotine intake. Nature 471:597-601.

Fredriksson R, Lagerstrom MC, Lundin LG, Schioth HB (2003) The G-protein-coupled receptors in the human genome form five main families. Phylogenetic analysis, paralogon groups, and fingerprints. Molecular pharmacology 63:1256-1272.

Fremeau RT, Jr., Troyer MD, Pahner I, Nygaard GO, Tran CH, Reimer RJ, Bellocchio EE, Fortin D, Storm-Mathisen J, Edwards RH (2001) The expression of vesicular glutamate transporters defines two classes of excitatory synapse. Neuron 31:247-260.

Fritzius T, Bettler B (2019) The organizing principle of GABAB receptor complexes: Physiological and pharmacological implications. Basic & clinical pharmacology & toxicology.

Fritzius T, Turecek R, Seddik R, Kobayashi H, Tiao J, Rem PD, Metz M, Kralikova M, Bouvier M, Gassmann M, Bettler B (2017) KCTD Hetero-oligomers Confer Unique Kinetic Properties on Hippocampal GABAB Receptor-Induced K+ Currents. The Journal of neuroscience : the official journal of the Society for Neuroscience 37:1162-1175.

Fujimoto K (1995) Freeze-fracture replica electron microscopy combined with SDS digestion for cytochemical labeling of integral membrane proteins. Application to the immunogold labeling of intercellular junctional complexes. Journal of cell science 108 (Pt 11):3443-3449.

Fukui M, Nakamichi N, Yoneyama M, Ozawa S, Fujimori S, Takahata Y, Nakamura N, Taniura H, Yoneda Y (2008) Modulation of cellular proliferation and differentiation through GABA(B) receptors expressed by undifferentiated neural progenitor cells isolated from fetal mouse brain. Journal of cellular physiology 216:507-519.

Furukawa M, He YJ, Borchers C, Xiong Y (2003) Targeting of protein ubiquitination by BTB-Cullin 3-Roc1 ubiquitin ligases. Nature cell biology 5:1001-1007.

Gamper N, Reznikov V, Yamada Y, Yang J, Shapiro MS (2004) Phosphatidylinositol [correction] 4,5-bisphosphate signals underlie receptor-specific Gq/11-mediated modulation of N-type Ca2+ channels. The Journal of neuroscience : the official journal of the Society for Neuroscience 24:10980-10992.

Gamse JT, Kuan YS, Macurak M, Brosamle C, Thisse B, Thisse C, Halpern ME (2005) Directional asymmetry of the zebrafish epithalamus guides dorsoventral innervation of the midbrain target. Development (Cambridge, England) 132:4869-4881.

Gandla J, Lomada SK, Lu J, Kuner R, Bali KK (2017) miR-34c-5p functions as pronociceptive microRNA in cancer pain by targeting Cav2.3 containing calcium channels. Pain 158:1765-1779.

Gardon O, Faget L, Chu Sin Chung P, Matifas A, Massotte D, Kieffer BL (2014) Expression of mu opioid receptor in dorsal diencephalic conduction system: new insights for the medial habenula. Neuroscience 277:595-609.

Gasparini S, Kasyanov AM, Pietrobon D, Voronin LL, Cherubini E (2001) Presynaptic R-type calcium channels contribute to fast excitatory synaptic transmission in the rat hippocampus. The Journal of neuroscience : the official journal of the Society for Neuroscience 21:8715-8721.

Gassmann M, Bettler B (2012) Regulation of neuronal GABA(B) receptor functions by subunit composition. Nature reviews Neuroscience 13:380-394.

Gharbi N, Zhao XF, Ellingsen S, Fjose A (2012) Zebrafish enhancer trap line showing maternal and neural expression of kctd15a. Development, growth & differentiation 54:241-252.

Groenewegen HJ, Ahlenius S, Haber SN, Kowall NW, Nauta WJ (1986) Cytoarchitecture, fiber connections, and some histochemical aspects of the interpeduncular nucleus in the rat. The Journal of comparative neurology 249:65-102.

Gurevich VV, Gurevich EV (2019) GPCR Signaling Regulation: The Role of GRKs and Arrestins. Frontiers in pharmacology 10:125.

Hamill GS, Lenn NJ (1984) The subnuclear organization of the rat interpeduncular nucleus: a light and electron microscopic study. The Journal of comparative neurology 222:396-408.

Hamill GS, Olschowka JA, Lenn NJ, Jacobowitz DM (1984) The subnuclear distribution of substance P, cholecystokinin, vasoactive intestinal peptide, somatostatin, leu-enkephalin, dopamine-beta-hydroxylase, and serotonin in the rat interpeduncular nucleus. The Journal of comparative neurology 226:580-596.

Harada H, Shigemoto R (2016) Immunogold Protein Localization on Grid-Glued Freeze-Fracture Replicas. Methods in molecular biology (Clifton, NJ) 1474:203-216.

Hashikawa Y, Hashikawa K, Basiri ML, Liu Y, Johnston NL, Ahmad OR, Stuber GD (2019) Transcriptional and Spatial Resolution of Cell Types in the Mammalian Habenula. bioRxiv 772376.

Helbig KL, Lauerer RJ, Bahr JC, Souza IA, Myers CT, Uysal B, Schwarz N, Gandini MA, Huang S, Keren B, Mignot C, Afenjar A, Billette de Villemeur T, Heron D, Nava C, Valence S, Buratti J, Fagerberg CR, Soerensen KP, Kibaek M, Kamsteeg EJ, Koolen DA, Gunning B, Schelhaas HJ, Kruer MC, Fox J, Bakhtiari S, Jarrar R, Padilla-Lopez S, Lindstrom K, Jin SC, Zeng X, Bilguvar K, Papavasileiou A, Xing Q, Zhu C, Boysen K, Vairo F, Lanpher BC, Klee EW, Tillema JM, Payne ET, Cousin MA, Kruisselbrink TM, Wick MJ, Baker J, Haan E, Smith N, Sadeghpour A, Davis EE, Katsanis N, Task Force for Neonatal G, Corbett MA, MacLennan AH, Gecz J, Biskup S, Goldmann E, Rodan LH, Kichula E, Segal E, Jackson KE, Asamoah A, Dimmock D, McCarrier J, Botto LD, Filloux F, Tvrdik T, Cascino GD, Klingerman S, Neumann C, Wang R, Jacobsen JC, Nolan MA, Snell RG, Lehnert K, Sadleir LG, Anderlid BM, Kvarnung M, Guerrini R, Friez MJ, Lyons MJ, Leonhard J, Kringlen G, Casas K, El Achkar CM, Smith LA, Rotenberg A, Poduri A, Sanchis-Juan A, Carss KJ, Rankin J, Zeman A, Raymond FL, Blyth M, Kerr B, Ruiz K, Urquhart J, Hughes I, Banka S, Deciphering Developmental Disorders S, Hedrich UBS, Scheffer IE, Helbig I, Zamponi GW, Lerche H, Mefford HC (2019) De Novo Pathogenic Variants in CACNA1E Cause Developmental and Epileptic Encephalopathy with Contractures, Macrocephaly, and Dyskinesias. American journal of human genetics 104:562.

Herkenham M, Nauta WJ (1977) Afferent connections of the habenular nuclei in the rat. A horseradish peroxidase study, with a note on the fiber-of-passage problem. The Journal of comparative neurology 173:123-146.

Herkenham M, Nauta WJ (1979) Efferent connections of the habenular nuclei in the rat. The Journal of comparative neurology 187:19-47.

Hoptman MJ (2015) Impulsivity and aggression in schizophrenia: a neural circuitry perspective with implications for treatment. CNS spectrums 20:280-286.

Hsu YW, Wang SD, Wang S, Morton G, Zariwala HA, de la Iglesia HO, Turner EE (2014) Role of the dorsal medial habenula in the regulation of voluntary activity, motor function, hedonic state, and primary reinforcement. The Journal of neuroscience : the official journal of the Society for Neuroscience 34:11366-11384.

Husken U, Stickney HL, Gestri G, Bianco IH, Faro A, Young RM, Roussigne M, Hawkins TA, Beretta CA, Brinkmann I, Paolini A, Jacinto R, Albadri S, Dreosti E, Tsalavouta M, Schwarz Q, Cavodeassi F, Barth AK, Wen L, Zhang B, Blader P, Yaksi E, Poggi L, Zigman M, Lin S, Wilson SW, Carl M (2014) Tcf7l2 is required for left-right asymmetric differentiation of habenular neurons. Current biology : CB 24:2217-2227.

Indriati DW, Kamasawa N, Matsui K, Meredith AL, Watanabe M, Shigemoto R (2013) Quantitative localization of Cav2.1 (P/Q-type) voltage-dependent calcium channels in Purkinje cells:

somatodendritic gradient and distinct somatic coclustering with calcium-activated potassium channels. The Journal of neuroscience : the official journal of the Society for Neuroscience 33:3668-3678.
Iwahori N (1977) A Golgi study on the habenular nucleus of the cat. The Journal of comparative neurology 72:319-344.
Jeong JY, Kweon HJ, Suh BC (2016) Dual Regulation of R-Type CaV2.3 Channels by M1 Muscarinic Receptors. Molecules and cells 39:322-329.
Ji AX, Chu A, Nielsen TK, Benlekbir S, Rubinstein JL, Prive GG (2016) Structural Insights into KCTD Protein Assembly and Cullin3 Recognition. Journal of molecular biology 428:92-107.
Kang MI, Kobayashi A, Wakabayashi N, Kim SG, Yamamoto M (2004) Scaffolding of Keap1 to the actin cytoskeleton controls the function of Nrf2 as key regulator of cytoprotective phase 2 genes. Proceedings of the National Academy of Sciences of the United States of America 101:2046-2051.
Kato AS, Witkin JM (2018) Protein complexes as psychiatric and neurological drug targets. Biochemical pharmacology 151:263-281.
Kim U, Chang SY (2005) Dendritic morphology, local circuitry, and intrinsic electrophysiology of neurons in the rat medial and lateral habenular nuclei of the epithalamus. The Journal of comparative neurology 483:236-250.
Kimm T, Bean BP (2014) Inhibition of A-type potassium current by the peptide toxin SNX-482. The Journal of neuroscience : the official journal of the Society for Neuroscience 34:9182-9189.
Kobayashi Y, Sano Y, Vannoni E, Goto H, Suzuki H, Oba A, Kawasaki H, Kanba S, Lipp HP, Murphy NP, Wolfer DP, Itohara S (2013) Genetic dissection of medial habenula-interpeduncular nucleus pathway function in mice. Frontiers in behavioral neuroscience 7:17.
Koppensteiner P, Melani R, Ninan I (2017) A Cooperative Mechanism Involving Ca(2+)-Permeable AMPA Receptors and Retrograde Activation of GABAB Receptors in Interpeduncular Nucleus Plasticity. Cell reports 20:1111-1122.
Kreusch A, Pfaffinger PJ, Stevens CF, Choe S (1998) Crystal structure of the tetramerization domain of the Shaker potassium channel. Nature 392:945-948.
Kubota M, Murakoshi T, Saegusa H, Kazuno A, Zong S, Hu Q, Noda T, Tanabe T (2001) Intact LTP and fear memory but impaired spatial memory in mice lacking Ca(v)2.3 (alpha(IE)) channel. Biochemical and biophysical research communications 282:242-248.
Kulik A, Nakadate K, Nyiri G, Notomi T, Malitschek B, Bettler B, Shigemoto R (2002) Distinct localization of GABA(B) receptors relative to synaptic sites in the rat cerebellum and ventrobasal thalamus. The European journal of neuroscience 15:291-307.
Kuzmiski JB, Barr W, Zamponi GW, MacVicar BA (2005) Topiramate inhibits the initiation of plateau potentials in CA1 neurons by depressing R-type calcium channels. Epilepsia 46:481-489.
Latorraca NR, Venkatakrishnan AJ, Dror RO (2017) GPCR Dynamics: Structures in Motion. Chemical reviews 117:139-155.
Laviv T, Vertkin I, Berdichevsky Y, Fogel H, Riven I, Bettler B, Slesinger PA, Slutsky I (2011) Compartmentalization of the GABAB receptor signaling complex is required for presynaptic inhibition at hippocampal synapses. The Journal of neuroscience : the official journal of the Society for Neuroscience 31:12523-12532.
Lecourtier L, Kelly PH (2007) A conductor hidden in the orchestra? Role of the habenular complex in monoamine transmission and cognition. Neuroscience and biobehavioral reviews 31:658-672.
Lefkowitz RJ (2013) A brief history of G-protein coupled receptors (Nobel Lecture). Angewandte Chemie (International ed in English) 52:6366-6378.
Lenn NJ (1976) Synapses in the interpeduncular nucleus: electron microscopy of normal and habenula lesioned rats. The Journal of comparative neurology 166:77-99.

Lenn NJ (1978) Effect of neonatal deafferentation on synaptogenesis in the rat interpeduncular nucleus. The Journal of comparative neurology 181:93-115.
Lenn NJ, Hamill GS (1984) Subdivisions of the interpeduncular nucleus: a proposed nomenclature. Brain research bulletin 13:203-204.
Lenn NJ, Wong V, Hamill GS (1983) Left-right pairing at the crest synapses of rat interpeduncular nucleus. Neuroscience 9:383-389.
Liu Z, Xiang Y, Sun G (2013) The KCTD family of proteins: structure, function, disease relevance. Cell & bioscience 3:45.
Lopez-Sanchez I, Garcia-Marcos M, Mittal Y, Aznar N, Farquhar MG, Ghosh P (2013) Protein kinase C-theta (PKCtheta) phosphorylates and inhibits the guanine exchange factor, GIV/Girdin. Proceedings of the National Academy of Sciences of the United States of America 110:5510-5515.
Lujan R, Aguado C, Ciruela F, Cozar J, Kleindienst D, de la Ossa L, Bettler B, Wickman K, Watanabe M, Shigemoto R, Fukazawa Y (2018) Differential association of GABAB receptors with their effector ion channels in Purkinje cells. Brain structure & function 223:1565-1587.
Mann EO, Kohl MM, Paulsen O (2009) Distinct roles of GABA(A) and GABA(B) receptors in balancing and terminating persistent cortical activity. The Journal of neuroscience : the official journal of the Society for Neuroscience 29:7513-7518.
Margeta-Mitrovic M, Mitrovic I, Riley RC, Jan LY, Basbaum AI (1999) Immunohistochemical localization of GABA(B) receptors in the rat central nervous system. The Journal of comparative neurology 405:299-321.
Marqueze-Pouey B, Wisden W, Malosio ML, Betz H (1991) Differential expression of synaptophysin and synaptoporin mRNAs in the postnatal rat central nervous system. The Journal of neuroscience : the official journal of the Society for Neuroscience 11:3388-3397.
Masugi-Tokita M, Shigemoto R (2007) High-resolution quantitative visualization of glutamate and GABA receptors at central synapses. Current opinion in neurobiology 17:387-393.
Masugi-Tokita M, Tarusawa E, Watanabe M, Molnar E, Fujimoto K, Shigemoto R (2007) Number and density of AMPA receptors in individual synapses in the rat cerebellum as revealed by SDS-digested freeze-fracture replica labeling. The Journal of neuroscience : the official journal of the Society for Neuroscience 27:2135-2144.
McDonough SI, Mintz IM, Bean BP (1997) Alteration of P-type calcium channel gating by the spider toxin omega-Aga-IVA. Biophysical journal 72:2117-2128.
McLaughlin I, Dani JA, De Biasi M (2017) The medial habenula and interpeduncular nucleus circuitry is critical in addiction, anxiety, and mood regulation. Journal of neurochemistry 142 Suppl 2:130-143.
Melani R, Von Itter R, Jing D, Koppensteiner P, Ninan I (2019a) Opposing effects of an atypical glycinergic and substance P transmission on interpeduncular nucleus plasticity. Neuropsychopharmacology : official publication of the American College of Neuropsychopharmacology 44:1828-1836.
Melani R, Von Itter R, Jing D, Koppensteiner P, Ninan I (2019b) Opposing effects of an atypical glycinergic and substance P transmission on interpeduncular nucleus plasticity. 44:1828-1836.
Melnick A, Ahmad KF, Arai S, Polinger A, Ball H, Borden KL, Carlile GW, Prive GG, Licht JD (2000) In-depth mutational analysis of the promyelocytic leukemia zinc finger BTB/POZ domain reveals motifs and residues required for biological and transcriptional functions. Molecular and cellular biology 20:6550-6567.
Metz M, Gassmann M, Fakler B, Schaeren-Wiemers N, Bettler B (2011) Distribution of the auxiliary GABAB receptor subunits KCTD8, 12, 12b, and 16 in the mouse brain. The Journal of comparative neurology 519:1435-1454.
Miki T, Kaufmann WA, Malagon G, Gomez L, Tabuchi K, Watanabe M, Shigemoto R, Marty A (2017) Numbers of presynaptic Ca(2+) channel clusters match those of functionally defined vesicular

docking sites in single central synapses. Proceedings of the National Academy of Sciences of the United States of America 114:E5246-e5255.
Mochida S (2018) Presynaptic calcium channels. Neuroscience research 127:33-44.
Molas S, DeGroot SR, Zhao-Shea R, Tapper AR (2017) Anxiety and Nicotine Dependence: Emerging Role of the Habenulo-Interpeduncular Axis. Trends in pharmacological sciences 38:169-180.
Mroz ED, Brownstein MJ, Leeman SE (1976) Evidence for substance P in the habenulo-interpeduncular tract. Brain research 113:597-599.
Muller CS, Haupt A, Bildl W, Schindler J, Knaus HG, Meissner M, Rammner B, Striessnig J, Flockerzi V, Fakler B, Schulte U (2010) Quantitative proteomics of the Cav2 channel nano-environments in the mammalian brain. Proceedings of the National Academy of Sciences of the United States of America 107:14950-14957.
Nakamura Y, Harada H, Kamasawa N, Matsui K, Rothman JS, Shigemoto R, Silver RA, DiGregorio DA, Takahashi T (2015) Nanoscale distribution of presynaptic Ca(2+) channels and its impact on vesicular release during development. Neuron 85:145-158.
Neugebauer NM, Einstein EB, Lopez MB, McClure-Begley TD, Mineur YS, Picciotto MR (2013) Morphine dependence and withdrawal induced changes in cholinergic signaling. Pharmacology, biochemistry, and behavior 109:77-83.
Neumaier F, Alpdogan S, Hescheler J, Schneider T (2018) Protein phosphorylation maintains the normal function of cloned human Cav2.3 channels. The Journal of general physiology 150:491-510.
Newcomb R, Szoke B, Palma A, Wang G, Chen X, Hopkins W, Cong R, Miller J, Urge L, Tarczy-Hornoch K, Loo JA, Dooley DJ, Nadasdi L, Tsien RW, Lemos J, Miljanich G (1998) Selective peptide antagonist of the class E calcium channel from the venom of the tarantula Hysterocrates gigas. Biochemistry 37:15353-15362.
Palkovits M, Saavedra JM, Kobayashi RM, Brownstein M (1974) Choline acetyltransferase content of limbic nuclei of the rat. Brain research 79:443-450.
Pang X, Liu L, Ngolab J, Zhao-Shea R, McIntosh JM, Gardner PD, Tapper AR (2016) Habenula cholinergic neurons regulate anxiety during nicotine withdrawal via nicotinic acetylcholine receptors. Neuropharmacology 107:294-304.
Parajuli LK, Nakajima C, Kulik A, Matsui K, Schneider T, Shigemoto R, Fukazawa Y (2012) Quantitative regional and ultrastructural localization of the Ca(v)2.3 subunit of R-type calcium channel in mouse brain. The Journal of neuroscience : the official journal of the Society for Neuroscience 32:13555-13567.
Paus T, Bernard M, Chakravarty MM, Davey Smith G, Gillis J, Lourdusamy A, Melka MG, Leonard G, Pavlidis P, Perron M, Pike GB, Richer L, Schumann G, Timpson N, Toro R, Veillette S, Pausova Z (2012) KCTD8 gene and brain growth in adverse intrauterine environment: a genome-wide association study. Cerebral cortex (New York, NY : 1991) 22:2634-2642.
Pereverzev A, Mikhna M, Vajna R, Gissel C, Henry M, Weiergraber M, Hescheler J, Smyth N, Schneider T (2002) Disturbances in glucose-tolerance, insulin-release, and stress-induced hyperglycemia upon disruption of the Ca(v)2.3 (alpha 1E) subunit of voltage-gated Ca(2+) channels. Molecular endocrinology (Baltimore, Md) 16:884-895.
Pin JP, Bettler B (2016) Organization and functions of mGlu and GABAB receptor complexes. Nature 540:60-68.
Qin C, Luo M (2009) Neurochemical phenotypes of the afferent and efferent projections of the mouse medial habenula. Neuroscience 161:827-837.
Quick MW, Ceballos RM, Kasten M, McIntosh JM, Lester RA (1999) Alpha3beta4 subunit-containing nicotinic receptors dominate function in rat medial habenula neurons. Neuropharmacology 38:769-783.

Rajagopal S, Shenoy SK (2018) GPCR desensitization: Acute and prolonged phases. Cellular signalling 41:9-16.

Ren J, Qin C, Hu F, Tan J, Qiu L, Zhao S, Feng G, Luo M (2011) Habenula "cholinergic" neurons co-release glutamate and acetylcholine and activate postsynaptic neurons via distinct transmission modes. Neuron 69:445-452.

Ricoy UM, Frerking ME (2014) Distinct roles for Cav2.1-2.3 in activity-dependent synaptic dynamics. Journal of neurophysiology 111:2404-2413.

Rolland B, Simon N, Franchitto N (2018) Safety Challenges of Using High Dose Baclofen for Alcohol Use Disorder: A Focused Review. Frontiers in psychiatry 9:367.

Rubio ME, Matsui K, Fukazawa Y, Kamasawa N, Harada H, Itakura M, Molnar E, Abe M, Sakimura K, Shigemoto R (2017) The number and distribution of AMPA receptor channels containing fast kinetic GluA3 and GluA4 subunits at auditory nerve synapses depend on the target cells. Brain structure & function 222:3375-3393.

Saegusa H, Kurihara T, Zong S, Minowa O, Kazuno A, Han W, Matsuda Y, Yamanaka H, Osanai M, Noda T, Tanabe T (2000) Altered pain responses in mice lacking alpha 1E subunit of the voltage-dependent Ca2+ channel. Proceedings of the National Academy of Sciences of the United States of America 97:6132-6137.

Schmidt M, Lohmann B, Hammer K, Haupenthal S, Nehls MV, Jakobs KH (1998) Gi- and protein kinase C-mediated heterologous potentiation of phospholipase C signaling by G protein-coupled receptors. Molecular pharmacology 53:1139-1148.

Schneider T, Alpdogan S, Hescheler J, Neumaier F (2018) In vitro and in vivo phosphorylation of the Cav2.3 voltage-gated R-type calcium channel. Channels (Austin, Tex) 12:326-334.

Schneider T, Dibue-Adjei M, Neumaier F, Akhtar I, Hescheler J, Kamp MA, Tevoufouet EE (2015) R-Type Voltage-Gated Ca(2)(+) Channels in Cardiac and Neuronal Rhythmogenesis. Current molecular pharmacology 8:102-108.

Schneider T, Dibue M, Hescheler J (2013) How "Pharmacoresistant" is Cav2.3, the Major Component of Voltage-Gated R-type Ca2+ Channels? Pharmaceuticals (Basel, Switzerland) 6:759-776.

Schramm M, Vajna R, Pereverzev A, Tottene A, Klockner U, Pietrobon D, Hescheler J, Schneider T (1999) Isoforms of alpha1E voltage-gated calcium channels in rat cerebellar granule cells--detection of major calcium channel alpha1-transcripts by reverse transcription-polymerase chain reaction. Neuroscience 92:565-575.

Schweitz H, Heurteaux C, Bois P, Moinier D, Romey G, Lazdunski M (1994) Calcicludine, a venom peptide of the Kunitz-type protease inhibitor family, is a potent blocker of high-threshold Ca2+ channels with a high affinity for L-type channels in cerebellar granule neurons. Proceedings of the National Academy of Sciences of the United States of America 91:878-882.

Schwenk J, Metz M, Zolles G, Turecek R, Fritzius T, Bildl W, Tarusawa E, Kulik A, Unger A, Ivankova K, Seddik R, Tiao JY, Rajalu M, Trojanova J, Rohde V, Gassmann M, Schulte U, Fakler B, Bettler B (2010) Native GABA(B) receptors are heteromultimers with a family of auxiliary subunits. Nature 465:231-235.

Schwenk J, Perez-Garci E, Schneider A, Kollewe A, Gauthier-Kemper A, Fritzius T, Raveh A, Dinamarca MC, Hanuschkin A, Bildl W, Klingauf J, Gassmann M, Schulte U, Bettler B, Fakler B (2016) Modular composition and dynamics of native GABAB receptors identified by high-resolution proteomics. Nature neuroscience 19:233-242.

Seddik R, Jungblut SP, Silander OK, Rajalu M, Fritzius T, Besseyrias V, Jacquier V, Fakler B, Gassmann M, Bettler B (2012) Opposite effects of KCTD subunit domains on GABA(B) receptor-mediated desensitization. The Journal of biological chemistry 287:39869-39877.

Shumake J, Edwards E, Gonzalez-Lima F (2003) Opposite metabolic changes in the habenula and ventral tegmental area of a genetic model of helpless behavior. Brain research 963:274-281.

Simpson LL (1988) Targeting drugs and toxins to the brain: magic bullets. International review of neurobiology 30:123-147.

Siwek ME, Muller R, Henseler C, Broich K, Papazoglou A, Weiergraber M (2014) The CaV2.3 R-type voltage-gated Ca2+ channel in mouse sleep architecture. Sleep 37:881-892.

Skoblov M, Marakhonov A, Marakasova E, Guskova A, Chandhoke V, Birerdinc A, Baranova A (2013) Protein partners of KCTD proteins provide insights about their functional roles in cell differentiation and vertebrate development. BioEssays : news and reviews in molecular, cellular and developmental biology 35:586-596.

Smith MA, Katsouri L, Virtue S, Choudhury AI, Vidal-Puig A, Ashford MLJ, Withers DJ (2018) Calcium Channel CaV2.3 Subunits Regulate Hepatic Glucose Production by Modulating Leptin-Induced Excitation of Arcuate Pro-opiomelanocortin Neurons. Cell reports 25:278-287 e274.

Soong TW, Stea A, Hodson CD, Dubel SJ, Vincent SR, Snutch TP (1993) Structure and functional expression of a member of the low voltage-activated calcium channel family. Science (New York, NY) 260:1133-1136.

Soria-Gomez E, Busquets-Garcia A, Hu F, Mehidi A, Cannich A, Roux L, Louit I, Alonso L, Wiesner T, Georges F, Verrier D, Vincent P, Ferreira G, Luo M, Marsicano G (2015) Habenular CB1 Receptors Control the Expression of Aversive Memories. Neuron 88:306-313.

Stogios PJ, Downs GS, Jauhal JJ, Nandra SK, Prive GG (2005) Sequence and structural analysis of BTB domain proteins. Genome biology 6:R82.

Stotz SC, Spaetgens RL, Zamponi GW (2000) Block of voltage-dependent calcium channel by the green mamba toxin calcicludine. The Journal of membrane biology 174:157-165.

Sugawara K, Shibasaki T, Takahashi H, Seino S (2016) Structure and functional roles of Epac2 (Rapgef4). Gene 575:577-583.

Sutherland RJ (1982) The dorsal diencephalic conduction system: a review of the anatomy and functions of the habenular complex. Neuroscience and biobehavioral reviews 6:1-13.

Takahashi M, Seagar MJ, Jones JF, Reber BF, Catterall WA (1987) Subunit structure of dihydropyridine-sensitive calcium channels from skeletal muscle. Proceedings of the National Academy of Sciences of the United States of America 84:5478-5482.

Tanabe T, Takeshima H, Mikami A, Flockerzi V, Takahashi H, Kangawa K, Kojima M, Matsuo H, Hirose T, Numa S (1987) Primary structure of the receptor for calcium channel blockers from skeletal muscle. Nature 328:313-318.

Tanaka J, Matsuzaki M, Tarusawa E, Momiyama A, Molnar E, Kasai H, Shigemoto R (2005) Number and density of AMPA receptors in single synapses in immature cerebellum. The Journal of neuroscience : the official journal of the Society for Neuroscience 25:799-807.

Teng X, Aouacheria A, Lionnard L, Metz KA, Soane L, Kamiya A, Hardwick JM (2019) KCTD: A new gene family involved in neurodevelopmental and neuropsychiatric disorders. CNS neuroscience & therapeutics 25:887-902.

Turecek R, Schwenk J, Fritzius T, Ivankova K, Zolles G, Adelfinger L, Jacquier V, Besseyrias V, Gassmann M, Schulte U, Fakler B, Bettler B (2014) Auxiliary GABAB receptor subunits uncouple G protein betagamma subunits from effector channels to induce desensitization. Neuron 82:1032-1044.

Turner TJ, Lampe RA, Dunlap K (1995) Characterization of presynaptic calcium channels with omega-conotoxin MVIIC and omega-grammotoxin SIA: role for a resistant calcium channel type in neurosecretion. Molecular pharmacology 47:348-353.

Vajna R, Schramm M, Pereverzev A, Arnhold S, Grabsch H, Klockner U, Perez-Reyes E, Hescheler J, Schneider T (1998) New isoform of the neuronal Ca2+ channel alpha1E subunit in islets of Langerhans and kidney--distribution of voltage-gated Ca2+ channel alpha1 subunits in cell lines and tissues. European journal of biochemistry 257:274-285.

Van Bogaert P, Aeby A, De Borchgrave V, De Cocq C, Deprez M, De Tiege X, de Tourtchaninoff M, Dubru JM, Foulon M, Ghariani S, Grisar T, Legros B, Ossemann M, Tugendhaft P, van Rijckevorsel K, Verheulpen D, Groupe de travail des centres francophones de reference de l'epilepsie r (2006) The epileptic syndromes with continuous spikes and waves during slow sleep: definition and management guidelines. Acta neurologica Belgica 106:52-60.

Varoqui H, Schafer MK, Zhu H, Weihe E, Erickson JD (2002) Identification of the differentiation-associated Na+/PI transporter as a novel vesicular glutamate transporter expressed in a distinct set of glutamatergic synapses. The Journal of neuroscience : the official journal of the Society for Neuroscience 22:142-155.

Vigot R, Barbieri S, Brauner-Osborne H, Turecek R, Shigemoto R, Zhang YP, Lujan R, Jacobson LH, Biermann B, Fritschy JM, Vacher CM, Muller M, Sansig G, Guetg N, Cryan JF, Kaupmann K, Gassmann M, Oertner TG, Bettler B (2006) Differential compartmentalization and distinct functions of GABAB receptor variants. Neuron 50:589-601.

Weiergraber M, Henry M, Krieger A, Kamp M, Radhakrishnan K, Hescheler J, Schneider T (2006) Altered seizure susceptibility in mice lacking the Ca(v)2.3 E-type Ca2+ channel. Epilepsia 47:839-850.

Weiergraber M, Pereverzev A, Vajna R, Henry M, Schramm M, Nastainczyk W, Grabsch H, Schneider T (2000) Immunodetection of alpha1E voltage-gated Ca(2+) channel in chromogranin-positive muscle cells of rat heart, and in distal tubules of human kidney. The journal of histochemistry and cytochemistry : official journal of the Histochemistry Society 48:807-819.

Wells CA, Betke KM, Lindsley CW, Hamm HE (2012) Label-free detection of G protein-SNARE interactions and screening for small molecule modulators. ACS chemical neuroscience 3:69-78.

Westenbroek RE, Hell JW, Warner C, Dubel SJ, Snutch TP, Catterall WA (1992) Biochemical properties and subcellular distribution of an N-type calcium channel alpha 1 subunit. Neuron 9:1099-1115.

Westenbroek RE, Sakurai T, Elliott EM, Hell JW, Starr TV, Snutch TP, Catterall WA (1995) Immunochemical identification and subcellular distribution of the alpha 1A subunits of brain calcium channels. The Journal of neuroscience : the official journal of the Society for Neuroscience 15:6403-6418.

Wheeler DB, Randall A, Tsien RW (1994) Roles of N-type and Q-type Ca2+ channels in supporting hippocampal synaptic transmission. Science (New York, NY) 264:107-111.

Williams ME, Marubio LM, Deal CR, Hans M, Brust PF, Philipson LH, Miller RJ, Johnson EC, Harpold MM, Ellis SB (1994) Structure and functional characterization of neuronal alpha 1E calcium channel subtypes. The Journal of biological chemistry 269:22347-22357.

Wu J, Yan Z, Li Z, Yan C, Lu S, Dong M, Yan N (2015) Structure of the voltage-gated calcium channel Cav1.1 complex. Science (New York, NY) 350:aad2395.

Wu LG, Saggau P (1995) Block of multiple presynaptic calcium channel types by omega-conotoxin-MVIIC at hippocampal CA3 to CA1 synapses. Journal of neurophysiology 73:1965-1972.

Xie K, Allen KL, Kourrich S, Colon-Saez J, Thomas MJ, Wickman K, Martemyanov KA (2010) Gbeta5 recruits R7 RGS proteins to GIRK channels to regulate the timing of neuronal inhibitory signaling. Nature neuroscience 13:661-663.

Yamaguchi T, Danjo T, Pastan I, Hikida T, Nakanishi S (2013) Distinct roles of segregated transmission of the septo-habenular pathway in anxiety and fear. Neuron 78:537-544.

Yang L, Katchman A, Morrow JP, Doshi D, Marx SO (2011) Cardiac L-type calcium channel (Cav1.2) associates with gamma subunits. FASEB journal : official publication of the Federation of American Societies for Experimental Biology 25:928-936.

Zaman T, Lee K, Park C, Paydar A, Choi JH, Cheong E, Lee CJ, Shin HS (2011) Cav2.3 channels are critical for oscillatory burst discharges in the reticular thalamus and absence epilepsy. Neuron 70:95-108.

Zamponi GW, Striessnig J, Koschak A, Dolphin AC (2015) The Physiology, Pathology, and Pharmacology of Voltage-Gated Calcium Channels and Their Future Therapeutic Potential. Pharmacological reviews 67:821-870.

Zawlik I, Zakrzewska M, Witusik M, Golanska E, Kulczycka-Wojdala D, Szybka M, Piaskowski S, Wozniak K, Zakrzewski K, Papierz W, Liberski PP, Rieske P (2006) KCTD11 expression in medulloblastoma is lower than in adult cerebellum and higher than in neural stem cells. Cancer genetics and cytogenetics 170:24-28.

Zhang J, Tan L, Ren Y, Liang J, Lin R, Feng Q, Zhou J, Hu F, Ren J, Wei C, Yu T, Zhuang Y, Bettler B, Wang F, Luo M (2016) Presynaptic Excitation via GABAB Receptors in Habenula Cholinergic Neurons Regulates Fear Memory Expression. Cell 166:716-728.

Zhang JF, Randall AD, Ellinor PT, Horne WA, Sather WA, Tanabe T, Schwarz TL, Tsien RW (1993) Distinctive pharmacology and kinetics of cloned neuronal Ca2+ channels and their possible counterparts in mammalian CNS neurons. Neuropharmacology 32:1075-1088.

Zhang L, Wang H, Luan S, Yang S, Wang Z, Wang J, Zhao H (2017) Altered Volume and Functional Connectivity of the Habenula in Schizophrenia. Frontiers in human neuroscience 11:636.

Zheng S, Abreu N, Levitz J, Kruse AC (2019) Structural basis for KCTD-mediated rapid desensitization of GABAB signalling. Nature 567:127-131.

Zollman S, Godt D, Prive GG, Couderc JL, Laski FA (1994) The BTB domain, found primarily in zinc finger proteins, defines an evolutionarily conserved family that includes several developmentally regulated genes in Drosophila. Proceedings of the National Academy of Sciences of the United States of America 91:10717-10721.